INFORMATION TO USERS

This manuscript has been reproduced from the microfilm master. UMI films the text directly from the original or copy submitted. Thus, some thesis and dissertation copies are in typewriter face, while others may be from any type of computer printer.

The quality of this reproduction is dependent upon the quality of the copy submitted. Broken or indistinct print, colored or poor quality illustrations and photographs, print bleedthrough, substandard margins, and improper alignment can adversely affect reproduction.

In the unlikely event that the author did not send UMI a complete manuscript and there are missing pages, these will be noted. Also, if unauthorized copyright material had to be removed, a note will indicate the deletion.

Oversize materials (e.g., maps, drawings, charts) are reproduced by sectioning the original, beginning at the upper left-hand corner and continuing from left to right in equal sections with small overlaps.

Photographs included in the original manuscript have been reproduced xerographically in this copy. Higher quality 6" x 9" black and white photographic prints are available for any photographs or illustrations appearing in this copy for an additional charge. Contact UMI directly to order.

Bell & Howell Information and Learning
300 North Zeeb Road, Ann Arbor, MI 48106-1346 USA
800-521-0600

Hadron Properties in a Generalized Nambu-Jona Lasinio Model

By

Xiangdong Li

A dissertation submitted to the Graduate Faculty in Physics in partial fulfillment of the requirements for the degree of Doctor of Philosophy, The City University of New York

2000

This manuscript has been read and accepted for the Graduate Faculty in Physics in satisfaction of the dissertation requirement for the degree of Doctor of Philosophy.

9/1/99
Date

Carl M. Shakin
Chair of Examining Committee

9/1/99
Date

Louis S. Celenza
Executive Officer

Carl M. Shakin

Louis S. Celenza

M.K. Liou

Victor Franco

J. Birman

Supervisory Committee

THE CITY UNIVERSITY OF NEW YORK

Abstract

Hadron Properties in a Generalized Nambu-Jona Lasinio Model

By

Xiangdong Li

Advisor: Distinguished Professor Carl Shakin

In this work we calculate the properties of the sigma meson using a generalized Nambu-Jona-Lasinio model that includes a model of confinement. We describe, in some detail, how the sigma coupling to states in the two-pion continuum may be calculated, when using a Lorentz-vector confining interaction. We provide a general procedure for calculating various loop diagrams in Minkowski momentum space for quarks in the presence of the confining interaction. We study the properties of the signa meson by considering t-channel scalar-isoscalar exchange between two quarks.

We study the pseudoscalar octet of Goldstone bosons as well as the η'. We are particularly interested in the properties of the η' and in the mixing of the η^0 (singlet) and η^8 (octet) modes. It is found that the value of the vacuum-polarization integral in each

mesonic channel increases rapidly as one approaches the qq continuum in a model without confinement, since there is cusp behavior at the qq thresholds. That is not a problem in the description of the low-mass mesons (π, κ, η), but makes the study of the η' problematic in a theory without confinement. With our model of Lorentz-vector confinement, we have shown in an earlier work that the Goldstone theorem is satisfied.

As usual, we found a relation between the Bethe-Salpeter equation and the Schwinger-Dyson equation for zero-energy modes. The approximation we adopt for our calculations, made in Minkowski momentum space, is to take the constituent masses of the up, down and strange quarks to be independent of momentum. Here, we present values for the meson masses and the meson decay constants. We also calculate the decay rates of the processes $\eta \to \gamma + \gamma$ and $\eta' \to \gamma + \gamma$ for one particular model of confinement. As part of our analysis, we describe how the triangle (anomaly) diagram, governing the process $\eta' \to \gamma + \gamma$, may be calculated when using one version of our confining interaction. Our calculated rates for the processes $\eta \to \gamma + \gamma$ and $\eta' \to \gamma + \gamma$ are in good agreement with the experimental values.

Acknowledgements

To Professor Carl M. Shakin, my thesis advisor, I wish to express my deepest gratitude for his valuable guidance and constant encouragement throughout this thesis work. His help was important in bring this work to completion.

I would also like to express my sincere gratitude to Professor Louis S. Celenza of Brooklyn College of the CUNY for the help given to me during the course of this work.

I wish to acknowledge with gratitude to Department of Physics of Brooklyn College and the Research Foundation of the CUNY for the financial support during the course of this work, and the Brooklyn College Computer Center for allowing me to use their facilities.

Table of Contents

I. Introduction

In this work we study a generalized version of the Nambu-Jona-Lasinio (NJL) model that includes a description of confinement. The NJL model is quite interesting, even in the absence of a model of confinement, since it provides a specific model of the generation of mass via the breaking of the chiral symmetry exhibited by the Lagrangian by the ground state of the theory. This phenomenon is called "spontaneous symmetry breaking" and corresponds to the case where there is a continuous set of degenerate vacuum states.

In this Introduction, we will summarize some of the results reported upon in this thesis. In Section II we introduce a model for the self-energy of a quark and proceed to solve the Schwinger-Dyson and Bethe-Salpeter equations for our model. We show that our analysis is consistent with the Goldstone theorem. That is, the pion has zero mass, if the current quark masses are zero. We use a confining interaction with a (Dirac) matrix structure that leads to simple equations for the self-energy and for a vertex function that serves to sum a ladder of confining interactions. We consider spacelike values of q^2, and carry out our analysis in a Euclidean momentum space. For timelike q^2, we use calculational procedures that we have developed in other work in order to exhibit properties of the confining vertex. We find that the strength of the zero-range quark-quark interaction of the NJL model needs to be increased to compensate for the presence of the confining interaction, if we wish to obtain the same value of the momentum-dependent constituent quark mass (at $k^2 = 0$) as the constant value, m_q, obtained in the absence of the confining interaction. For the spacelike values of

q^2 considered here, we see that the effects due to the introduction of our model of confinement are small. (However, such effects are very important for timelike q^2. Their consideration is essential, if we wish to study mesons, such as the rho and omega, in our model.)

In Section III and IV we study the scalar-isoscalar section of the generalized NJL model. In Section III we use an SU(2)-flavor version of the model and in Section IV we study the SU(3)-flavor version. This work is directed toward understanding the properties of the sigma meson. A recent analysis by Törnqvist and Roos suggests that the sigma meson has a mass of 860 MeV with a width of 880 MeV[To96]. We investigate this matter and describe, in some detail, how the sigma coupling to states in the two-pion continuum may be calculated, when using a Lorentz-vector confining interaction. As part of our work we provide a general procedure for calculating various loop diagrams in Minkowski momentum space for quarks in the presence of the confining interaction. We study the properties of the sigma meson by considering t-channel scalar-isoscalar exchange between two quarks. The resulting quark-quark T matrix, $t_{qq}(q^2)$, has $\mathrm{Re}\, t_{qq}(q^2) = 0$ for $q^2 = (0.823\ \mathrm{GeV})^2$. Thus, we have $m_\sigma = 0.823\ \mathrm{GeV}$. However, the coupling of the sigma to the two-pion states is so large as to make $|t_{qq}(q^2)|$ a rather smooth function over a broad range of q^2. Therefore, we do not attempt to assign a width for the resonance.

In Section IV we study the nonstrange scalar-isoscalar states of the generalized Nambu−Jona-Lasinio model that includes both the 't Hooft interaction and a model of confinement. As in Section III, we also include coupling of the $q\bar{q}$ states to the two-pion

continuum in our analysis. (Our study is limited to energies $q^2 \leq 1.8$ GeV^2, since to go beyond $q^2 = 2.0$ GeV^2 we need to change our method of calculation.) After introducing octet-singlet mixing we find two states, σ_1 and σ_2, at energies of 1.00 GeV and 1.28 GeV, respectively. The first of these is predominantly a SU(3) - singlet, while the second state is rather strongly mixed. Of particular interest for nuclear physics is the behavior of the quark-quark T matrix for small spacelike values of q^2. Because of a strong q^2-dependence of the T matrix at the opening of the two-pion continuum at $q^2 = 4m_\pi^2$, the *effective* mass that parametrizes scalar-isoscalar exchange in the T matrix is about 520 MeV. Thus, in a model of the nucleon-nucleon interaction, whose ingredients are a T matrix for the interaction of off-mass-shell quarks and valence-quark nucleon form factors, we can provide a basis for the use of a low-mass *effective* σ meson in nuclear physics.

In Section V we study the pseudoscalar octet of Goldstone bosons as well as the η'. We are particularly interested in the properties of the η' and in the mixing of the η^0 (singlet) and η^8 (octet) modes. It is found that the value of the vacuum-polarization integral in each mesonic channel increases rapidly as one approaches the $q\bar{q}$ continuum in a model without confinement, since there is cusp behavior at the $q\bar{q}$ thresholds. That is not a problem in the description of the low-mass mesons (π, K, η), but makes the study of the η' problematic in a theory without confinement. With our model of Lorentz-vector confinement, we show in in Section II that the Goldstone theorem is satisfied. As usual, we found a relation between the Bethe-Salpeter equation and the Schwinger-Dyson equation for zero-energy modes. The inclusion of confinement,

however, leads to a momentum-dependent self-energy for the quark. The approximation we adopt for our calculations in Section III, IV and V, made in Minkowski momentum space, is to take the constituent masses of the up, down and strange quarks to be independent of momentum. (We hope to assess the validity of such an approximation in a future work.) In Sect V, we present values for the meson masses and the meson decay constants. We also calculate the decay rates of the processes $\eta \to \gamma + \gamma$ and $\eta' \to \gamma + \gamma$ for one particular model of confinement. As part of our analysis, we describe how the triangle (anomaly) diagram, governing the process $\eta' \to \gamma + \gamma$, may be calculated when using one version of our confining interaction. (That calculation cannot be made for the η', if one does not include a model of confinement.) Our calculated rates for the processes $\eta \to \gamma + \gamma$ and $\eta' \to \gamma + \gamma$ are in good agreement with the experimental values.

II. Chiral Symmetry Breaking in the Presence of a Confining Interaction

2.1. Introduction

In recent years, we have seen numerous applications of the Nambu–Jona-Lasinio (NJL) model in the study of chiral symmetry breaking and in the description of hadron properties [Kl92, Vo91]. Usually, confinement is neglected, so that the theory may be applied to study the pion and the "sigma meson". In previous work, it has been shown how a confining interaction (a linear potential) introduced in momentum-space calculations removes the unitarity cut associated with the quark and antiquark going on mass shell. The resulting formalism then only has cuts when hadrons go on mass shell [Ce95a, Ce95b]. In previous work it was assumed that the constituent quark mass had a constant value that was obtained from the gap equation, without confinement. In the present work, the confining interaction is included in the Schwinger-Dyson equation and, therefore, a self-energy for the quark that varies with k^2, the square of the quark momentum, is obtained.

It is usually thought that confinement is not particularly important for the study of the low-energy hadron spectrum. In this work we wish to put such suggestions on a more quantitative basis and to obtain guidance as to the implementation of a more comprehensive treatment of low-lying mesonic states, including the pseudoscalar octet and the η'. The organization of this section is as follows. In Section 2.2 we describe the confining interaction that we use in this work. In Section 2.3, we present equations for the quark self-energy, $\Sigma(k) = B(k^2)\not{k} + A(k^2)$. In Section 2.4, we introduce a vertex function that serves to sum a "ladder" of confining interactions and present results of our

calculations of that quantity. In Section 2.5, we discuss the vertex function associated with the entire interaction of the generalized NJL model. We show that the Goldstone theorem is satisfied, with the zero-mass pion as the Goldstone boson. The calculation of quark-antiquark loop integrals (polarization diagrams) is described in Section 2.6. Section 2.7 contains a summary and some conclusions, while Section 2.8 serves as an Appendix.

2.2. The NJL Model with a Confining Interaction

In this section we will use the SU(2)-flavor version of our model, where the Lagrangian is

$$\mathcal{L} = \bar{q}(x)\left(i\partial - m_q^0\right)q(x) + \frac{G_S}{2}\left[\left(\bar{q}(x)\,q(x)\right)^2 + \left(\bar{q}(x)\,i\gamma_5\,\vec{\tau}q(x)\right)^2\right] + \mathcal{L}_{conf} \quad . \tag{2.2.1}$$

Where m_q^0 is the current quark mass. We will use

$$\mathcal{L}_{conf} = \left[\bar{q}(x)\gamma^\mu q(x)\,V^C(x-y)\bar{q}(y)\gamma_\mu q(y) - \bar{q}(x)\gamma^\mu\gamma_5 q(x)\,V^C(x-y)\bar{q}(y)\gamma_\mu\gamma_5 q(y)\right] \quad . \tag{2.2.2}$$

(The advantages of using this form will be made clear as we proceed.) Thus, the confining interaction is

$$\bar{V}(x-y) = V^C(x-y)\left[\gamma^\mu(1)\gamma_\mu(2) - \gamma^\mu(1)\gamma_5(1)\gamma_\mu(2)\gamma_5(2)\right] \quad . \tag{2.2.3}$$

In an earlier work $V^C(r) = \kappa r\exp(-\mu r)$ was used with $\mu = 0.050$ GeV. The parameter μ is introduced to make the Fourier transform of $V^C(r)$ less singular and, thus, facilitate our numerical calculations. The Fourier transform of $V^C(r)$ is

$$V^C(\vec{k}-\vec{k}') = -4\pi\kappa\left\{\frac{2}{\left[(\vec{k}-\vec{k}')^2+\mu^2\right]^2} - \frac{8\mu^2}{\left[(\vec{k}-\vec{k}')^2+\mu^2\right]^3}\right\} \quad . \tag{2.2.4}$$

However, for calculations in a Euclidean momentum space, that we report upon in this work, it is necessary to treat all the components of the momentum transfer on the same footing. Therefore, we will use

$$V_E^C(k-k') = -4\pi\kappa\left\{\frac{2}{\left(k_E^2+\mu^2\right)^2} - \frac{8\mu^2}{\left(k_E^2+\mu^2\right)^3}\right\}, \tag{2.2.5}$$

where k_E^μ is the momentum transfer in the Euclidean momentum space.

It is useful to write

$$\bar{V}(x-y) = V^C(x-y)\sum_{i=1}^{2} O_i(1)\,O_i(2) \tag{2.2.6}$$

with $O_1 = \gamma^\mu$ and $O_2 = i\gamma^\mu\gamma_5$. [See Eq. (2.2.3).] (We will use a bar over a letter to denote a quantity that has Dirac matrix indices.)

For the interaction of Eq. (2.2.3), the Lagrangian has chiral symmetry, if $m_q^0 = 0$. Indeed, each of the terms in Eq. (2.2.3) respects chiral symmetry. Our motivation in combining the terms, as in Eq. (2.2.3), is to achieve a particularly simple form for the self-energy and vertex functions. For example, if we write the self-energy as $\Sigma(k^2) = B(k^2)\not{k} + A(k^2)$, we find that $B(k^2) = 0$. Also, if we consider a scalar or pseudoscalar vertex for the confining interaction, $\bar{F}_S(q^2, q\cdot k, k^2)$ or $\bar{F}_P(q^2, q\cdot k, k^2)$, we find that, when Eq. (2.2.3) is used, $\bar{F}_P(q^2, q\cdot k, k^2) = F_P(q^2, q\cdot k, k^2)\gamma_5\tau^i$ and $\bar{F}_S(q^2, q\cdot k, k^2) = F_S(q^2, q\cdot k, k^2)\cdot\mathbb{I}$. Here $\mathbb{I}$ denotes the unit matrix in the space of Dirac matrices. That is, the simple structure of the vertex operators of the NJL model is maintained in the presence of confinement, if $\bar{V}(x-y)$ of Eq. (2.2.3) is used. In the case we need to refer to that interaction, we may call it a $V-A$ form. That designation is in keeping with the current practice, where one speaks of "scalar confinement" or "vector confinement".

We now write the quark propagator as

$$iS(k) = \frac{i}{\not{k} - \Sigma(k) + i\epsilon} \quad , \tag{2.2.7}$$

with $\Sigma(k) = B(k^2)\not{k} + A(k^2)$. This propagator is represented by a double line in Fig. 2. In Fig. 2.1a we see the equation for the quark self-energy, $\Sigma(k)$. There, the wavy line is the confining interaction. The filled circle in Fig. 2.1a denotes the element iG_S, where G_S is defined in Eq. (2.2.1). In the absence of the first term of Fig. 2.1a, we would reproduce the gap equation of the standard NJL model. In that case, one has a constant value for the constituent mass, $\Sigma(k) = m_q$, with $m_q \sim 250 - 350$ MeV.

In Fig. 2.1b, we show the integral equation for the quark propagator, $iS(k)$, given in terms of a massless propagator (single line) and the self-energy, $\Sigma(k)$.

2.3. The Quark Self-Energy

We write the quark self-energy as $\Sigma(k) = B(k^2)\not{k} + A(k^2)$. From the equation depicted in Fig. 2.1b, we find that $B(k^2) = 0$ and that $A(k^2)$ satisfies the equation

$$A(k^2) = i\int \frac{d^4k'}{(2\pi)^4} \frac{\left[8V^C(k-k') + 4n_c n_f G_S\right]}{k'^2 - A^2(k'^2)} A(k'^2) \quad . \tag{2.3.1}$$

Note that, if $V^C = 0$, $A(k^2)$ is a constant. In that case, we have

$$m_q = 4n_c n_f G_S i\int \frac{d^4k'}{(2\pi)^4} \frac{m_q}{k'^2 - m_q^2} \quad . \tag{2.3.2}$$

Thus, since $m_q^0 = 0$ at this point, m_q may be factored out to yield the equation

$$1 = 4n_c n_f G_S i\int \frac{d^4k'}{(2\pi)^4} \frac{1}{k'^2 - m_q^2} \quad . \tag{2.3.3}$$

Solutions of Eq. (2.3.1) have been obtained by using a Euclidean momentum space. One may use either a covariant cutoff, where $k_E^2 < \Lambda_E^2$, or the Pauli-Villars regularization procedure, among other possibilities. We have done both kinds of calculations; however, the Pauli-Villars method is to be preferred, since it preserves the symmetries of the theory.

First, we note that, if $G_S = 7.91$ GeV^{-2} and $\kappa = 0$, and if we use a Euclidean momentum-space cutoff of $\Lambda_E = 1.0$ GeV, we find $m_q = 241$ MeV. Once we include a finite value for κ, we no longer obtain a constant mass. That is, $A(k^2)$ depends upon k^2 as shown in Fig. 2.2. For the result shown in Fig. 2.2, we put $\kappa = 0.140/8$ GeV$^2 = 0.0175$ GeV^2. The factor of (1/8) in our choice for κ serves to convert a value of κ appropriate to scalar confinement to a value appropriate to the

interaction given in Eqs. (2.2.3) and (2.2.4). A factor of 2 is obtained since we have two terms in Eq. (2.2.3) and a factor of 4 arises from the Lorentz character of the interaction.

We now choose G_S' such that $A(0) \simeq m_q$, where m_q was the value obtained for $\kappa = 0$. We find that $G_S' = 8.95$ GeV^{-2} yields $A(0) = 239$ MeV. Values for $A(k^2)$ for $\kappa = 0.0175$ GeV^2 and $G_S' = 8.95$ GeV^{-2} are given in Fig. 2.2. (We use the notation G_S' when $\kappa \neq 0$.) The k^2 dependence of $A(k^2)$ is not strong. Going from $k^2 = 0$ to $k^2 = -1.0$ GeV^2 only increases $A(k^2)$ by 22 percent. (We have $A(k^2) = 293$ MeV when $k^2 = -1$ GeV^2.)

2.4. The Vertex Function of the Confining Interaction

We now consider a vertex function that sums a "ladder" of confining interactions. The equation for the pseudoscalar vertex is then obtained from the evaluation of the diagrams of Fig. 2.3 [Ce95a, Ce95b]

$$\bar{F}^i_P(q,k) = \gamma_5\tau_i + \sum_{j=1}^{2} i\int \frac{d^4k'}{(2\pi)^4} V^C(k-k')O_j(1)S(k'+q/2)\bar{F}^i_P(q,k')S(k'-q/2)O_j(2) \quad . \tag{2.4.1}$$

We define $A_+(q,k') = A\left((k'+q/2)^2\right)$ and $A_-(q,k') = A\left((k'-q/2)^2\right)$ and make use of the relation

$$\begin{aligned}\gamma^\mu\Big[\big(k'+\not{q}/2+A_+(q,k')\big)\gamma_5\big(k'-\not{q}/2+A_-(q,k')\big)\Big]\gamma_\mu \\ -\gamma_5\gamma^\mu\Big[\big(k'+\not{q}/2+A_+(q,k')\big)\gamma_5\big(k'-\not{q}/2+A_-(q,k')\big)\Big]\gamma_\mu\gamma_5 \\ = 8\big[(k'+q/2)\cdot(k'-q/2)-A_+(q,k')A_-(q,k')\big]\gamma_5 \quad .\end{aligned} \tag{2.4.2}$$

We also define

$$N_P(q,k') = k'^2 - q^2/4 - A_+(q,k')A_-(q,k') \quad , \tag{2.4.3}$$

so that, if we put

$$\bar{F}^i_P(q,k) = \gamma_5\tau^i F_P(q,k) \quad , \tag{2.4.4}$$

we see that the function $F_P(q,k)$ satisfies the integral equation

$$F_P(q,k) = 1 + i\int \frac{d^4k'}{(2\pi)^4}\,\frac{8V^C(k-k')N_P(q,k')F_P(q,k')}{D\left((k'+q/2)^2\right)D\left((k'-q/2)^2\right)} \quad . \tag{2.4.5}$$

In Eq. (2.4.5), we have used the definition $D(p^2) = p^2 - A^2(p^2)$.

An entirely similar equation may be written for the scalar confining vertex, where we put $\bar{F}_S(q,k) = F_S(q,k)\mathbf{I}$. Thus,

$$F_S(q,k) = \mathbf{I} + i\int \frac{d^4k'}{(2\pi)^4} \frac{8V^C(k-k')N_S(q,k')F_S(q,k')}{D\left((k'+q/2)^2\right) D\left((k'-q/2)^2\right)} \quad , \tag{2.4.6}$$

with

$$N_S(q,k') = k'^2 - q^2/4 + A_+(q,k')A_-(q,k') \quad . \tag{2.4.7}$$

Note the difference sign for the last term of Eqs. (2.4.3) and (2.4.7).

In the past, for $q^2 > 0$, the equation for $F_S(q,k)$ was solved by computing the k'_0 integral in the complex k'_0 plane [Ce95a, Ce95b]. There are two poles in the lower-half plane arising from the quark propagators. For one pole, the quark is on its positive mass shell. For the other pole, the antiquark is on its negative mass shell. [We have also neglected any poles that would arise if we admit energy transfer in $V^C(k-k')$. We continue to make that approximation for our calculations for timelike $q^2(q^2 > 0)$.]

For the function $F_P(q^2, q\cdot k, k^2)$, let us consider the case where the quark is on its mass positive shell, so that $k^0 + q^0/2 = E_q(\vec{k}+\vec{q})$. The resulting function is a function of only two variables. In the frame where $\vec{q}=0$, we define

$$\Gamma_S^{+-}(q^0, |\vec{k}|) = F_S(q^2, q\cdot k, k^2)\,|_{k^0+q^0/2=E_q(\vec{k})} \quad . \tag{2.4.8}$$

Similarly, we consider the case where the antiquark is on its negative mass shell. In that case, we define

$$\Gamma_S^{-+}(q^0, |\vec{k}|) = F_S(q^2, q\cdot k, k^2)\,|_{k^0-q^0/2=E_q(\vec{k})} \quad . \tag{2.4.9}$$

These functions satisfy coupled equations of the form

$$\begin{bmatrix} \Gamma_s^{+-}(q^0, |\vec{k}|) \\ \Gamma_s^{-+}(q^0, |\vec{k}|) \end{bmatrix} = \begin{bmatrix} 1 \\ 1 \end{bmatrix} - 4\int \frac{d^3k'}{(2\pi)^3} V^C(k-k') \begin{bmatrix} \frac{1}{q^0 - 2E_q(\vec{k}')} - \frac{1}{q^0 + 2E_q(\vec{k}')} \\ \frac{1}{q^0 - 2E_q(\vec{k}')} - \frac{1}{q^0 + 2E_q(\vec{k}')} \end{bmatrix} \begin{bmatrix} \Gamma_s^{+-}(q^0, |\vec{k}'|) \\ \Gamma_s^{-+}(q^0, |\vec{k}'|) \end{bmatrix}$$

(2.4.10)

We see, however, from the last equation that

$$\Gamma_s^{+-}(q^0, |\vec{k}|) = \Gamma_s^{-+}(q^0, |\vec{k}|) \quad . \tag{2.4.11}$$

Discarding the superscripts, we have a single integral equation

$$\Gamma_s(q^0, |\vec{k}|) = 1 - 4\int \frac{d^3k'}{(2\pi)^3} \frac{4E_q(\vec{k}')}{(q^0)^2 - [2E_q(\vec{k}')]^2} V^C(k-k')\Gamma_s(q^0, |\vec{k}'|) \quad .$$

(2.4.12)

In Fig. 2.4 we present values of $\Gamma_s(q^0, |\vec{k}|)$ for several values of $q^0 \geq 0$. It may be seen from the figure that $\Gamma_s(q^0, |\vec{k}|)$ for large $|\vec{k}|$ is about 0.6 to 0.7. Those values are related to a cutoff placed on the three momenta in the integral equation, $\Lambda_3 = 0.702$ GeV($|\vec{k}'| \leq \Lambda_3$). However, the integral equation does not need to be regulated, since the integrals converge as $|\vec{k}'| \to \infty$. If one puts Λ_3 equal to several GeV, the various $\Gamma_s(q^0, |\vec{k}|)$ go rapidly to 1 with increasing $|\vec{k}|$ for all q^0 values considered here. We recall that it is the zeroes of the confining vertex functions for $k_{on}^2 = (q^0/2)^2 - m_q^2$ that remove the $q\bar{q}$ cut in various vacuum polarization diagrams. Such cuts would appear for $q^2 > 4m_q^2$ in the absence of a model for confinement [Ce95a, Ce95b]. The zeroes of $\Gamma_P(q^0, |\vec{k}|)$ are indicated in Fig. 2.4 by small dots. For those curves without such dots, q^0 is too small ($q^0 < 2m_q$) to lead to on-mass-shell quarks in the absence of confinement.

2.5. The Vertex Function for the Total Interaction and the Goldstone Boson of the Generalized NJL Model

In this Section we discuss a vertex function, $\bar{F}_T(q,k)$, that includes the effects of both the confining interaction and the (zero-range) NJL interaction. The integral equation for that quantity is depicted in Fig. 2.5. That integral equation reads, in the pion channel,

$$\bar{F}_T(q,k) = \gamma_5 + \sum_{j=1}^{2} i\int \frac{d^4k'}{(2\pi)^4} V^C(k-k')O_j(1)S(q/2+k')\gamma_5 S(-q/2+k')O_j(2)\bar{F}_T(q,k')$$

$$+ n_c n_f i G_S \int \frac{d^4k'}{(2\pi)^4} Tr\left[S(q/2+k')\gamma_5 S(-q/2+k')\gamma_5\right]\bar{F}_T(q,k') \quad . \tag{2.5.1}$$

In the last equation, we have already factored out the isospin matrix that appears in the driving term, $\gamma_5\tau^i$. We then define $\bar{F}_T(q,k) = \gamma_5 F_T(q,k)$ where $F_T(q,k)$ is a scalar function. We have

$$F_T(q,k) = 1 + i\int \frac{d^4k'}{(2\pi)^4} \frac{\left[8N_P(q,k')V^C(k-k') - n_c n_f G_S M(q,k')\right]F_T(q,k')}{D_+(q,k')D_-(q,k')} \quad , \tag{2.5.2}$$

where we have put $D_+(q,k') \equiv D\left((q/2+k')^2\right)$ and $D_-(q,k') \equiv D\left((q/2-k')^2\right)$. Note that $N_P(q,k)$ was given previously in Eq. (2.4.3) Here, we have also defined

$$M(q,k) = 4\left[\frac{q^2}{4} - k^2 + A_+(q,k)A_-(q,k)\right] \quad . \tag{2.5.3}$$

We now consider the limit $q \to 0$. We have $D_+(0,k) = D_-(0,k) = D(k^2)$, $N_P(0,k) = D(k^2)$, and $M(0,k) = -4D(k^2)$. Therefore,

$$F_T(0,k) = 1 + i\int \frac{d^4k'}{(2\pi)^4}\frac{\left[8V^C(k-k') + 4n_c n_f G_S\right]}{D(k'^2)}F_T(0,k') \quad . \tag{2.5.4}$$

If there is a boundstate at zero energy, the homogeneous version of Eq. (2.5.4) will have a solution. Thus, we consider

$$F_T(0,k) = 1 + i\int \frac{d^4k'}{(2\pi)^4}\frac{\left[8V^C(k-k') + 4n_c n_f G_S\right]}{D(k'^2)}F_T(0,k') \quad . \tag{2.5.5}$$

However, the gap equation, was

$$A(k^2) = i\int \frac{d^4k'}{(2\pi)^4}\frac{\left[8V^C(k-k') + 4n_c n_f G_S\right]}{D(k'^2)}A(k'^2) \quad . \tag{2.5.6}$$

Thus, we see that $F_T(0,k)$ is proportional to $A(k^2)$ and we have a zero-mass state. The pion is the Goldstone boson, as expected.

It is sometimes useful to define the wave function

$$\psi_T(k^2) = n\frac{1}{k^2 - A^2(k^2)}A(k^2) \tag{2.5.7}$$

where n is a normalization factor.

We have

$$\left[k^2 - A^2(k^2)\right]\psi_T(k^2) = i\int \frac{d^4k'}{(2\pi)^4}\left[8V^C(k-k') + 4n_c n_f G_S\right]\psi_T(k'^2) \tag{2.5.8}$$

2.6. Calculation of Polarization Diagrams

In the original NJL model, the quark loop integrals for the scalar-isoscalar and pseudoscalar-isovector channels are [Vo91]

$$-iJ_S(q^2) = (-1)i^2 n_f n_c \int \frac{d^4k}{(2\pi)^4} Tr\left[S(k+q/2)S(k-q/2)\right] \quad , \qquad (2.6.1)$$

and

$$-iJ_P(q^2) = (-1)i^2 n_f n_c \int \frac{d^4k}{(2\pi)^4} Tr\left[\gamma_5 S(k+q/2)\gamma_5 S(k-q/2)\right] \quad . \qquad (2.6.2)$$

Here $S(k) = [\not{k} - m_q + i\epsilon]^{-1}$, etc. For the generalized model, we have

$$\frac{\hat{J}_S(q^2)}{i} = (-1)i^2 n_f n_c \int \frac{d^4k}{(2\pi)^4} F_S(q,k) Tr\left[S(k+q/2)S(k-q/2)\right] \qquad (2.6.3)$$

where, now, $S(k) = [\not{k} - A(k^2) + i\epsilon]^{-1}$, etc. Also,

$$\frac{\hat{J}_P(q^2)}{i} = (-1)i^2 n_c n_f \int \frac{d^4k}{(2\pi)^4} F_P(q,k) Tr\left[\gamma_5 S(k+q/2)\gamma_5 S(k-q/2)\right] \qquad (2.6.4)$$

These simple forms arise in the *V-A* model of confinement considered here. For $q^2 \leq 0$, the evaluation may be made by going over to a Euclidean momentum space.

2.7. Discussion

Work that has some relation to ours was carried out by Gross and Milana [Gr91,Gr92]. These authors obtained coupled equations for meson wave functions, in the presence of a confining interaction, by performing integrals in the complex k_0' plane and picking up the poles of the quark propagators, as was done in our work when q^2 was timelike. However, the formalism used in [Gr91] does not yield a zero-mass pion unless the confining potential satisfies a constraint. (The constraint used is a relativistic generalization of the relation $V^C(r) = 0$, for $r = 0$.)

The appropriate Lorentz transformation properties of the confinement interaction is a matter of some uncertainty. Scalar confinement has been popular, since it provides a good representation of spin-orbit effects in heavy quark systems. However, a number of authors have suggested that better results may be obtained with vector confinement. In particular, Münz [Mu96] has noted that the Salpeter equation used for the study of meson structure is unstable for scalar confinement [Pa95], while vector confinement works well. Studies of Swanson and Isgur [Sw97] and of Adam Szczepaniak [Sz97] also suggest the importance of vector confinement. Further, Resag and Münz have used vector confinement and have only kept the term involving γ_0 [Re95]. In addition, Münz has used equal amounts of scalar and vector confinement, again keeping only the γ_0 term of the vector-confinement interaction [Mu96].

In the work reported here, we have shown that the *V-A* form of the confining interaction yields simple equations for the quark self-energy and for the pseudoscalar vertex function. Thus, we could carry out our analysis without solving coupled,

nonlinear equations for $A(k^2)$ and $B(k^2)$. We could also deal with a single scalar function $F_P(q, k)$, rather than with four such functions that characterize the pseudoscalar vertex in the general case. On the other hand, we do not recommend the *V-A* form for the study of meson spectra. We believe that vector confinement provides a more satisfactory model and also allows us to write a Lagrangian with chiral symmetry. We will consider vector confinement in the following. The equations that will be studied are more complicated than those considered in the present section. We anticipate that, for vector confinement, we will again need to increase the value of G_S to compensate for the confining interaction and that modifications of the size found in this work will be found for the quark self-energy and polarization diagrams. Results of some calculations for the case of vector confinement are reported in the Appendix.

In this Section we have shown that one may write a Lagrangian that has chiral symmetry when we include a model of confinement. However, our wor has a number of limitatios and further work is required. For example, our analysis has made in a Euclidean momentum space. We would like to have results for timelike values of the momentum as well. One might attempt to continue the results for spacelike momenta into the timelike region, but we do not believe that the accuracy of such a procedure is known and we do not adopt that approach. On the other hand, we have made a large number of calculations in Minkowsi space for timelike values of the momenta [Ce95a, Ce95b]. We have used an approach similar to that of Gross and Milana [Gr91,Gr92] in that we have only considered the singularities of the quark propagators, when completing integrals in the complex k'_0 plane. That is a correct procedure, if the confining potential has no

singularities in the plane. Therefore, we have neglected energy transfer when using the confining interaction in Minkowsi-space calculations. Thus, we see that our Euclidean-space calculations reported here are not entirely consistent with our Minkowski-space calculations reported upon elsewhere [Ce95a, Ce95b]. We hope to study this problem in the future. While the Lorentz structure of the confining interaction may be considered an open question, we have shown that confining interactions that preserve chiral symmetry may be used for various studies. Such potentials are to be preferred, since they are consistent with the properties that a good effective interaction for low-energy QCD should have. Their use is essential, if we are to study the effects of confinement in the case of the pseudoscalar octet (Goldstone Bosons).

2.8. Appendix: Self-energy for Lorentz-Vector Confinement

In this Appendix, we wish to study the self-energy, $\Sigma(k) = B(k^2)\not{k} + A(k^2)$, and the vertex function, $\bar{F}_T(q, k)$, for pure vector confinement. In this case we find the coupled nonlinear equations

$$A(k^2) = i\int \frac{d^4k'}{(2\pi)^4} \frac{\left[4V^C(k-k') + 4n_c n_f G_S\right]}{k'^2\left[1 - B(k')\right]^2 - A^2(k'^2)} A(k'^2) \tag{2.8.1}$$

and

$$k^2B(k^2) = -i\int \frac{d^4k'}{(2\pi)^4} \frac{2(k\cdot k')\left[1 - B(k'^2)\right] V^C(k-k')}{k'^2\left[1 - B(k')\right]^2 - A^2(k'^2)} \quad . \tag{2.8.2}$$

The pseudoscalar vertex function is more complicated than in the *V-A* model, since there are now four scalar functions of three variables to be calculated. We may write, in the general case,

$$\bar{F}_T(q, k) = \gamma_5\left[a_1(k, q) + \not{k}a_2(k, q) + \not{q}a_3(k, q) + \not{q}\not{k}a_4(k, q)\right] \quad , \tag{2.8.3}$$

with $a_1(k, q) = a_1(k^2, k\cdot q, q^2)$, etc. However, $\bar{F}_T(q, k)$ is simpler, if we consider the case $q = 0$:

$$\bar{F}_T(0, k) = \gamma_5\left[a_1(k^2) + \not{k}a_2(k^2)\right] \quad , \tag{2.8.4}$$

where $a_1(k^2) = a_1(0, k)$, etc.

The vertex function for the total interaction satisfies the equation

$$\bar{F}_T(0,k) = \gamma_5 + i\int \frac{d^4k'}{(2\pi)^4} V^C(k-k')\gamma^\mu S(k')\bar{F}_T(0,k')S(k')\gamma_\mu + n_c n_f i G_S \int \frac{d^4k'}{(2\pi)^4} Tr\left[S(k')\bar{F}_T(0,k')S(k')\gamma_5\right] . \tag{2.8.5}$$

We now make use of Eq. (2.8.4) and find that

$$a_1(k^2) = 1 + i\int \frac{d^4k'}{(2\pi)^4} \frac{\left[4V^C(k-k') + 4n_c n_f G_S\right]a_1(k'^2)}{k'^2\left[1-B(k'^2)\right]^2 - A^2(k'^2)} \tag{2.8.6}$$

and

$$k^2 a_2(k^2) = -i\int \frac{d^4k'}{(2\pi)^4} \frac{2(k\cdot k')(k-k')a_2(k'^2)}{k'^2\left[1-B(k'^2)\right]^2 - A(k'^2)} . \tag{2.8.7}$$

Now, let us ask if Eq. (2.8.5) has a homogeneous solution. We write Eq. (2.8.6), with the "driving term" removed, as

$$a_1(k^2) = i\int \frac{d^4k'}{(2\pi)^4} \frac{\left[4V^C(k-k') + 4n_c n_f G_S\right]a_1(k'^2)}{k'^2\left[1-B(k'^2)\right]^2 - A^2(k'^2)} . \tag{2.8.8}$$

Now consider Eq. (2.8.7) and (2.8.8). We see that comparison to Eq. (2.8.1) shows that $a_1(k^2) \sim A(k^2)$. Further, we may put $a_2(k^2) = 0$, since Eq. (2.8.7) is homogeneous. Thus, in the chiral limit, the vertex for $q = 0$ is $\bar{F}_T^i(0,k) = \gamma_5 \tau^i F_T(k^2)$, where $F_T(k^2)$ is proportional to $A(k^2)$. Since there is no driving term, $F_T(k^2)$ is related to the pion wave function

$$\psi_T(k^2) = \eta \frac{1}{k^2\left[1-B(k^2)\right]^2 - A(k^2)} A(k^2) , \tag{2.8.9}$$

where η is a normalization constant. [Recall Eq. (2.4.7).] We remark that

$$\left\{k^2\left[1-B(k^2)\right]^2-A^2(k^2)\right\}\psi_T(k^2) = i\int\frac{d^4k'}{(2\pi)^4}\left[4V^C(k-k')+4n_c n_f G_S\right]\psi_T(k'^2) \tag{2.8.10}$$

in the case of vector confinement. Results for $A(k^2)$ and $B(k^2)$ calculated with vector confinement are shown in Fig. 2.6.

III. Calculation of the Properties of the Sigma Meson in a with Lorentz-Vector Confinement

3.1. Introduction

It is well known that the SU(2)-flavor version of the Nambu−Jona-Lasinio (NJL) model predicts a scalar-isoscalar meson with mass $m_\sigma^2 = (2m_q)^2 + m_\pi^2$, where m_q is the constituent quark mass [Vo91, Kl92, Ha94]. (We have usually used $m_q = 260$ MeV in our work, so that $m_\sigma = 540$ MeV.) Since there is no low-mass sigma meson in the data tables, it is of interest to consider what happens to the low-mass state predicted by the NJL model as we introduce confinement and coupling to the two-pion continuum. In a recent work Törnqvist and Roos [To96], who use a unitary quark model, suggest Breit-Wigner parameters for the sigma of m_σ = 860 MeV and Γ_σ = 880 MeV. As we will see, our results are generally consistent with the parameters found in Ref. [To96].

In this work we will use the NJL model, generalized to include a model of confinement. We will use Lorentz-vector confinement, rather than the Lorentz-scalar confinement usually used, since the use of vector confinement allows us to maintain the chiral symmetry of the Lagrangian. (That feature is particularly important, if we wish to study the pseudoscalar octet of Goldstone bosons, for example.) We have performed two types of calculations. In Section II we carried out our calculations in a Euclidean momentum space and were able to do a fully covariant calculation in which we allowed energy transfer via the confining interaction. That work was limited to spacelike values of the momentum, $q^2 < 0$. On the other hand, when we have considered timelike excitations ($q^2 > 0$), we have neglected energy transfer by the confining interaction.

Our method of calculation for timelike q^2 is similar to that used by Gross and Milana [Gr91, Gr92] who assume that the only important singularities to be taken into account when completing integrals over loop four-momenta, k^μ, are those associated with the quark propagators. (A review of our formalism for the case of Lorentz-scalar confinement may be found in Ref. [Ce95a].) In the work reported in this Section, we will be concerned with the timelike region and will neglect energy transfer by the confining interaction. That avoids the necessity of considering singularities associated with that interaction when performing loop integrals.

We will begin our discussion by describing the covariant formalism, which may be used in Euclidean-space calculations. We will then go on to neglect energy transfer. In that approximation, we will provide results for vertex functions of the confining interaction using the formalism presented in Ref. [Ce95a].

The Lagrangian of our model was given in Eq. (2.2.1). Here, we choose

$$\mathcal{L}_{\text{conf}} = \frac{1}{4}\bar{q}(x)\gamma^\mu q(x)\, V^C(x-y)\bar{q}(y)\gamma_\mu q(y) \quad , \tag{3.1.1}$$

where $V^C(r) = \kappa r \exp[-\mu r]$. Since our calculations are made in momentum space, we include a small parameter, $\mu = 0.030$ GeV, to soften the singularities of the Fourier transform of $V^C(r)$. We include the factor 1/4 in Eq. (3.1.1) so that the value of κ we quote can be directly compared to the value of κ used in the case of Lorentz-scalar confinement, $\kappa \simeq 0.20$ GeV^2.

The organization of our work is as follows. In Section 3.2 we define a vertex function that serves to sum a "ladder" of confining interactions. This vertex, when inserted into the quark-antiquark (polarization) loop diagrams, removes the unphysical $q\bar{q}$

unitary cut, so that the loop integral is real. In Section 3.3 we describe the calculation of polarization diagrams and provide a value for the mass of the sigma in the presence of confinement. In Section 3.4 we study the coupling of the sigma to states of two pions and in Section 3.5 we show how we may calculate the contribution to the sigma self-energy due to the coupling to the two-pion continuum. (Again, confinement plays an important role in removing unphysical $q\bar{q}$ cuts in the sigma self-energy.) In Section 3.5 we calculate the imaginary part of the self-energy due to coupling to the two-pion states and go on to calculate the real part using a once-subtracted dispersion relation. (Note that, while the polarization diagrams are of order n_c, the self-energy diagrams considered in Section 3.5 are of order 1 in the standard counting of color factors.) In Section 3.6, we study the quark-quark T matrix for scalar-isoscalar t-channel exchange and show that the coupling to the two-pion continuum is so large as to leave only slight evidence of the presence of the sigma. Section 3.7 contains further discussion and some conclusions.

3.2. Vertex Functions for Lorentz-Vector Confinement

We have considered (Lorentz) scalar confinement in our earlier work [Ce95a,Ce93a,Ce93c]. However, we have shown that, if one uses Lorentz-vector confinement, one may maintain the chiral symmetry of the Lagrangian, if the current quark mass, m_q^0, is zero. Therefore, we will continue our use of Lorentz-vector confinement in this work. In this section we will consider a scalar-isoscalar vertex function. (We use the notation $S(p) = [\not{p} - m_q + i\epsilon]^{-1}$ for the quark propagator, with m_q being the constituent quark mass.)

With reference to Fig. 3.1a, we define a vertex that satisfies the (inhomogeneous) equation

$$\bar{\Gamma}_S(q,k) = 1 + i\int \frac{d^4k'}{(2\pi)^4}\gamma^\mu S(q/2+k')\bar{\Gamma}_S(q,k')S(-q/2+k')\gamma_\mu V^C(k-k')/4 \quad , \tag{3.2.1}$$

where, in the covariant formalism,

$$V^C(k-k') = -8\pi\kappa\left\{\frac{1}{\left[(k-k')^2-\mu^2\right]^2} + \frac{4\mu^2}{\left[(k-k')^2-\mu^2\right]^3}\right\} \quad . \tag{3.2.2}$$

In the figure, the filled triangular area is the vertex $\bar{\Gamma}_S(q,k)$. In general, one may write

$$\bar{\Gamma}_S(q,k) = a_1(q^2,q\cdot k,k^2) + \hat{\not{k}}a_2(q^2,q\cdot k,k^2) + \not{q}a_3(q^2,q\cdot k,k^2) + 2i\sigma_{\mu\nu}q^\mu k^\nu a_4(q,q\cdot k,k^2) \quad . \tag{3.2.3}$$

Here $\hat{k}^\mu = k^\mu - (k\cdot q)q^\mu/q^2$. [In some cases, we will insert a bar over quantities that have Dirac matrix indices; for example, we wrote $\bar{\Gamma}_S(q,k)$ in Eqs. (3.2.1) and (3.2.3).] We will not need to consider the general case given in Eq. (3.2.3), since the functions we

calculate will not depend upon the variable $q\cdot k$. (That feature has its origin in our neglect of energy-transfer dependence in the confining interaction.)

When we perform loop integrals in Minkowski space we will first integrate over the timelike component, k'_0. In the complex k'_0 plane we encounter poles due to the quarks, or antiquarks, going on mass shell. (The contour is usually chosen so that we have poles due to the quarks going on their positive mass shell, while the antiquarks go on their negative mass shell, when we evaluate polarization diagrams.) In Figs. 3.1c and 3.1d we indicate the nature of the calculation in which the quark is on mass shell. In this case, the relevant vertex will be denoted as $\Gamma_S^{+-}(q,k)$ and, for $\vec{q}=0$, we will write $\Gamma_S^{+-}(q^0,|\vec{k}|)$. Other vertex functions that appear in our analysis will be denoted as Γ_S^{-+}, Γ_S^{++} and Γ_S^{--}. We may relate these functions to $\bar{\Gamma}_S(q,k)$ by the following procedure. We first define the standard Dirac projection operators

$$\Lambda^{(+)}(\vec{k}) = \frac{\not{k}+m_q}{2m_q} \quad , \tag{3.2.4}$$

with $k^\mu=[E(\vec{k}),\vec{k}]$, and

$$\Lambda^{(-)}(-\vec{k}) = \frac{\not{\tilde{k}}+m_q}{2m_q} \quad , \tag{3.2.5}$$

with $\tilde{k}^\mu=[-E(\vec{k}),\vec{k}]$. Thus, we now define

$$\Lambda^{(+)}(\vec{k})\bar{\Gamma}_S\Lambda^{(+)}(\vec{k}) = \Gamma_S^{++}(q,k)\Lambda^{(+)}(\vec{k})\Lambda^{(+)}(\vec{k}) \quad , \tag{3.2.6}$$

$$= \Gamma_S^{++}(q,k)\Lambda^{(+)}(\vec{k}) \quad , \tag{3.2.7}$$

$$\Lambda^{(-)}(-\vec{k})\bar{\Gamma}_S\Lambda^{(-)}(-\vec{k}) = \Gamma_S^{--}(q,k)\Lambda^{(-)}(-\vec{k}) \quad , \tag{3.2.8}$$

$$\Lambda^{(+)}(\vec{k})\bar{\Gamma}_S\Lambda^{(-)}(-\vec{k}) = \Gamma_S^{+-}(q,k)\Lambda^{(+)}(\vec{k})\Lambda^{(-)}(-\vec{k}) \quad , \tag{3.2.9}$$

and

$$\Lambda^{(-)}(-\vec{k})\bar{\Gamma}_S\Lambda^{(+)}(\vec{k}) = \Gamma_S^{-+}(q,k)\Lambda^{(-)}(-\vec{k})\Lambda^{(+)}(\vec{k}) \quad . \tag{3.2.10}$$

Usually, we will work in the frame where $\vec{q}=0$, so that the various functions we have defined will depend upon q^0 and $|\vec{k}|$. In Sections 3.3 and 3.4, we will see how these functions arise naturally in our Minkowski-space calculations of loop integrals. As we will see, the set of Γ's will be linearly related to the functions a_1, a_2, a_3 and a_4. We may write equations for either set of functions by using standard projection operator and trace techniques, starting with Eq. (3.2.1). We first present the results for the functions defined in Eq. (3.2.3). For vector confinement, we find that $a_4 = 0$ and that

$$a_1(q,-k) = a_1(q,k) \tag{3.2.11}$$

$$= a_1(q^2,(k\cdot q)^2,k^2) \quad , \tag{3.2.12}$$

$$a_2(q,-k) = a_2(q,k) \tag{3.2.13}$$

$$= a_2(q^2,(k\cdot q)^2,k^2) \quad , \tag{3.2.14}$$

and

$$a_3(q,-k) = -a_3(q,k) \tag{3.2.15}$$

$$= (k\cdot q)\tilde{a}_3\left(q^2,(k\cdot q)^2,k^2\right) \quad . \tag{3.2.16}$$

Now, if $V^C(k)$ is independent of k^0, we also have $a_3 = 0$.

We now neglect energy transfer and find the following equations are obtained for the two remaining functions. Integrating over k_0', and writing $E(k) = [k^2 + m_q^2]^{1/2}$, we have

$$a_1(q,k) = 1 + 4\pi \int \frac{k'^2 dk'}{(2\pi)^3} \frac{(-8\overline{k'}^2)\, V_0^C(k,k')[a_1(q,k') + m_q a_2(q,k')]}{E(k')\left[q_0^2 - (2E(k'))^2\right]} \quad . \tag{3.2.17}$$

and

$$a_2(q,k) = -4\pi \int \frac{k'^2 dk'}{(2\pi)^3} V_1^C(k,k') \frac{\frac{k'}{k}(4m_q)\left[a_1(q,k') + m_q a_2(q,k')\right]}{E(k')\left[q_0^2 - (2E(k'))^2\right]} \quad . \tag{3.2.18}$$

In these equations $k' = |\overline{k'}|$ and $k = |\overline{k}|$, and

$$V_l^C(k,k') = \frac{1}{2}\int_{-1}^{1} dx P_l(x)\, V_C(\overline{k}^2 + \overline{k'}^2 - 2kk'x)/4 \quad . \tag{3.2.19}$$

The functions $a_1(q,k)$ and $a_2(q,k)$ are related to the functions $\Gamma_S^{+-}(q,k)$, $\Gamma_S^{-+}(q,k)$, etc. We find that $\Gamma_S^{+-}(q,k) = \Gamma_S^{-+}(q,k)$ and $\Gamma_S^{++}(q,k) = \Gamma_S^{--}(q,k)$, with

$$\Gamma_S^{+-}(q,k) = a_1(q,k) + m_q a_2(q,k) \tag{3.2.20}$$

and

$$\Gamma_S^{++}(q,k) = a_1(q,k) - \frac{\overline{k}^2}{m_q} a_2(q,k) \quad . \tag{3.2.21}$$

These last two relations may be obtained by writing $\overline{\Gamma}_S(q,k) = a_1(q,k) + \hat{k} a_2(q,k)$ and then using the definitions of $\Gamma_S^{+-}(q,k)$, $\Gamma_S^{-+}(q,k)$, etc., given in Eqs. (3.2.6)-(3.2.10). Using the equations for $a_1(q,k)$ and $a_2(q,k)$ given above, and Eqs. (3.2.20)-(3.2.21),

we find that, when $\overline{q}=0$,

$$\Gamma^{+-}(q^0,k) = 1+4\pi\int\frac{k'^2dk'}{(2\pi)^3}\frac{-8\overline{k}'^2}{E(k')}\frac{\left[V_0^C(k,k')+\frac{m_q^2}{2kk'}V_1^C(k,k')\right]}{(q^0)^2-\left(2E(k')\right)^2}\Gamma^{+-}(q^0,k') \quad , \tag{3.2.22}$$

and

$$\Gamma^{++}(q^0,k) = 1+4\pi\int\frac{k'^2dk'}{(2\pi)^3}\frac{-8\overline{k}'^2}{E(k')}\frac{\left[V_0^C(k,k')-\frac{k}{2k'}V_1^C(k,k')\right]}{(q^0)^2-\left(2E(k')\right)^2}\Gamma^{+-}(q^0,k') \quad . \tag{3.2.23}$$

(We recall that $\Gamma_S^{+-}(q,k)=\Gamma_S^{-+}(q,k)$ and $\Gamma_S^{++}(q,k)=\Gamma_S^{--}(q,k)$, if the k^0 dependence of $V^C(k)$ is ignored. Also note that $\Gamma_S^{++}(q,k)$ may be obtained from $\Gamma_S^{+-}(q,k)$ by using Eq. (3.2.23).)

Values calculated for $\Gamma_S^{+-}(q,|\overline{k}|)$ are given in Fig. 3.2 for several values of q^0. Note that when <u>both</u> the quark and antiquark go on their (positive) mass shell, we have $q^0=2[\overline{k}_{on}^2+m_q^2]^{1/2}$ and $\Gamma_S^{+-}(q^0,|\overline{k}_{on}|)=0$. This last relation may be used to show how our model of confinement removes unitary cuts that would otherwise arise when the quark and antiquark both go on their positive mass shell.

In Fig. 3.3 we show values obtained for $\Gamma_S^{++}(q^0,|\overline{k}|)$. The functions shown in Figs. 3.2 and 3 will be needed for the calculations described in the following sections.

3.3. Polarization Diagrams and the Mass of the Sigma Meson

It is useful to determine the parameters for the sigma meson resonance by studying a quark-quark T matrix evaluated for t-channel scalar-isoscalar exchange processes. (The T matrix we study may be defined even if the quarks are confined.) If we drop reference to Dirac matrices and isospin factors, the polarization diagrams may be summed to yield

$$t_{qq}(q^2) = -\frac{G_S}{1 - G_S J_S(q^2)} \quad , \tag{3.3.1}$$

where

$$-iJ_S(q^2) = (-1)n_c n_f \mathrm{Tr} \int \frac{d^4k}{(2\pi)^4} iS(\frac{q}{2}+k)\, iS(-\frac{q}{2}+k) \quad , \tag{3.3.2}$$

with $S(p) = [\not{p} - m_q + i\epsilon]^{-1}$. [See Fig. 4.] When we include confinement, we define

$$t_{qq}(q^2) = -\frac{G_S}{1 - G_S \hat{J}_S(q^2)} \quad , \tag{3.3.3}$$

where $\hat{J}_S(q^2)$ is defined in terms of the confining vertex, $\bar{\Gamma}_S(q,k)$,

$$-i\hat{J}_S(q^2) = n_c n_f \mathrm{Tr} \int \frac{d^4k}{(2\pi)^4} S\left[\frac{q}{2}+k\right] \bar{\Gamma}_S(q,k) S\left[-\frac{q}{2}+k\right] \quad . \tag{3.3.4}$$

[See Fig. 5.] As a next step, we use the relation

$$S(k) = \frac{m_q}{E(\vec{k})}\left[\frac{\Lambda^{(+)}(\vec{k})}{k^0 - E(\vec{k}) + i\epsilon} - \frac{\Lambda^{(-)}(-\vec{k})}{k^0 + E(\vec{k}) - i\epsilon}\right] \tag{3.3.5}$$

in Eq. (3.3.4). [See Eqs. (3.2.4) and (3.2.5).] Therefore, if we work in the frame where $\vec{q}=0$,

$$-i\hat{J}_S(q^2) = -n_c n_f \mathrm{Tr}\int \frac{d^4k}{(2\pi)^4}\frac{m_q}{E(\vec{k})}\left[\frac{\Lambda^{(+)}(\vec{k})\,\bar{\Gamma}_S(q,k)\,\Lambda^{(-)}(-\vec{k})}{\left[\frac{q^0}{2}+k^0-E(\vec{k})+i\epsilon\right]\left[-\frac{q^0}{2}+k^0+E(\vec{k})-i\epsilon\right]}\right.$$

$$\left.+\frac{\Lambda^{(-)}(-\vec{k})\,\bar{\Gamma}_S(q,k)\,\Lambda^{(+)}(\vec{k})}{\left[\frac{q^0}{2}+k^0+E(\vec{k})-i\epsilon\right]\left[-\frac{q^0}{2}+k^0-E(k)+i\epsilon\right]}\right], \tag{3.3.6}$$

where we have kept only the non-zero terms. The first term in Eq. (3.6) introduces $\Gamma_S^{++}(q,k)$ and the second introduces $\Gamma_S^{--}(q,k)$. If we evaluate the integral in the lower part of the complex k^0 plane, the first term in Eq. (3.3.6) leads to the quark being on its positive mass shell, $q^0/2 + k^0 = E(\vec{k})$, while the second term leads to the antiquark being on its negative mass shell, $-q^0/2 + k^0 = E(\vec{k})$. The singularity that would otherwise appear in the result when both the quark and the antiquark go on their positive mass shell is eliminated by the fact that $\Gamma_S^{+-}(q,k) = 0$ at that point (where $q^0 = 2E(\vec{k})$ and $k^0 = 0$).

In Fig. 3.6 we show the results of calculations of $J_S(q^2)$ and $\hat{J}_S(q^2)$ for $q^2 \geq 0$. We note that $J_S(q^2)$ is complex for $q^2 > 4m_q^2$, while $\hat{J}_S(q^2)$ is a real function.

We may determine the mass of the sigma meson by solving the equation

$$G_S^{-1} - J_S(m_\sigma^2) = 0 \ , \tag{3.3.7}$$

or the equation

$$G_S^{-1} - \hat{J}_S(m_\sigma^2) = 0 \ . \tag{3.3.8}$$

For Eq. (3.3.7), we use $G_S = 7.91\ \mathrm{GeV}^{-2}$, $m_q = 260$ MeV and a cutoff on the magnitude

of $\vec{k}$, $|\vec{k}| \leq \Lambda_3$. The cutoff is chosen so that our Minkowski-space calculation yields the same value

for $J_S(0)$ as a Euclidean space calculation of that quantity made with a cutoff $\Lambda_E = 1.0$ GeV. In that manner, we choose $\Lambda_3 = 0.689$ GeV. (Note that $J_S(0) = 0.088$ GeV^2.) The upper horizontal line in Fig. 3.6 corresponding to $G_S^{-1} = (7.91 \text{ GeV}^{-2})^{-1}$ yields a graphical solution of Eq. (3.3.7) with $m_\sigma = 540$ MeV. That value is just above the beginning of the two-quark continuum at $q^2 = (2m_q)^2$.

Now, if we solve Eq. (3.3.8) rather than Eq. (3.3.7), we see that m_σ takes on a larger value. For example, a graphical solution of Eq. (3.3.8) appears in Fig. 3.6, where we now use the lower horizontal line corresponding to $G_S^{-1} = (8.516 \text{ GeV}^{-2})^{-1}$. (The larger value of G_S used at this point has its origin in our model of confinement. If we write the quark self-energy as $\Sigma(p) = A(p^2) + \not{p}B(p^2)$ and calculate $A(p^2)$ and $B(p^2)$ for the NJL interaction plus the confining interaction, we find that $A(p^2)$ varies with p^2, unlike the case of the NJL interaction alone, where $A(p^2)$ is a constant. We also found that $B(p^2)$ is small. We then adjust G_S so that $A(0)$ has the same value, m_q, that it had when there was no confining interaction. Since the confining interaction behaves as a repulsive interaction, we have to increase G_S to keep $A(0) = m_q$, with the result that $G_S = 7.91$ GeV^{-2} is replaced by $G_S = 8.516$ GeV^{-2}.) Returning to Fig. 3.6, we see that we have $m_\sigma \simeq 800$ MeV, which is an increase of about 260 MeV above the value of $m_\sigma = 540$ MeV found in the absence of confinement.

The quark-quark T matrix can be extended to include diagrams involving $\hat{K}_S(q^2)$, some of which are shown in Fig. 3.4. In that case, we have

$$t_{qq}(q^2) = -\frac{G_S}{1 - G_S\left[\hat{J}_S(q^2) + \hat{K}_S(q^2)\right]} \quad , \tag{3.3.9}$$

$$= -\frac{G_S}{1 - G_S\left[\hat{J}_S(q^2) + \mathrm{Re}\,\hat{K}_S(q^2)\right] - iG_S\,\mathrm{Im}\,\hat{K}_S(q^2)} \quad . \tag{3.3.10}$$

In the next section we will describe the methods that are used to calculate $\hat{K}_S(q^2)$. The presence of $\mathrm{Re}\,\hat{K}_S(q^2)$ moves the sigma mass upward by a small amount. However, introduction of $\mathrm{Im}\,\hat{K}_S(q^2)$ has a rather dramatic effect on the properties of the sigma resonance.

3.4. Coupling to the Two-Pion Continuum: Calculation of the Amplitude $q + \bar{q} \to \pi + \pi$ in the Scalar-Isoscalar Channel

We will first concentrate on the calculation of $\mathrm{Im}\,\hat{K}_S(q^2)$. Once that calculation is completed, we will use a once-subtracted dispersion relation to calculate $\mathrm{Re}\,\hat{K}_S(q^2)$. Basic to the calculation of $\mathrm{Im}\,\hat{K}_S(q^2)$ is the evaluation of the diagram shown in Fig. 3.7 for the case of on-mass-shell pions. There, we have $(q/2 + \kappa)^2 = (q/2 - \kappa)^2 = m_\pi^2$, so that $q \cdot \kappa = 0$.

In the general case, we can define an amplitude

$$\mathscr{F}_S(q, \kappa) = \mathrm{Tr} i \int \frac{d^4k}{(2\pi)^4} \left[S(k - \kappa)\gamma_5 S(q/2 + k) \bar{\Gamma}_S(q, k)\, S(-q/2 + k)\gamma_5 \right] . \quad (3.4.1)$$

[See Fig. 3.7.] Now, if the pions are on-mass-shell, we may define

$$F_1(q^2) = \mathscr{F}_S(q^2, q \cdot \kappa = 0, \kappa^2 = m_\pi^2 - q^2/4) \quad . \quad (3.4.2)$$

[See Fig. 3.8.] We will also find it useful to introduce

$$F_2(\kappa^2) = \mathscr{F}_S(0, 0, \kappa^2) \quad . \quad (3.4.3)$$

[See Fig. 3.8.] We will need values of $F_2(\kappa^2)$ when we calculate $\mathrm{Re}\,\hat{K}_S(0)$. (The latter quantity will be needed when we form the once-subtracted dispersion relation.)

We now describe the procedure used to calculate $\mathscr{F}_S(q, \kappa)$ in Minkowski space. First, we use Eq. (3.3.5) to write each of the three propagators in Eq. (3.4.1) in terms of $S^{(+)}$ and $S^{(-)}$. That yields eight terms. We now note that, in each of these terms, $\bar{\Gamma}_S(q, k)$ is replaced by $\Gamma_S^{+-}(q, k)$, $\Gamma_S^{-+}(q, k)$, $\Gamma_S^{++}(q, k)$ or $\Gamma_S^{--}(q, k)$, depending upon the location of the $S^{(+)}$ and $S^{(-)}$ factors. (For example,

$S^{(+)}(q/2+k)\bar{\Gamma}_S(q,k)S^{(-)}(-q/2+k)$ gives rise to a factor of $\Gamma_S^{+-}(q,k)$, etc.) As a next step, we complete the integral over k^0 in the complex k^0 plane. The terms with three $S^{(+)}$ factors, or three $S^{(-)}$ factors, all have their poles in the same half-plane and, therefore, do not contribute to the integral. For the remaining six terms, we choose to complete the k^0 integral either in the upper-half or the lower-half k^0 plane, depending upon where there is only a single pole. The resulting six terms are depicted in Fig. 3.7. There, a cross on a line denotes a quark on its positive mass shell, while an open circle on a line denotes an antiquark on its negative mass shell. For each diagram in Fig. 3.7a, one has a factor of $\Gamma_S^{+-}(q,k)$ and for the diagrams of Fig. 3.7b, one has a factor of $\Gamma_S^{-+}(q,k)$; however, these two vertex functions are equal, if the interaction does not depend upon energy transfer. Similarly, diagrams of Fig. 3.7c give rise to a factor of $\Gamma_S^{++}(q,k)$, which is equal to the function $\Gamma_S^{--}(q,k)$ arising from the other diagram in Fig. 3.7c. The result of these calculations is (for $\vec{q}=0$)

$$\mathcal{F}_S(q,\kappa) = 4\int \frac{d^3k}{(2\pi)^3}\left\{\frac{(-\vec{k}\cdot\vec{\kappa})}{2m_q^2}\left[\frac{\Gamma_S^{+-}(q^0,k)}{(q^0-2E(\vec{k}))\left[\frac{q^0}{2}-(E(\vec{k})+E(\vec{k}-\vec{\kappa}))\right]}\right.\right.$$

$$\left.+\frac{\Gamma^{-+}(q,k)}{(q^0+2E(\vec{k}))\left[\frac{q^0}{2}+(E(\vec{k})+E(\vec{k}-\vec{\kappa}))\right]}\right]$$

$$\left.-\frac{1}{4m_q^2}\frac{[E^2(\vec{k})+E(\vec{k})E(\vec{k}-\vec{\kappa})-\vec{k}\cdot\vec{\kappa}][\Gamma^{++}(q^0,k)+\Gamma^{--}(q^0,k)]}{\left[\left[\frac{q^0}{2}\right]^2-(E(\vec{k})+E(\vec{k}-\vec{\kappa}))^2\right]}\right\}, \tag{3.4.4}$$

where $k = |\vec{k}|$. From this function, we may obtain $F_1(q^2)$ and $F_2(\kappa^2)$ as special cases.

In Fig. 3.9, we show the values we have found for $F_2(\kappa^2)$. Values for $\kappa^2 \leq 0$ are obtained by evaluating the relevant integral in Euclidean space, where we neglect the effects of confinement. Values for $\kappa^2 \geq 0$ are obtained using the methods described in this section. If we choose a cutoff for the loop integrals evaluated for $\kappa^2 \geq 0$ to be $|\vec{k}| \leq \Lambda_3$, with $\Lambda_3 = 0.816$ GeV, we find that the value at $\kappa^2 = 0$ for both calculations is the same. [See Fig. 3.9.] (Recall that for loop diagrams with two quark propagators, the appropriate value of Λ_3 was found to be 0.689 GeV.) We note that confinement effects are small for $q^2 \leq 0$, so that for $F_2(\kappa^2) = \mathcal{F}_S(0,0,\kappa^2)$, these effects are relatively unimportant.

3.5. The Sigma Self-Energy Including Coupling to the Two-Pion Continuum

Once we have calculated $F_1(q^2)$, we may calculate $\mathrm{Im}\,\hat{K}_S(q^2) = (1/2)\,\mathrm{Disc}\,\hat{K}_S(q^2)$, where the discontinuity is taken across the two-pion cut that starts at $q^2 = 4m_\pi^2$. We have

$$\begin{aligned}\mathrm{Disc}\,\hat{K}_S(q^2) &= g_{\pi qq}^4 I_f n_c^2 s(-1)\int \frac{d^4\kappa}{(2\pi)^4}\left[F_1(q^2)\right]^2 \\ &\times\left(-2\pi i\delta^{(+)}\left[(q/2+\kappa)^2 - m_\pi^2\right]\right) \\ &\times\left(-2\pi i\delta^{(+)}\left[(q/2-\kappa)^2 - m_\pi^2\right]\right)\ ,\end{aligned} \tag{3.5.1}$$

where $I_f = 12$ is an isospin factor, $n_c^2 = 9$ is a color factor and $s = 2$ is a symmetry factor. Also, the superscript (+) on the delta functions denotes the fact that we choose only the part of the delta function in which the pions are on their positive mass shell.

Now, when $\bar{q} = 0$,

$$-(2\pi)^2\int\frac{d^4\kappa}{(2\pi)^4}\delta^{(+)}\left[\left(\frac{q}{2}+\kappa\right)^2 - m_\pi^2\right]\delta^{(+)}\left[\left(\frac{q}{2}-\kappa\right)^2 - m_\pi^2\right] = -\frac{1}{8\pi\omega(\bar{\kappa})}\bar{\kappa} \tag{3.5.2}$$

where $\bar{\kappa} = [(q^0/2)^2 - m_\pi^2]^{1/2}$, $\omega(\bar{\kappa}) = [\bar{\kappa}^2 + m_\pi^2]^{1/2}$ and $q^0 = 2\omega(\bar{\kappa})$. Thus,

$$\mathrm{Im}\,\hat{K}_S(q^2) = \frac{1}{2}g_{\pi qq}^4 I_f n_c^2 s\left[F_1(q^2)\right]^2\left[\frac{\bar{\kappa}}{8\pi\omega(\bar{\kappa})}\right]\theta(q^2 - 4m_\pi^2)\ . \tag{3.5.3}$$

Values of $\mathrm{Im}\,\hat{K}_S(q^2)$, calculated using Eq. (3.5.3), are given in Fig. 3.10 for the case $g_{\pi qq} = 2.68$. That value for $g_{\pi qq}$ was first obtained in Ref. [Na92]. (A simple estimate of $g_{\pi qq}$ may be found by working in the chiral limit, $m_q^0 = 0$, and evaluating

$$\frac{g_{\sigma qq}^2(0)}{m_\sigma^2} = \frac{G_S}{1 - G_S \hat{J}_S(0)} \quad . \tag{3.5.4}$$

Then, one may put $g_{\pi qq} = g_{\sigma qq}$. A more accurate value is found by using the relation

$$g_{\pi qq}^{-2}(m_\pi^2) = \frac{\partial J_P(q^2)}{\partial q^2}\Big|_{q^2 = m_\pi^2} \quad , \tag{3.5.5}$$

where $J_P(q^2)$ is the value of the (polarization) loop integral in the pseudoscalar channel.

Once we have calculated $\mathrm{Im}\,\hat{K}_S(q^2)$, we can obtain $\mathrm{Re}\,\hat{K}_S(q^2)$ by means of a once-subtracted dispersion relation

$$\mathrm{Re}\,\hat{K}_S(q^2) = \hat{K}_S(0) - \frac{\mathrm{P}}{\pi} q^2 \int_{4m_\pi^2} ds \, \frac{\mathrm{Im}\hat{K}_S(s)}{s(q^2 - s)} \quad . \tag{3.5.6}$$

As a next step, we need to calculate $\hat{K}_S(0)$, which may be obtained in terms of $F_2(\kappa^2)$. We have

$$\hat{K}_S(0) = g_{\pi qq}^4 I_f n_c^2 s i \int \frac{d^4\kappa}{(2\pi)^4} \left[\frac{i}{\kappa^2 - m_\pi^2} \right]^2 \left[F_2(\kappa^2) \right]^2 \quad . \tag{3.5.7}$$

This integral may be completed by going over to a Euclidean momentum space. Using the values of $F_2(\kappa^2)$ given in the last section, and again using $g_{\pi qq} = 2.68$, we find $\hat{K}_S(0) = 0.0108\ \mathrm{GeV}^2$. Using that value in Eq. (3.5.3), we find the values of $\mathrm{Re}\,\hat{K}_S(q^2)$ shown in Fig. 3.11. (The sharp peak in that function is due to the rapid opening of the two-pion channel at $q^2 = 4m_\pi^2$.)

Note that, if we write

$$\mathrm{Im}\,\hat{K}_S(q^2) = \left[1 - \frac{4m_\pi^2}{q^2}\right]^{1/2} K_0\,\theta(q^2 - 4m_\pi^2) \quad , \tag{3.5.8}$$

with K_0 a constant, we have an accurate approximation for $\mathrm{Im}\,\hat{K}_S(q^2)$. We can then complete the integrals in Eq. (3.5.6) with the result, for $q^2 > 4m_\pi^2$, where

$$\mathrm{Re}\,\hat{K}_S(q^2) = \hat{K}_S(0) + \frac{2K_0}{\pi}\left[1 + \frac{x}{2}\ln\left[\frac{1-x}{1+x}\right]\right] \quad , \tag{3.5.9}$$

$$x \equiv \left[1 - \frac{4m_\pi^2}{q^2}\right]^{1/2} \quad . \tag{3.5.10}$$

For $0 < q^2 < 4m_\pi^2$, we have

$$\mathrm{Re}\,\hat{K}_S(q^2) = \hat{K}_S(0) + \frac{2K_0}{\pi}\left[1 - \left|\,1 - \frac{4m_\pi^2}{q^2}\,\right|^{1/2} \tan^{-1}\left[\frac{q^2}{|\,q^2 - 4m_\pi^2\,|}\right]^{1/2}\right] \quad . \tag{3.5.11}$$

We now have enough informaton to calculate $\hat{J}_S(q^2) + \mathrm{Re}\,\hat{K}_S(q^2)$. That quantity is shown in Fig. 3.12.

3.6. Calculation of the Quark-Quark Scattering Amplitude for t-Channel Scalar-Isoscalar Exchange

Since we now have values of $\hat{J}_S(q^2) + \mathrm{Re}\,\hat{K}_S(q^2)$ and $\mathrm{Im}\,\hat{K}_S(q^2)$, we are able to obtain $t_{qq}(q^2)$ that was defined in Eqs. (3.3.9)-(3.3.10). In Fig. 3.13 we show $\mathrm{Re}\,t_{qq}(q^2)$ as a solid line and $\mathrm{Im}\,t_{qq}(q^2)$ as a dotted line. Note that $\mathrm{Re}\,t_{qq}(q^2)$ has a zero at $q^2 = m_\sigma^2$, corresponding to the equation

$$G_S^{-1} - \left[J_S(m_\sigma^2) + \mathrm{Re}\,\hat{K}_S(m_\sigma^2)\right] = 0 \quad . \tag{3.6.1}$$

The very large negative value for $q^2 \simeq 4m_\pi^2$ seen for $\mathrm{Re}\,t_{qq}(q^2)$ has its origin in the opening of the two-pion channel at that energy.

In Fig. 3.14 we show values of $|\,t_{qq}(q^2)\,|^2$. Again, the large peak in that quantity reflects the opening of the two-pion channel at $q^2 = 4m_\pi^2$. It may be seen that there is little evidence for the presence of a resonance centered around $q^2 = m_\sigma^2$ due to the strong coupling to the two-pion continuum. To investigate this point further, we show $|\,t_{qq}(q^2)\,|^2$ in Fig. 3.15 using an expanded scale. One may note a small enhancement centered around $q^2 \sim 0.67$ GeV^2 that could be interpreted as a residual effect due to the presence of the sigma resonance.

3.7. Discussion

In a previous work we have studied the quark-quark T matrix, $t_{qq}(q^2)$, for spacelike values of q^2. In the present work we have extended our considerations to study $t_{qq}(q^2)$ in the timelike region. For $q^2 \leq 0$, and for $-q^2$ not too large, the approximation

$$t_{qq}(q^2) = \frac{g^2_{\sigma qq}}{q^2 - m^2_\sigma} \tag{3.7.1}$$

was found to be quite accurate, if $m_\sigma = 540$ MeV and $g_{\sigma qq} = 3.05$. In the present work, we may find $g^2_{\sigma qq}$ by writing

$$\frac{G_S}{1 - G_S\left[\hat{J}_S(0) + \hat{K}_S(0)\right]} = \frac{g^2_{\sigma qq}}{m^2_\sigma} \quad , \tag{3.7.2}$$

where $m_\sigma = 0.540$ GeV. For the parameters developed here, $\hat{J}_S(0) = 0.0708$ GeV^2 $\hat{K}_S(0) = 0.0108$ GeV^2, and $G_S = 8.516$ GeV^{-2}, we find $g_{\sigma qq} = 2.86$, if $m_\sigma = 0.540$ GeV. Thus, $t_{qq}(0) = -g^2_{\sigma qq}/m^2_\sigma = -28.0$ GeV^{-2}. [See Fig. 3.13.]

Equation (3.7.1) is useful in the spacelike domain if $-q^2 < 0.25$ GeV^2. For an accurate representation beyond that region, one may write

$$t_{qq}(q^2) = \frac{g^2_{\sigma qq}(q^2)}{q^2 - m^2_\sigma} \quad . \tag{3.7.3}$$

(Equation (3.7.3) may be used to define $g_{\sigma qq}(q^2)$.) Note that, although Eq. (3.7.1) represents the T matrix for a limited region of spacelike values of q^2, there is no low-mass scalar-isoscalar state in the timelike region. However, for calculation of the NN force, or for the study of nuclear matter, the momenta of the exchanged mesons are

spacelike. Therefore, we may conclude that, if one restricts oneself to the description of mesons with spacelike momenta, the introduction of a sigma "meson" with $m_\sigma = 540$ MeV is quite a good approximation. We have also seen that the use of a low-mass sigma for spacelike q^2 is not in contradiction to the fact that such a meson has not been seen. Also, in the present study, we have found little direct evidence for a more massive resonance in the timelike region because of the very strong coupling to the two-pion continuum of the scalar-isoscalar state. On the other hand, the zero of the real part of the T matrix, found using Eq. (3.6.1), does define a mass that the sigma would have, if $\mathrm{Im}\,\hat{K}_S(q^2)$ were neglected. We have also seen that there is a large peak in $|\,t_{qq}(q^2)\,|$ at $q^2 \sim 4m_\pi^2$. We do not know whether such an effect could be observed in some experiment. However, we again note that the T matrix for spacelike q^2 is not influenced by the peak at $q^2 \sim 4m_\pi^2$. For nuclear physics problems that are of interest to us, the mesons exchanged between nucleons (or between quarks) are spacelike, with Eq. (3.7.1) providing an accurate representation of the dynamics.

IV. Singlet-Octet Mixing of Scalar Mesons

4.1. Introduction

In the last section we studied the properties of the σ meson in a generalized Nambu−Jona-Lasinio (NJL) model with SU(2) flavor symmetry. In this work we wish to extend our considerations to a NJL model with SU(3) flavor symmetry and with the 't Hooft interaction added. Important theoretical developments and various applications of that model may be found in Refs. [Be88, Ha87,Kl90,Vo90,Ta97,Re96], while useful reviews appear in Refs. [Vo91,Kl92,Ha94]. Our motivation in studying the SU(3)-flavor version of the NJL model has its origin in some of our earlier work using the SU(2) version of that model [Sh97]. There we found that the quark-quark T matrix that describes scalar-isoscalar exchange could be well approximated by the exchange of an effective sigma meson of mass of about 500 MeV, if q^2 was small and spacelike. That result allowed us to understand some aspects of the one-boson-exchange model of the nucleon-nucleon interaction [Ma89] in the case of scalar-isoscalar exchange. (Since we had used constituent quark masses of about 260 MeV in our earlier work, our result might not be all that surprising.) It is of interest to see if our result for the mass of the effective σ is maintained if we use larger constituent quark masses and the SU(3)-flavor version of the NJL model. Thus, we are here more interested in the behavior of the quark-quark T matrix for small q^2 than in the spectroscopy in the region of 1 GeV, where the physical σ meson is to be found.

In a previous work dealing with the octet of pseudoscalar mesons and the η' we studied $\eta^0 - \eta^8$ mixing which gives rise to the physical states η and η'. When we

consider scalar mesons, the analogous problem is the mixing of σ^0 (singlet) with σ^8 (octet) states to yield the physical states which we denote as $\sigma_1, \sigma_2, \ldots$. Here, σ_1 has the lowest energy and is predominantly the $\sigma^0(1P)$. It is found that the next state, σ_2, is rather strongly mixed. Note that in the case of $\eta^0 - \eta^8$ mixing, it is the η' that is predominantly the singlet state. These features are characteristic of the 't Hooft interaction [Dm96].

The use of the SU(3)-flavor NJL model and the 't Hooft interaction to study the scalar octet and the scalar singlet has been described in Ref. [Dm96], where an extensive discussion of the experimental data for scalar meson spectroscopy is presented. In Ref. [Dm96], the states considered have energies equal to or greater than 1 GeV, so that one may question the use of the NJL model (without confinement) to describe the scalar mesons. This problem is avoided in Ref. [Dm96], since the energies of the scalar states are calculated using a bosonization procedure. That procedure is essentially a low-energy (or low-momentum) expansion. Therefore, in such an expansion one stays below the unitarity cuts whose thresholds are given in terms of the constituent quark masses. These thresholds are at $q^2 = (2m_u)^2$, $q^2 = (m_u + m_s)^2$, and $q^2 = (2m_s)^2$ in a model without confinement. One advantage of the methods we use in our work is that we can obtain both the energy and the width of the various mesonic states, since we are able to implement our program at fairly large values of q^2 (with $q^2 > 0$).

A useful approach to the problem of meson mixing is to study a quark-quark T matrix. When calculating the T matrix, one sums various t-channel exchange diagrams. If the T matrix is real, a single mixing angle appears in the formalism when we use a

orthogonal transformation to bring the T matrix to diagonal form. (A more elaborate parametrization is needed when T is complex.) The relevant equations describing singlet-octet mixing appear in the literature [Be88,Hu87,Vo90,Ta97,Re96]. In this work we exhibit these equations modified to include a model of confinement and coupling to the two-pion contiuum.

The organization of our work is as follows. In Section 4.2 we describe some characteristics of our generalized NJL model and describe how we implement our model of confinement. In Section 4.3 we discuss the calculation of vacuum polarization diagrams that involve a quark and an antiquark. In Section 4.4 we describe the formalism used in the calculation of $\sigma^0 - \sigma^8$ mixing. In Section 4.5 we describe the important role played by the coupling of $q\bar{q}$ states to the two-pion continuum. Numerical results are presented in Sections 4.6. In Section 4.7 we describe the dynamical origin of a low-mass (effective) σ meson for nuclear physics studies. The exchange of this effective meson is shown to provide a good representation of the quark-quark T matrix, if the exchanged momentum is spacelike $(q^2 \leq 0)$. Finally, Section 4.8 contains some further discussion and some conclusions.

4.2. Model of Confinement

In this section we introduce various vacuum polarization integrals that are an essential feature of the NJL model [Vo91,Kl92,Ha94]. We will then show how the introduction of a model of confinement removes unphysical $q\bar{q}$ cuts from the various loop integrals studied. In Section 4.5 we will also discuss the coupling of the $q\bar{q}$ states

to the two-pion continuum. (It is this feature that gives rise to the large widths obtained for the scalar states in some cases.)

In the last section we have studied the SU(2)-flavor version of the NJL model. In this section we consider the SU(3)-flavor version of the model, supplemented by the 't Hooft interaction. The Lagrangian we consider is

$$\mathcal{L} = \bar{q}(i\partial - m^0)q + G_s\sum_{i=0}^{8}\left[\left[\bar{q}\frac{\lambda^i}{2}q\right]^2 + \left[\bar{q}i\gamma_5\frac{\lambda^i}{2}q\right]^2\right] \qquad (4.2.1)$$

$$+ \frac{G_D}{2}\left\{\det[\bar{q}(1+\gamma_5)q] + \det[\bar{q}(1-\gamma_5)q]\right\} + \mathcal{L}_{\text{conf}} \ ,$$

where the $\lambda^i (i = 1, \ldots 8)$ are the Gell-Mann matrices in flavor space and $\lambda^0 = (2/3)^{1/2}\mathbf{I}$, with $\mathbf{I}$ being the unit matrix. In Eq. (4.2.1), m^0 denotes a quark mass matrix with diagonal elements, m_u^0, m_d^0, m_s^0. Here, we take $m_u^0 = m_d^0 = 5.5$ MeV and $m_s = 132$ MeV, which are the values used in Ref. [Vo91]. Further,

$$\mathcal{L}_{\text{conf}}^{(x)} = \int d^4y\,\bar{q}(x)\gamma^\mu q(x)\,V^C(x-y)\bar{q}(y)\gamma_\mu q(y) \ . \qquad (4.2.2)$$

This represents a Lorentz-vector confinement model [Ce97a]. For calculations made in Minkowski momentum space, we neglect any dependence of V^C on energy transfer. That is, $V^C(x-y)$ contains a delta function that serves to equate the times associated with points x and y in Eq. (4.2.2). We use $V^C(r) = \kappa r\exp(-\mu r)$ where κ is the "string tension" and μ is a small parameter used to soften the singularities of the Fourier transform of $V^C(r)$. The Fourier transform of $V^C(r)$ was given previously as
We have used $\mu = 0.020$ GeV, and for the Lorentz-vector confinement model of Eq. (3.2.2), we use $\kappa = 0.20/4$ GeV^2. We write κ in that manner, since κ for Lorentz-vector

$$V^C(\vec{k}-\vec{k}') = -8\pi\kappa\left[\frac{1}{[(\vec{k}-\vec{k}')^2+\mu^2]^2} - \frac{4\mu^2}{[(\vec{k}-\vec{k}')^2+\mu^2]^3}\right] . \quad (4.2.3)$$

confinement is about one-fourth of the equivalent parameter for scalar confinement. We make reference to the scalar confinement parameter, since it is a more commonly specified quantity.

Another confinement model is the V-A model that we have used in some of our earlier in Section II. In that model

$$\mathcal{L}_{\text{conf}}(x) = \int d^4y\left[\bar{q}(x)\gamma^\mu q(x)\,V^C(x-y)\,\bar{q}(y)\gamma_\mu q(y) - \bar{q}(x)\gamma^\mu\gamma_5 q(x)\,V^C(x-y)\bar{q}(y)\gamma_\mu\gamma_5 q(y)\right] . \quad (4.2.4)$$

For the V-A model, we put $\kappa = 0.20/8$ GeV^2, again making reference to the scalar confinement parameter, $\kappa = 0.20$ GeV^2.

Since we do not study strange mesons in this work, we may limit ourselves to the case where the flavor of the quark and antiquark at the vertex is the same. The V-A model leads to a particularly simple result, $\bar{\Gamma}_S(q,k) = \mathbb{I}\Gamma_S(q,k)$, where $\mathbb{I}$ denotes the unit matrix in flavor space and in the space of Dirac matrices, and where $\Gamma_S(q,k)$ is a scalar function [Ce97b]. This scalar function has a very important property. It is equal to zero when the quark and the antiquark both go on their positive mass shells. It is that feature that eliminates unphysical $q\bar{q}$ cuts from the various functions that arise upon performing loop integrals.

The situation in the case of Lorentz-vector confinement is more complicated since $\bar{\Gamma}_S(q,k)$ then contains several terms having different Dirac matrix structure. In that case it is useful to introduce the projection operators

$$\Lambda^{(+)}(\vec{k}) = \frac{\not{k} + m}{2m} \quad , \tag{4.2.5}$$

with $k^{\mu} = [E(\vec{k}), \vec{k}]$ and

$$\Lambda^{(-)}(-\vec{k}) = \frac{\not{\tilde{k}} + m}{2m} \quad , \tag{4.2.6}$$

with $\tilde{k}^{\mu} = [-E(\vec{k}), \vec{k}]$. Here $E(\vec{k}) = [\vec{k}^2 + m^2]^{1/2}$. In this case, we may define functions, $\Gamma^{-+}(q,k)$, $\Gamma^{+-}(q,k)$, etc.:

$$\Lambda^{(+)}(\vec{k})\bar{\Gamma}_S(q,k)\Lambda^{(-)}(-\vec{k}) = \Gamma^{+-}(q,k)\Lambda^{(+)}(\vec{k})\Lambda^{(-)}(-\vec{k}) \quad , \tag{4.2.7}$$

$$\Lambda^{(-)}(-\vec{k})\bar{\Gamma}_S(q,k)\Lambda^{(+)}(-\vec{k}) = \Gamma^{-+}(q,k)\Lambda^{(-)}(-\vec{k})\Lambda^{(+)}(\vec{k}) \quad , \tag{4.2.8}$$

$$\Lambda^{(+)}(\vec{k})\bar{\Gamma}_S(q,k)\Lambda^{(+)}(\vec{k}) = \Gamma^{++}(q,k)\Lambda^{(+)}(\vec{k}) \quad , \tag{4.2.9}$$

and

$$\Lambda^{(-)}(-\vec{k})\bar{\Gamma}_S(q,k)\Lambda^{(-)}(-\vec{k}) = \Gamma^{--}(q,k)\Lambda^{(-)}(-\vec{k}) \quad . \tag{4.2.10}$$

In the next section we discuss the use of these functions in the calculation of $q\bar{q}$ vacuum-polarization diagrams that are needed in our work.

4.3. Vacuum-Polarization Integrals

The basic integral for a quark and antiquark of a single flavor is obtained from the evaluation of the

$$-iJ(q^2) = (-1)n_c \mathrm{Tr} \int \frac{d^4k}{(2\pi)^4} iS(q/2+k) iS(-q/2+k) \quad , \tag{4.3.1}$$

where $S(p) = [\not{p} - m + i\epsilon]^{-1}$ is the quark propagator and m is the constituent quark mass. The introduction of confinement proceeds via the definition

$$-i\hat{J}(q^2) = n_c \mathrm{Tr} \int \frac{d^4k}{(2\pi)^4} S(q/2+k) \bar{\Gamma}_S(q,k) S(-q/s+k) \quad , \tag{4.3.2}$$

where $\bar{\Gamma}_S(q,k)$ is represented by the filled triangular area in Fig. 3.4. In the calculation of $\hat{J}(q^2)$ it is useful to introduce the representation

$$S(k) = \frac{m}{E(\vec{k})} \left[\frac{\Lambda^{(+)}(\vec{k})}{k^0 - E(\vec{k}) + i\epsilon} - \frac{\Lambda^{(-)}(-\vec{k})}{k^0 + E(\vec{k}) - i\epsilon} \right] \quad , \tag{4.3.3}$$

and work in the frame where $\vec{q} = 0$. Thus,

$$-i\hat{J}(q^2) = -n_c \mathrm{Tr} \int \frac{d^4k}{(2\pi)^4} \frac{m}{E(\vec{k})} \left[\frac{\Lambda^{(+)}(\vec{k}) \bar{\Gamma}_S(q,k) \Lambda^{(-)}(-\vec{k})}{[q^0/2 + k^0 - E(\vec{k}) + i\epsilon][-q^0/2 + k^0 + E(\vec{k}) - i\epsilon]} \right.$$

$$\left. + \frac{\Lambda^{(-)}(-\vec{k}) \bar{\Gamma}_S(q,k) \Lambda^{(+)}(\vec{k})}{[q^0/2 + k^0 + E(\vec{k}) - i\epsilon][-q^0/2 + k^0 - E(\vec{k}) + i\epsilon]} \right] \quad , \tag{4.3.4}$$

where m denotes the constituent quark mass. We proceed by evaluating the integral in the lower half of the complex k^0 plane. There are two contributions in which either the quark goes on its positive mass shell or the antiquark goes on its negative mass shell [Gr91,Gr92]. Thus, when $\Gamma^{+-}(q,k)$ appears in the final result, it has the quark on its positive mass shell and we write $\Gamma^{+-}(q^0, |\vec{k}|)$ for this function in the frame where

$\vec{q}=0$. On the other hand, $\Gamma^{-+}(q^0, |\vec{k}|)$ has the antiquark on its negative mass shell in the final result. When we neglected energy transfer in the confining interaction, we found that $\Gamma^{+-}(q^0, |\vec{k}|) = \Gamma^{-+}(q^0, |\vec{k}|)$ and $\Gamma^{++}(q^0, |\vec{k}|) = \Gamma^{--}(q^0, |\vec{k}|)$ for the case of vector confinement [Ce97a]. In Figs. 3.2 and 3.3 we show values obtained for $\Gamma^{+-}(q^0, |\vec{k}|)$ and $\Gamma^{++}(q^0, |\vec{k}|)$ in Section III, where we used a smaller constituent quark mass for the up and down quarks than that used here. (Here we use $m_u = m_d = 364$ MeV and $m_s = 522$ MeV.)

In the evaluation of the various functions $\hat{J}(q^2)$, we require a cutoff for the integral over $\vec{k}$. We choose $|\vec{k}| \leq \Lambda_3$, where Λ_3 is chosen such that the values for the condensates are the same as those presented in Ref. [Vo91]. There, a Euclidean momentum space cutoff of $\Lambda_E = 0.90$ GeV was used. We found that we should put $\Lambda_3 = 0.622$ GeV on the basis of this procedure.

It is important to understand that there are solutions of equation for $\bar{\Gamma}_S(q,k)$ when we drop the driving term. The solutions of the resulting (homogeneous) equation are just the vertex functions of the bound states in the confining potential. Since such states are present, $\bar{\Gamma}_S(q,k)$ will have poles at $q^2 = M_i^2$ where the M_i are the mass parameters for the bound states in the confining field. Therefore, $\hat{J}(q^2)$ will also have poles at $q^2 = M_i^2$.

4.4. Coupled Channel Dynamics for $\sigma^0 - \sigma^8$ Mixing

Here we study the quark-quark T matrix that describes scalar-isoscalar exchange. We generalize the equations presented in Refs. [Be88,Ha87,Kl90,Vo90,Ta97,Re96] to

include confinement and coupling to the two-pion continuum. It is useful to define effective coupling constants

$$G_{00}^{S} = \frac{1}{2}(G_S - G_D c_{00}) \ , \tag{4.4.1}$$

$$G_{88}^{S} = \frac{1}{2}(G_S - G_D c_{88}) \ , \tag{4.4.2}$$

$$G_{08}^{S} = -\frac{1}{2} G_D c_{08} \ , \tag{4.4.3}$$

where

$$c_{00} = -\frac{2}{3}(2 < \bar{u}u > + < \bar{s}s >) \ , \tag{4.4.4}$$

$$c_{88} = \frac{1}{3}(4 < \bar{u}u > - < \bar{s}s >) \ , \tag{4.4.5}$$

and

$$c_{08} = \frac{\sqrt{2}}{3}(< \bar{u}u > - < \bar{s}s >) \ . \tag{4.4.6}$$

[See Fig. 4.1.] In this work we do not introduce any new parameters. The parameter values are taken from [Ce97a] and, except for G_S, they are the same as those given in Ref. [Vo91]. We have $G_S = 21.53\ \text{GeV}^{-2}$, $G_D = -239.1\ \text{GeV}^{-5}$, $< \bar{u}u > = < \bar{d}d > = -(0.248\ \text{GeV})^3 = -0.01525\ \text{GeV}^3$ and $< \bar{s}s > = -(0.258\ \text{GeV})^3 = -0.01717\ \text{GeV}^3$. Recall that we also use $m_u^0 = m_d^0 = 5.5$ MeV, $m_s^0 = 132$ MeV, $m_u = m_d = 364$ MeV and $m_s = 522$ MeV.

It is useful to introduce a set of functions defined in terms of the functions defined previously,

$$\hat{J}_{00}(q^2) = \frac{2}{3}\left(\hat{J}_u(q^2) + \hat{J}_d(q^2) + \hat{J}_s(q^2)\right) \quad , \tag{4.4.7}$$

and

$$\hat{J}_{88}(q^2) = \frac{1}{3}\left(\hat{J}_u(q^2) + \hat{J}_d(q^2) + 4\hat{J}_s(q^2)\right) \quad , \tag{4.4.8}$$

$$\hat{J}_{08}(q^2) = \frac{\sqrt{2}}{3}\left(\hat{J}_u(q^2) + \hat{J}_d(q^2) - 2\hat{J}_s(q^2)\right) \quad . \tag{4.4.9}$$

We then define the matrices

$$G = \begin{bmatrix} G_{00}^S & G_{08}^S \\ G_{08}^S & G_{88}^S \end{bmatrix} \quad , \tag{4.4.10}$$

and

$$\hat{J}(q^2) = \begin{bmatrix} \hat{J}_{00}(q^2) & \hat{J}_{08}(q^2) \\ \hat{J}_{08}(q^2) & \hat{J}_{88}(q^2) \end{bmatrix} \quad . \tag{4.4.11}$$

In the next section we will introduce a set of functions that describe the coupling of the $q\bar{q}$ states to the two-pion continuum. Making use of the functions defined there, we introduce the matrix

$$\hat{K}(q^2) = \begin{bmatrix} \hat{K}_{00}(q^2) & \hat{K}_{08}(q^2) \\ \hat{K}_{08}(q^2) & \hat{K}_{88}(q^2) \end{bmatrix} \quad , \tag{4.4.12}$$

as well as the matrix

$$\bar{J}(q^2) = \hat{J}(q^2) + \hat{K}(q^2) \quad . \tag{4.4.13}$$

Note that $\hat{K}(q^2) = \mathrm{Re}\hat{K}(q^2) + i\,\mathrm{Im}\hat{K}(q^2)$, with $\mathrm{Im}\hat{K}(q^2)$ equal to zero when $q^2 < 4m_\pi^2$.

The T matrix, exclusive of Dirac matrices and flavor matrices, then satisfies the matrix equation

$$T(q^2) = -G + G\bar{J}(q^2)T(q^2) \quad , \tag{4.4.14}$$

or

$$T(q^2) = -(\mathbb{I} - G\bar{J}(q^2))^{-1}G \quad . \tag{4.4.15}$$

We also introduce the matrix

$$D(q^2) = \mathbf{I} - G\bar{J}(q^2) \tag{4.4.16}$$

$$= \begin{bmatrix} D_{11}(q^2) & D_{12}(q^2) \\ D_{21}(q^2) & D_{22}(q^2) \end{bmatrix} \quad , \tag{4.4.17}$$

with

$$D_{11}(q^2) = 1 - \left[G_{00}^S \bar{J}_{00}(q^2) + G_{08}^S \bar{J}_{08}(q^2)\right] \quad , \tag{4.4.18}$$

$$D_{12}(q^2) = -\left[G_{00}^S \bar{J}_{08}(q^2) + G_{08}^S \bar{J}_{88}(q^2)\right] \quad , \tag{4.4.19}$$

$$D_{21}(q^2) = -\left[G_{08}^S \bar{J}_{00}(q^2) + G_{88}^S \bar{J}_{08}(q^2)\right] \quad , \tag{4.4.20}$$

and

$$D_{22}(q^2) = 1 - \left[G_{08}^S \bar{J}_{08}(q^2) + G_{88}^S \bar{J}_{88}(q^2)\right] \quad . \tag{4.4.21}$$

With these definitions, we may write

$$T(q^2) = \begin{bmatrix} A_S(q^2) & B_S(q^2) \\ B_S(q^2) & C_S(q^2) \end{bmatrix} \quad , \tag{4.4.22}$$

with

$$A_S(q^2) = -\frac{1}{\det D(q^2)}\left[G_{00}^S - \left(G_{88}^S G_{00}^S - G_{08}^S G_{08}^S\right)\bar{J}_{88}(q^2)\right] \quad , \tag{4.4.23}$$

$$B_S(q^2) = -\frac{1}{\det D(q^2)}\left[G_{08}^S - \left(G_{08}^S G_{08}^S - G_{00}^S G_{88}^S\right)\bar{J}_{08}(q^2)\right] \quad , \tag{4.4.24}$$

and

$$C_S(q^2) = -\frac{1}{\det D(q^2)}\left[G_{88}^S - \left(G_{00}^S G_{88}^S - G_{08}^S G_{08}^S\right)\bar{J}_{00}(q^2)\right] \quad . \tag{4.4.25}$$

Note that in the absence of octet-singlet coupling $(G_{08}^S = \bar{J}_{08}(q^2) = 0)$, we have $B_S(q^2) = 0$,

$$A_S(q^2) = -\frac{G_{00}^S}{1 - G_{00}^S \bar{J}_{00}(q^2)} \tag{4.4.26}$$

and

$$C_S(q^2) = -\frac{G_{88}^S}{1 - G_{88}^S \bar{J}_{88}(q^2)} \quad . \tag{4.4.27}$$

If we use Eq. (4.4.26), we see that the masses of the scalar singlet mesons are given by the solution of the equation

$$\left(G_{00}^S\right)^{-1} - \mathrm{Re}\bar{J}_{00}\left(m_{\sigma'}^2\right) = 0 \quad . \tag{4.4.28}$$

Similarly, we have for the mass of the scalar octet mesons, the solution of the equation

$$\left(G_{88}^S\right)^{-1} - \mathrm{Re}\bar{J}_{88}\left(m_{\sigma'}^2\right) = 0 \quad . \tag{4.4.29}$$

As we will see, Eqs. (4.4.28) and (4.4.29) will have more than one solution.

We note that for $q^2 < 4m_\pi^2$, the T matrix is real. If $q^2 < 4m_\pi^2$, or if we neglect $\mathrm{Im}\hat{K}_S(q^2)$, we can bring T to a diagonal form with a real matrix

$$M(\theta) = \begin{pmatrix} \cos\theta & -\sin\theta \\ \sin\theta & \cos\theta \end{pmatrix} \quad , \tag{4.4.30}$$

where θ is a function of q^2.

Thus,

$$T_{\mathrm{diag}}(q^2) = M(\theta)T(q^2)M^{-1}(\theta) \quad , \tag{4.4.31}$$

$$= \begin{bmatrix} T_\sigma(q^2) & 0 \\ 0 & T_{\sigma'}(q^2) \end{bmatrix} \quad , \tag{4.4.32}$$

where

$$T_{\sigma}(q^2) = A_S(q^2)\cos^2\theta - 2B_S(q^2)\sin\theta\cos\theta + C_S(q^2)\sin^2\theta \quad , \qquad (4.4.33)$$

and

$$T_{\sigma'}(q^2) = A_S(q^2)\sin^2\theta + 2B_S(q^2)\sin\theta\cos\theta + C_S(q^2)\cos^2\theta \quad . \qquad (4.4.34)$$

Alternate expressions for $T_{\sigma}(q^2)$ and $T_{\sigma'}(q^2)$ that are generally valid are

$$T_{\sigma}(q^2) = \frac{A_S(q^2) + C_S(q^2)}{2} + \left\{ \left[\frac{A_S(q^2) - C_S(q^2)}{2} \right]^2 + B_S^2(q^2) \right\}^{1/2} \qquad (4.4.35)$$

and

$$T_{\sigma'}(q^2) = \frac{A_S(q^2) + C_S(q^2)}{2} - \left\{ \left[\frac{A_S(q^2) - C_S(q^2)}{2} \right]^2 + B_S^2(q^2) \right\}^{1/2} \qquad (4.4.36)$$

as may be seen by calculating the eigenvalues of the matrix $T(q^2)$ in the case $A_S(q^2)$, $B_S(q^2)$ and $C_s(q^2)$ are complex functions.

We can also see that the matrix $T(q^2)$ takes on a diagonal form when

$$\tan 2\theta(q^2) = \frac{2B_S(q^2)}{C_S(q^2) - A_S(q^2)} \qquad (4.4.37)$$

in the case that $q^2 < 4m_{\pi}^2$, or if $\mathrm{Im}\hat{K}_S(q^2) = 0$. Equation (4.4.37), therefore, provides the value of the mixing angle, $\theta(q^2)$, for the case in which $A_S(q^2)$, $B_S(q^2)$, and $C_S(q^2)$

are real functions. We find $\theta(q^2) = -12.6^0$ at $q^2 = 0$. (At low energies there is only small singlet-octet mixing.) .

It is useful to define the functions $d_\sigma(q^2)$ and $d_{\sigma'}(q^2)$, such that

$$T_\sigma(q^2) = \frac{d_\sigma(q^2)}{\det D(q^2)} \quad , \tag{4.4.38}$$

and

$$T_{\sigma'}(q^2) = \frac{d_{\sigma'}(q^2)}{\det D(q^2)} \quad . \tag{4.4.39}$$

If we neglect $\mathrm{Im}\hat{K}_s(q^2)$, or if $q^2 < 4m_\pi^2$, we may find the mass of the resonances that appear in $T_\sigma(q^2)$ or $T_{\sigma'}(q^2)$ from the equation

$$\det D(q^2) = 0 \quad . \tag{4.4.40}$$

In the general case, we can define meson masses by the condition

$$\mathrm{Re}[\det D(q^2)] = 0 \quad . \tag{4.4.41}$$

Equation (4.4.41) may be used in the presence of octet-singlet mixing and in the case that $\mathrm{Im}\hat{K}_s(q^2)$ is included in the analysis. Note that $\det D(q^2)$ will have a zero at each bound state or resonance. However, in some cases $d_\sigma(q^2)$, or $d_{\sigma'}(q^2)$, may have a corresponding zero such that the resonance is absent from $T_\sigma(q^2)$ or $T_{\sigma'}(q^2)$.

4.5. Coupling to the Two-Pion Continuum

We presented a detailed discussion of the calculation of $\hat{K}_S(q^2)$ when using the NJL model with SU(2) flavor symmetry in Ref. [Ce97a]. In Fig. 4.2a we exhibit the diagram that defines $K_S(q^2)$ for that theory in the absence of confinement. (Note that for the calculation of $K_S(q^2)$, the flavor matrix at the vertices is the unit matrix.) In Fig. 4.2b we add the confining vertex, so that the only discontinuity for $K_S(q^2)$ is that across the two-pion cut. We can calculate the discontinuity across the cut by placing the pions on mass shell, as denoted by a cross on the wavy lines in Fig. 4.2c. In Fig. 4.2d we show the form factor that has to be calculated when constructing $\mathrm{Im}\hat{K}_S(q^2)$.

In Section III we saw that we could write a once-subtracted dispersion relation to obtain $\mathrm{Re}\hat{K}_S(q^2)$ from the knowledge of $\hat{K}_S(0)$ and $\mathrm{Im}\hat{K}_S(q^2)$. (The calculation of $\hat{K}_S(0)$ required a separate calculation in which we evaluated the form factor of Fig. 4.2e for the case $q^\mu = 0$.) Our results for $\mathrm{Im}\hat{K}_S(0)$ and $\mathrm{Re}\hat{K}_S(q^2)$ are shown in Figs. 3.10 and 3.11.

We find that we can calculate the coupling of the $q\bar{q}$ states to the two-pion continuum in the model with SU(3) flavor symmetry by making use of our earlier calculation. The only modification is the different flavor factors that appear at the vertices. The appropriate definition is then

$$\hat{K}_{00}(q^2) = \frac{2}{3}\hat{K}_S(q^2) \quad , \tag{4.5.1}$$

$$\hat{K}_{88}(q^2) = \frac{1}{3}\hat{K}_S(q^2) \quad , \tag{4.5.2}$$

and

$$\hat{K}_{08}(q^2) = \frac{\sqrt{2}}{3}\hat{K}_S(q^2) \quad . \tag{4.5.3}$$

Therefore the matrix $\bar{J}(q^2) = \hat{J}(q^2) + \hat{K}(q^2)$, introduced earlier, has the elements

$$\bar{J}_{00}(q^2) = \frac{2}{3}\left[\hat{J}_u(q^2) + \hat{J}_d(q^2) + \hat{J}_s(q^2) + \hat{K}_S(q^2)\right] \quad , \tag{4.5.4}$$

$$\bar{J}_{88}(q^2) = \frac{1}{3}\left[\hat{J}_u(q^2) + \hat{J}_d(q^2) + 4\hat{J}_s(q^2) + \hat{K}_S(q^2)\right] \quad , \tag{4.5.5}$$

and

$$\bar{J}_{08}(q^2) = \frac{\sqrt{2}}{3}\left[\hat{J}_u(q^2) + \hat{J}_d(q^2) - 2\hat{J}_s(q^2) + \hat{K}_S(q^2)\right] \quad . \tag{4.5.6}$$

We have only considered the two-pion cut in the construction of $\mathrm{Im}\hat{K}_S(q^2)$. Other cuts appear in the case of SU(3) flavor symmetry. However, such cuts appear at higher energy and involve mesons having masses that are significantly larger than the mass of the pion. Their contribution to $\mathrm{Im}\hat{K}_S(q^2)$ is expected to be small.

It can be seen that $\hat{K}_S(q^2)$ only affects singlet states in the absence of singlet-octet coupling. In this model, octet states will take on a width due to their coupling to the singlet states. These comments will be bourne out when we inspect the form of the T matrix in the representation in which it is diagonal. For example, $\mathrm{Re}\hat{K}_S(q^2)$ exhibits strong cusplike behavior near $q^2 = 4m_\pi^2$. However, that behavior is only reflected in the component of the diagonalized T matrix that we denote as $T_\sigma(q^2)$. That component is

predominantly of SU(3)-singlet character since the mixing angle is small in the vicinity of $q^2 = 0$.

4.6. Numerical Results

When we introduce $\mathrm{Im}\,\hat{K}_S(q^2)$ into our analysis, the functions $A_S(q^2)$, $B_S(q^2)$ and $C_S(q^2)$ become complex. Also, when the T matrix is brought to diagonal form, $T_\sigma(q^2)$ and $T_{\sigma'}(q^2)$ will be complex functions. We begin our analysis by presenting values of $\mathrm{Re}[\det D(q^2)]$ in Fig. 4.3. The singlet-octet coupling moves two of the four states that originally appeared in the region $q^2 \leq 1.8$ GeV to higher energy. (The analysis of Ref. [Ce81] puts the lowest of these states at $q^2 \simeq 2.53$ GeV^2, which is outside the range of q^2 we are able to investigate in our work.) In Fig. 4.3 we see cusp behavior at $q^2 \equiv 4m_\pi^2$. (The singularity seen in Fig. 4.3 at $q^2 \simeq 1.48$ GeV^2 is due to a singularity of $\hat{J}_u(q^2)$. That singularity does not appear in the T matrix elements, as we will see.) Figure 4.4 shows the values of $\mathrm{Im}[\det D(q^2)]$.

In Fig. 4.5 we show both $\mathrm{Re}\,T_\sigma(q^2)$ [dashed line] and $\mathrm{Re}\,T_{\sigma'}(q^2)$ [solid line]. These curves have the following features. There are two zeros of $T_\sigma(q^2)$ for which the curve rises from negative values to positive values. These zeros correspond to resonances which we denote as σ_1 and σ_2. The values of $T_\sigma(q^2)$ exhibit strong cusp behavior at $q^2 \simeq 4m_\pi^2$. Note also that $T_{\sigma'}(q^2)$ has no resonances in the range shown, since the states that we may call σ_3 and σ_4 are now are at higher energies.

In Fig. 4.6 we show $\mathrm{Im}\,T_\sigma(q^2)$ [dashed line] and $\mathrm{Im}\,T_{\sigma'}(q^2)$ [solid line]. Again, strong cusp behavior is only seen in $\mathrm{Im}\,T_\sigma(q^2)$. The state σ_1 at $q^2 = 1.00$ GeV^2 has a large width and the width is quite asymmetric due to its proximity to the region of strong

cusp behavior. The state σ_2 has a relatively narrow width and the T matrix could be well approximated by the form

$$T_\sigma(q^2) = \frac{g^2}{q^2 - m^2 + im\Gamma} \tag{4.6.1}$$

with $m^2 = 1.63$ GeV^2, $\Gamma = 0.033$ GeV and $g^2 = 1.35$. The small value of g^2 means that this state is only weakly coupled to quarks. In case of the broad asymmetric resonance at $q^2 = 1.00$ GeV^2, we can ask what the resonance parameters would be in the case the behavior below $q^2 = 1.00$ GeV^2 was modified so as to make the resonance symmetric. In that case, we would have $\Gamma = 0.355$ GeV and $g^2 = 10.6$; however, a symmetric form does not provide a good representation of $T_\sigma(q^2)$. [See Fig. 4.6.]

4.7. Dynamical Origin of an Effective Low-Mass Scalar Meson for Nuclear Physics

In this work we have seen that the σ_1 and σ_2 mesons have masses of 1 GeV or greater. Therefore, it appears that the σ_1 meson cannot be identified with the low-mass scalar ($m_\sigma \simeq 550$ MeV) often used in the description of the nucleon-nucleon interaction that is based upon the one-boson-exchange model [Ma89]. In addition, a low-mass scalar plays an important role in the Walecka model [Se86] and in relativistic Brueckner-Hartree-Fock theory [Se86].

There is also a body of work that relates the mean sigma field in nuclei to an order parameter for partial restoration of chiral symmetry at finite baryon density [Ce81,Ce92a-b,Ce93,Sh94]. In that work the mean scalar field is related to the value

of the quark condensate in matter. The reduction of the condensate in matter satisfies a well-known model-independent relation

$$\langle \bar{q}q \rangle_\rho = \langle \bar{q}q \rangle_0 \left[1 - \frac{\sigma_N \rho}{m_\pi^2 f_\pi^2} \right] , \qquad (4.7.1)$$

to first-order in the baryon density ρ. In Eq. (4.7.1), σ_N is the pion-nucleon sigma term whose value is usually given as $\sigma_N = 45 \pm 8$ MeV, and $\langle \bar{q}q \rangle_0$ is the vacuum value of the condensate. Thus, the reduction of the condensate is about 35 percent in nuclear matter. That is similar to the reduction of the nucleon mass from its vacuum value as seen in the Walecka model [Se86]. If one argues that the nucleon mass is (approximately) proportional to the value of the quark condensate, a fairly consistent picture emerges, with the mean scalar field being an order parameter for the deviation of the condensate from its vacuum value.

In the present work we wish to show how an effective low-mass σ meson emerges from our study of the quark-quark T matrix of the generalized NJL model. To study this matter, we first consider Eq. (4.6.1), which may be used to parametrize the $T_\sigma(q^2)$ component of the T matrix, if we make Γ q^2-dependent. We stress that, since m_σ is about 1 GeV in that parametrization, that form is only appropriate for large q^2. However, in nuclear physics studies the exchanged mesons are spacelike ($q^2 \leq 0$), so we

may ask how $T_\sigma(q^2)$ should be parametrized in the spacelike region. With reference to Fig. 4.7, we see that inclusion of $\mathrm{Re}\hat{K}_S(q^2)$ when calculating $\det D(q^2)$ changes the behavior in a dramatic fashion.

Note that for $q^2 \leq 4m_\pi^2$, $\det D(q^2)$ is real. Near $q^2 = 0$, we may write $\det D(q^2) \simeq 0.97\,[(m_\sigma^{\text{eff}})^2 - q^2]$, with $m_\sigma^{\text{eff}} \simeq 0.520$ GeV. That means that for small spacelike values of q^2, we can put

$$T_\sigma(q^2) \simeq \frac{\left(g_{\sigma qq}^{\text{eff}}\right)^2}{q^2 - \left(m_\sigma^{\text{eff}}\right)^2} \quad . \tag{4.7.2}$$

Inspection of Fig. 4.4 yields an approximate value of $g_{\sigma qq}^{\text{eff}} = 3.32$. Note that the strong q^2 dependence for small q^2 in $T_\sigma(q^2)$ is almost entirely due to the cusplike behavior of $\det D(q^2)$.

The T matrix for off-mass-shell quarks can be used in a model of the nucleon-nucleon force that is based upon that T matrix and valence-quark form factors of the nucleon. [See Fig. 4.8.] That model has been developed in a number of works [Sh95a,Sh94,Sh97,Ce96a-b]. Since the T matrix in the model considered here is parametrized by isoscalar-scalar exchange with $m_\sigma^{\text{eff}} \simeq 520$ MeV, we see how we may understand one important feature of the boson-exchange model and of the Walecka model.

It is important to note that while inclusion of the cusplike behavior of $\mathrm{Re}\hat{K}_S(q^2)$ leads to a significant change when going from m_σ to m_σ^{eff}, the value of

$\det D(q^2)$ near $q^2 = 0$ is only reduced from its value in the absence of $\mathrm{Re}\,\hat{K}_S(q^2)$ by about 25 percent. That means that the predominant feature in scalar-isoscalar exchange in the nucleon-nucleon interaction is the exchange of the σ_1 meson, which we saw to be predominantly the $\sigma^0(1P)$ in our model.

4.8. Discussion

In this work we have found two low-lying states that have energies of 1.00 GeV and 1.28 GeV. The first of these states which we have denoted as σ_1, is predominantly the $\sigma^0(1P)$, while the state σ_2 is strongly mixed and has a rather small width for decay to two pions. Also, σ_2 is only weakly coupled to quarks. On the other hand, the state σ_1 is a quite broad and asymmetric resonance, as may be seen in Fig. 4.6. Clearly, coupling to the two-pion continuum is important over quite a broad range of energies for the σ_1. The situation is simpler for $q^2 \leq 4m_\pi^2$, where the T matrix is well approximated by the exchange of an effective σ meson that has a mass parameter, $m_\sigma^{eff} \simeq 520$ MeV. This small mass parameter has its origin in the cusplike behavior of $T_\sigma(q^2)$ at small q^2 which is due to the rapid opening of the two-pion channel.

We have identified the effective σ meson with the low-mass scalar that is extensively used in nuclear structure studies and studies of the nucleon-nucleon interaction. A schematic representation of the wave function of this scalar is $\sigma = (\bar{u}u + \bar{d}d + \bar{s}s)/\sqrt{3}$ in a first approximation. The consequences of this identification will be explored in a future work. In such future work, it should be possible to extend our analysis to an energy region beyond $q^2 = 1.8$ GeV^2. However, such an extension requires that we modify our procedure for calculation of the vacuum polarization diagrams $\hat{J}(q^2)$.

V. Phenomenological Confinement Model for Pseudoscalar Mesons

5.1. Introduction

In this work we will discuss our generalized version of the SU(3)-flavor Nambu−Jona-Lasinio (NJL) model as appled to pseudoscalar mesons. Our model, and the version of the NJL model usually studied, contains an interaction between three quarks, introduced by 't Hooft, that serves to break the U(1) symmetry of the original model. Our generalized version also includes a model of confinement, described in previous sections, that allows us to study the properties of the η' meson which is the continuum of the NJL model in the absence of a confinement model. We will again use a Lorentz-vector form of confinement, since that form allows us to develop an approximation which preserves chiral symmetry. (Another model of confinement, which preserves chiral symmetry, will also be described in this work.) The Lagrangian of the generalized model is, for SU(3) flavor symmetry,

$$\mathcal{L} = \bar{q}(i\partial - m^0)q(x) + G_S\sum_{i=0}^{8}\left[\left[\bar{q}\frac{\lambda^i}{2}q\right]^2 + \left[\bar{q}i\gamma_5\frac{\lambda^i}{2}q\right]^2\right] + \frac{G_D}{2}\left\{\det\left[\bar{q}(1+\gamma_5)q\right] + \det\left[\bar{q}(1-\gamma_5)q\right]\right\} + \mathcal{L}_{conf} \quad , \tag{5.1.1}$$

where the λ^i ($i = 1, \ldots 8$) are the Gell-Mann matrices in flavor space and $\lambda^0 = (2/3)^{1/2}\mathbf{I}$, with $\mathbf{I}$ being the unit matrix. In Eq. (5.1.1), m^0 denotes a quark mass matrix with diagonal elements, m_u^0, m_d^0, m_s^0. Here, we take $m_u^0 = m_d^0 = 5.5$ MeV and $m_s^0 = 132$ MeV. Further,

$$\mathcal{L}_{\text{conf}} = \bar{q}(x)\gamma^{\mu}q(x)\,V^{C}(x-y)\bar{q}(y)\gamma_{\mu}q(y) \quad . \tag{5.1.2}$$

For calculations made in Minkowski momentum space, we neglect any dependence of V^C on energy transfer. We again take $V^C(r) = \kappa r \exp[-\mu r]$.

$$V^{C}(\vec{k}-\vec{k}') = -8\pi\kappa\left[\frac{1}{[(\vec{k}-\vec{k}')^2+\mu^2]^2} - \frac{4\mu^2}{[(\vec{k}-\vec{k}')^2+\mu^2]^3}\right] \quad . \tag{5.1.3}$$

In this section we will use μ=0.020 GeV and κ=0.20/4 GeV^2.

Another confinement model that yields particularly simple equations for vertex functions is a V-A form introduced in Section II:

$$\mathcal{L}_{\text{conf}} = \bar{q}(x)\gamma^{\mu}q(x)\,V^{C}(x-y)\bar{q}(y)\gamma_{\mu}q(y) - \bar{q}(x)\gamma^{\mu}\gamma_5 q(x)\,V^{C}(x-y)\bar{q}(y)\gamma_{\mu}\gamma_5 q(y) \quad . \tag{5.1.4}$$

This choice simplifies the calculation of the rates for $\eta \to 2\gamma$ and $\eta' \to 2\gamma$, since only a single scalar function, $\Gamma_P(q,k)$, is needed to characterize the vertex associated with the confining field: $\bar{\Gamma}_P(q,k) = \gamma_5\Gamma_P(q,k)$. (See Section 5.9 and 5.10.)

As we proceed we will present results for both Lorentz-vector confinement and for the V-A form. There is some reason to believe that the Lorentz-vector form is to be preferred over the Lorentz-scalar form usually used in the study of heavy mesons [Sz97]. We do not know of any use of the V-A form other than that of Ref. [Ce97b]. However, it is interesting to see if the V-A form yields a useful phenomenology, since it is particularly easy to use in various calculations. The organization of our work is as follows. In Section 5.2 we will discuss a relation between the Schwinger-Dyson equation and the Bethe-Salpeter equation that allows us to show that, in the absence of current

quark masses, our model yields zero-mass Goldstone bosons [Ce97b]. In Section 5.3 we discuss some of the vacuum polarization diagrams of the generalized NJL model. In Section 5.4 we describe the various effective coupling constants of the model [Vo91], as well as the polarization diagrams needed to calculate the mesonic states of the SU(3)-flavor NJL model. In Section 5.5 we describe a quark-antiquark T matrix, including coupling of the octet and singlet states via SU(3) symmetry breaking effects. (Since we have included a model of confinement, our T matrix is only defined for off-mass-shell quarks, such as those found in hadrons.) We also present our results for the masses of the π, K, η and η' mesons, and for the mixing angle for $\eta^0 - \eta^8$ mixing in Section 5.5. (We neglect $\pi - a_1$ mixing.) In Section 5.6 we calculate the decay widths for $\eta \to \gamma + \gamma$ and $\eta' \to \gamma + \gamma$ using the V-A confining interaction. In Section 5.7 we describe the calculations of the mesonic decay constants, f_π, f_K, f_η and $f_{\eta'}$. Finally, Section 5.8 contains some further discussion and conclusions. The appendices that comprise Sections 5.9 and 5.10 are denoted to a description of some aspects of our models of confinement.

5.2. Goldstone Bosons in a Generalized NJL Model

In an earlier work we showed how, if $m^0 = 0$, one can relate the Bethe-Salpeter equation for zero-energy pseudoscalar bound states to the Schwinger-Dyson equation for the quark self-energy [4]. The relevant equations are depicted in Fig. 5.1. (In Section II we considered the SU(2)-flavor version of the model, for simplicity.) In Fig. 5.1, Σ is the quark self-energy, while V^c is the confining field. The crosshatched triangular area is the vertex function for pseudoscalar bound states. [See Sections 5.9 and 5.10]

We showed that, if one introduces Lorentz-vector confinement, or the V-A model, in the standard SU(2)-flavor version of the NJL model, one finds a zero-mass Goldstone boson (the pion) and a relation between the self-energy, $\Sigma(p) = A(p^2) + \not{p}B(p^2)$, and the vertex function. We will not repeat the discussion of Section II, except to point out that our analysis was limited to spacelike p^2. It was found that $A(p^2)$ and $B(p^2)$ are p^2 - dependent, if the confining field, V^C, is added to the zero-range interaction of the NJL model, whose strength is parameterized by G_S. [See Fig. 5.1] We do not, as yet, have a procedure for extending $A(p^2)$ and $B(p^2)$ to the timelike region, $p^2 > 0$. Therefore, we will carry out our calculations in Minkowski momentum space with $B = 0$ and a constant value for $A(p^2)$; that is, $A(p^2) = m_q$, where m_q is the constituent quark mass obtained when we do not include confinement. When we go over to the model with SU(3)-flavor symmetry, there are three constituent masses, m_u, m_d and m_s. In the absence of confinement, one has the gap equations

$$m_u = m_u^0 - G_S <\bar{u}u> - G_D <\bar{d}d> <\bar{s}s> \quad , \tag{5.2.1}$$

$$m_d = m_d^0 - G_S <\bar{d}d> - G_D <\bar{u}u> <\bar{s}s> \quad , \tag{5.2.2}$$

$$m_s = m_s^0 - G_S <\bar{s}s> - G_D <\bar{u}u> <\bar{d}d> \quad , \tag{5.2.3}$$

where $<\bar{u}u>$, $<\bar{d}d>$ and $<\bar{s}s>$ are the condensates calculated in the NJL model [Vo91]. Since we will only make a modest increase in G_S relative to the value used in Ref. [Vo91], Eqs. (5.2.1)-(5.2.3) will be satisfied approximately. In order to obtain

some estimate of the effects due to the lack of self-consistency in our formalism, we write

$$m_u = m_u^0 - G_S<\bar{u}u> - G_D<\bar{d}d><\bar{s}s> + \Delta m_u \ , \qquad (5.2.4)$$

$$m_d = m_d^0 - G_S<\bar{d}d> - G_D<\bar{u}u><\bar{s}s> + \Delta m_d \ , \qquad (5.2.5)$$

$$m_s = m_s^0 - G_S<\bar{s}s> - G_D<\bar{u}u><\bar{d}d> + \Delta m_s \ , \qquad (5.2.6)$$

where the various Δm might represent an average correction to these equations due to the inclusion of the confining field in the gap equations. If we put $\Delta m_u = \Delta m_d \simeq -32$ MeV and $\Delta m_s \simeq -35$ MeV, Eqs. (5.2.4)-(5.2.6) will be satisfied in our model. Note that the values of G_D, m_u, m_d, m_s, $<\bar{u}u>$, $<\bar{d}d>$ and $<\bar{s}s>$ are the same as those used in Ref. [Vo91]. [See Table 5.1 for values of G_S, G_D, the constituent masses, and the condensates.]

In our work we use a three-momentum cutoff for Minkowski-space integrals, $\Lambda_3 = 0.622$ GeV, that yields the same values for the condensates as those calculated in Ref. [Vo91], where a Euclidean-space momentum cutoff of $\Lambda_E = 0.90$ GeV was used. (In most studies of the NJL model, the cutoff, Λ_E or Λ_3, is adjusted so that the meson decay constants are given correctly. We do not adopt that procedure here, since we wish to use the same quark mass values and condensate values as those obtained in Ref. [Vo91].)

As noted above, in this work we will include a model of confinement and use constant values for the constituent quark masses. Ideally, in some future work, we would like to include a momentum-dependent quark self-energy. However, at this time it is still of interest to see the features of the generalized NJL model that follow from the use of constant values for the constituent quark masses. We use the parameters found in Ref. [Vo91]; however, we need to make a small increase in G_S to compensate for the presence of the confining field. Therefore, G_S and κ are the only free parameters in our analysis. We take the value of κ from our earlier work, so that G_S remains as the only free parameter in our study. In practice, we fix G_S so that m_π is given correctly. Therefore, m_K, m_η and $m_{\eta'}$ are predictions of our model, as are f_π, f_K, f_η and $f_{\eta'}$, the meson decay constants. In addition, we calculate the transition rates for the decays $\eta \to 2\gamma$ and $\eta' \to 2\gamma$ using the V-A confinement model.

5.3. Vacuum Polarization diagrams

Important elements of the NJL model are vacuum polarization diagrams of the type shown in Fig. 3.4. For the purposes of this work, we will first introduce diagrams with quarks of a single flavor. For example, we may write

$$J_u(q^2) = n_c \mathrm{Tr} i \int \frac{d^4k}{(2\pi)^4} \left[i\gamma_5 S_u(q/2+k) i\gamma_5 S_u(-q/2+k) \right] , \qquad (5.3.1)$$

where $S_u(p) = [\not{p} - m_u + i\epsilon]^{-1}$ is the propagator of an up quark and $n_c = 3$ is the number of colors. In a similar fashion, we define $J_d(q^2)$ and $J_s(q^2)$. We may also define an integral with one up and one strange quark

$$J_{us}(q^2) = n_c \mathrm{Tr} i \int \frac{d^4k}{(2\pi)^4} \left[i\gamma_5 S_u(q/2+k) i\gamma_5 S_s(-q/2+k) \right] \quad . \qquad (5.3.2)$$

Note that the integral defined in Eq. (5.3.1) becomes complex for $q^2 > (2m_u)^2$, while $J_{us}(q^2)$ is complex for $q^2 > (m_u + m_s)^2$.

Our model of confinement is implemented by replacing $i\gamma_5$ by $i\bar{\Gamma}(q,k)$ at a single vertex. [See Fig. 3.1, Sections 5.9 and 5.10] Thus, we define

$$\hat{J}_u(q^2) = n_c \mathrm{Tr} i \int \frac{d^4k}{(2\pi)^4} \left[S_u(q/2+k) i\bar{\Gamma}(q,k) S_u(-q/2+k) i\gamma_5 \right] \quad , \qquad (5.3.3)$$

with corresponding definitions for $\hat{J}_d(q^2)$ and $\hat{J}_s(q^2)$. Further, $J_{us}(q^2)$ is replaced by

$$\hat{J}_{us}(q^2) = n_c \mathrm{Tr} i \int \frac{d^4k}{(2\pi)^4} \left[S_u(q/2+k) i\bar{\Gamma}(q,k) S_s(-q/2+k) i\gamma_5 \right] \quad . \qquad (5.3.4)$$

One procedure for the evaluation of such integrals is to first complete the integral in the complex k^0 plane [Gr91]. To that end, we again use the representation of the propagator

$$S(k) = \frac{m}{E(\vec{k})} \left[\frac{\Lambda^{(+)}(\vec{k})}{k^0 - E(\vec{k}) + i\epsilon} - \frac{\Lambda^{(-)}(-\vec{k})}{k^0 + E(\vec{k}) - i\epsilon} \right] \quad , \qquad (5.3.5)$$

with

$$\Lambda^{(+)}(\vec{k}) = \frac{\not{k} + m}{2m} \quad , \qquad (5.3.6)$$

and

$$\Lambda^{(-)}(-\vec{k}) = \frac{\tilde{k}+m}{2m} \quad , \tag{5.3.7}$$

where $k^{\mu} = [E(\vec{k}),\ \vec{k}]$ and $\tilde{k}^{\mu} = [-E(\vec{k}),\ \vec{k}]$. Here, $E(\vec{k}) = [\vec{k}^2 + m^2]^{1/2}$.

It is then useful to define $\Gamma^{+-}(q,\ k)$ and $\Gamma^{-+}(q,\ k)$ by means of the equations

$$\Lambda^{(+)}(\vec{k})\bar{\Gamma}(q,k)\Lambda^{(-)}(-\vec{k}) = \Gamma^{+-}(q,k)\Lambda^{(+)}(\vec{k})\gamma_5\Lambda^{(-)}(-\vec{k}) \quad , \tag{5.3.8}$$

and

$$\Lambda^{(-)}(-\vec{k})\bar{\Gamma}(q,k)\Lambda^{(+)}(\vec{k}) = \Gamma^{-+}(q,k)\Lambda^{(-)}(-\vec{k})\gamma_5\Lambda^{(+)}(\vec{k}) \quad . \tag{5.3.9}$$

(Further details concerning the calculation of these vertex functions may be found in the Section 5.9 and 5.10). If we use Eq. (5.3.5) in Eq. (5.3.3), we find that only two terms contribute. Thus, for $\vec{q}=0$,

$$\hat{J}_u(q^2) = n_c \mathrm{Tr} i\int \frac{d^4k}{(2\pi)^4}\frac{m_u^2}{E_u^2(\vec{k})}\left[\frac{\Lambda^{(+)}(\vec{k})\bar{\Gamma}(q,k)\Lambda^{(-)}(-k)\gamma_5}{\left(q^0/2+k^0-E_u(\vec{k})+i\epsilon\right)\left(-q^0/2+k^0+E_u(\vec{k})-i\epsilon\right)}\right.$$

$$\left. + \frac{\Lambda^{(-)}(-\vec{k})\bar{\Gamma}(q,k)\Lambda^{(+)}(\vec{k})\gamma_5}{\left(q^0/2+k^0+E_u(\vec{k})-i\epsilon\right)\left(-q^0/2+k^0-E_u(\vec{k})+i\epsilon\right)}\right] \tag{5.3.10}$$

or

$$\hat{J}_u(q^2) = 2n_c i\int \frac{d^4k}{(2\pi)^4}\left[\frac{\Gamma^{+-}(q,k)}{\left(q^0/2+k^0-E_u(k)+i\epsilon\right)\left(-q^0/2+k^0+E_u(\vec{k})-i\epsilon\right)}\right. \tag{5.3.11}$$

$$\left. + \frac{\Gamma^{-+}(q,k)}{\left(q^0/2+k^0+E_u(\vec{k})-i\epsilon\right)\left(-q^0/2+k^0-E_u(\vec{k})+i\epsilon\right)}\right] .$$

The k^0 integral is completed in the lower-half plane, with the result that, with $\vec{q}=0$,

$$\hat{J}_u(q^2) = -2n_c\int \frac{d^3k}{(2\pi)^3}\left[\frac{\Gamma_u^{+-}(q^0,|\vec{k}|)}{q^0-2E_u(\vec{k})} - \frac{\Gamma_u^{-+}(q^0,|\vec{k}|)}{q^0+2E_u(\vec{k})}\right] . \tag{5.3.12}$$

Note that in obtaining Eq. (5.3.12), we see that $\Gamma^{+-}(q^0,|\vec{k}|)$ in Eq. (5.3.12) is the value of $\Gamma^{+-}(q,k)$ with the quark on its positive mass shell, while $\Gamma^{-+}(q^0,|\vec{k}|)$ has the antiquark on its negative mass shell. Also, when $q^0=2E_u(\vec{k})$, we have $\Gamma_u^{+-}(q^0,|\vec{k}|)=0$. [See Fig. 5.2.] Therefore, the first term in the bracket appearing in Eq. (5.3.12) is real and finite. (Thus, we need not keep an $i\epsilon$ in the denominator of the first term of Eq. (5.3.12).)

Values obtained for $\hat{J}_u(q^2)=\hat{J}_d(q^2)$, $\hat{J}_s(q^2)$ and $\hat{J}_{us}(q^2)$ are given in Fig. 5.4. There, we have used $|\vec{k}|\le\Lambda_3$ with $\Lambda_3=0.622$ GeV, $m_u=364$ MeV and $m_s=522$ MeV. (The calculation of $\Gamma_u^{+-}(q^0,|\vec{k}|)$ and $\Gamma_u^{-+}(q^0,|\vec{k}|)$ is described in Appendix A and the values obtained are shown in Figs. 5.2 and 5.3.)

The result given in Eq. (5.3.12) may be simplified if we use the V-A model developed in Section II. There, we saw that there was only a single function to consider. That is, we can write the confinement vertex for the up quark as $\bar{\Gamma}_u(q,k)=\gamma_5\Gamma_P^u(q,k)$, where $\Gamma_P^u(q,k)$ is a scalar function. We also have $\bar{\Gamma}_s(q,k)=\gamma_5\Gamma_P^s(q,k)$,

$\bar{\Gamma}_d(q,k) = \gamma_5 \Gamma_P^d(q,k)$, and $\bar{\Gamma}_{us}(q,k) = \gamma_5 \Gamma_P^{us}(q,k)$. (In this work $\Gamma_P^u(q,k) = \Gamma_P^d(q,k)$, since $m_u = m_d$. Further details concerning the function $\Gamma_P(q,k)$ are given in Section 5.10.) For the V-A model, we then may write Eq. (5.3.12) as

$$\hat{J}_u(q^2) = -2n_c \int \frac{d^3k}{(2\pi)^3} \Gamma_P^u(q^0, |\vec{k}|) \frac{4E_u(\vec{k})}{(q^0)^2 - \left[2E_u(\vec{k})\right]^2} , \qquad (5.3.13)$$

with a similar definition for $\hat{J}_d(q^2)$ and $\hat{J}_s(q^2)$. (The unequal mass case is discussed in Section 5.10.) Again, we note that $\Gamma_P^u(q^0, k_{on}) = 0$, when $q^0 = 2E_u(\vec{k}_{on})$. In a similar fashion, $\Gamma_P^s(q^0, k_{on}) = 0$ when $q^0 = 2E_s(\vec{k}_{on})$, etc.

5.4. The Quark-Antiquark Interaction

In terms of the parameters, G_S and G_D, that appear in Eq. (5.1.1), it is useful to define a series of effective coupling constants [Vo91]. The definition involves the quark condensates $<\bar{u}u> = <\bar{d}d>$ and $<\bar{s}s>$. We make use of the results of Ref. [Vo91] to write

$$G_\pi = \frac{1}{2}\left(G_S + G_D <\bar{s}s>\right) \qquad (5.4.1)$$

$$G_K = \frac{1}{2}\left(G_S + G_D <\bar{u}u>\right) \qquad (5.4.2)$$

$$G_{\eta^0} = \frac{1}{2}\left(G_S + G_D c_{00}\right) \qquad (5.4.3)$$

$$G_{\eta'} = \frac{1}{2}\left(G_S + G_D c_{88}\right) \tag{5.4.4}$$

and

$$G_{08} = \frac{1}{2}\left(G_D c_{08}\right) \ . \tag{5.4.5}$$

In these equations, with $<\bar{u}u> = <\bar{d}d>$, we have

$$c_{00} = -\frac{2}{3}\left(2<\bar{u}u> + <\bar{s}s>\right) \ , \tag{5.4.6}$$

$$c_{88} = \frac{1}{3}\left(4<\bar{u}u> - <\bar{s}s>\right) \ , \tag{5.4.7}$$

and

$$c_{08} = \frac{\sqrt{2}}{3}\left(<\bar{u}u> - <\bar{s}s>\right) \ . \tag{5.4.8}$$

(These effective coupling constants are proportional to those defined by Vogl and Weise [Vo91].) It is also useful to introduce the following functions

$$\hat{J}_{\pi}(q^2) = \hat{J}_u(q^2) + \hat{J}_d(q^2) \tag{5.4.9}$$

$$\hat{J}_K(q^2) = 2\hat{J}_{us}(q^2) \tag{5.4.10}$$

$$\hat{J}_{\eta'}(q^2) = \frac{2}{3}\left[\hat{J}_u(q^2) + \hat{J}_d(q^2) + \hat{J}_s(q^2)\right] \tag{5.4.11}$$

$$\hat{J}_{\eta^s}(q^2) = \frac{1}{3}\left[\hat{J}_u(q^2) + \hat{J}_d(q^2) + 4\hat{J}_s(q^2)\right] \tag{5.4.12}$$

$$\hat{J}_{08}(q^2) = \frac{\sqrt{2}}{3}\left[\hat{J}_u(q^2) + \hat{J}_d(q^2) - 2\hat{J}_s(q^2)\right] . \tag{5.4.13}$$

The values of $\hat{J}_\pi(q^2)$, $\hat{J}_K(q^2)$, $\hat{J}_{\eta^0}(q^2)$ and $\hat{J}_{\eta^s}(q^2)$ were calculated with vector confinement and are given in Fig. 5.5. In Figs. 5.6 and 5.7, we compare the values of these functions with the same functions calculated without confinement, $J_\pi(q^2)$, $J_K(q^2)$, $J_{\eta^0}(q^2)$ and $J_{\eta^s}(q^2)$. For the low-mass mesons, π, K, η^8, the integrals that include confinement are about 10-20 percent smaller than those that do not include confinement. Note that $J_\pi(q^2)$, $J_{\eta^0}(q^2)$ and $J_{\eta^s}(q^2)$ become complex above $q^2 = (2m_u)^2$, while $J_K(q^2)$ is complex for $q^2 > (m_u + m_s)^2$. Thus, we see that, if we are to describe the η^0 (or the η'), we need to use the generalized model that includes confinement.

The functions of Eqs. (5.4.9)-(5.4.13) and the effective coupling constants may be used to define T matrices that describe the interaction of quarks. [See Fig. 4.1.] Since we have introduced a model of confinement, these T matrices are only defined for the interaction of off-mass-shell quarks, such as those bound in a nucleon, for example. (There are no asymptotic free-quark states in this model.) We can separate the Dirac and flavor matrices to write

$$\bar{T}_P^{ij}(q^2) = i\gamma_5(1)\lambda^i(1)T_{ij}(q^2)i\gamma_5(2)\lambda^j(2) \tag{5.4.14}$$

where the λ^i are the Gell-Mann matrices ($i = 1, \ldots 8$) plus $\lambda^0 = (2/3)\mathbf{I}$. We now drop reference to the Dirac and flavor matrices and consider the various $T(q^2)$. If we neglect $\pi - a_1$ mixing, the T matrices for the pion and kaon channels are given by simple expressions,

$$T_\pi(q^2) = -\frac{G_\pi}{1 - G_\pi \hat{J}_\pi(q^2)} \quad , \tag{5.4.15}$$

and

$$T_K(q^2) = -\frac{G_K}{1 - G_K \hat{J}_K(q^2)} \quad . \tag{5.4.16}$$

[See Fig. 4.1.] Note that the equations

$$G_\pi^{-1} - \hat{J}_\pi(m_\pi^2) = 0 \quad , \tag{5.4.17}$$

and

$$G_K^{-1} - \hat{J}_K(m_K^2) = 0 \quad , \tag{5.4.18}$$

determine the masses of the pion and kaon in the model with confinement. Also, if we were to neglect $\eta^0 - \eta^8$ mixing, we would find the masses of the η^0 and η^8 from the equations

$$G_{\eta^0}^{-1} - \hat{J}_{\eta^0}(m_{\eta^0}^2) = 0 \quad , \tag{5.4.19}$$

and

$$G_{\eta^8}^{-1} - \hat{J}_{\eta^8}(m_{\eta^8}^2) = 0 \quad . \tag{5.4.20}$$

These equations follow, if $G_{08} = \hat{J}_{08}(q^2) = 0$. The mixing of the η^0 and η^8, which depends upon the values of G_{08} and $\hat{J}_{08}(q^2)$, is described in the next section.

5.5. Coupled-Channel Effects: $\eta^0 - \eta^8$ Mixing

The calculation of the $q\bar{q}$ interaction is made somewhat more complicated by the mixing of the singlet state (η^0) with the octet state (η^8) to produce the physical states, η and η'. The masses of the η and η' may be obtained by studying the equation that determines the T matrix [ta95]. It is useful to use a matrix notation. We define the matrix

$$G = \begin{bmatrix} G_{\eta^8} & G_{08} \\ G_{08} & G_{\eta^0} \end{bmatrix} , \tag{5.5.1}$$

where G_{08} serves to mix the singlet and octet states. We also introduce the matrix

$$\hat{J}(q^2) = \begin{bmatrix} \hat{J}_{\eta^8}(q^2) & \hat{J}_{08}(q^2) \\ \hat{J}_{08}(q^2) & \hat{J}_{\eta^0}(q^2) \end{bmatrix} . \tag{5.5.2}$$

The T matrix satisfies the matrix equation

$$T(q^2) = -G + G\hat{J}(q^2)T(q^2) , \tag{5.5.3}$$

or

$$\left(1 - G\hat{J}(q^2)\right)T(q^2) = -G . \tag{5.5.4}$$

Thus

$$T(q^2) = -\left(1 - G\hat{J}(q^2)\right)^{-1} G . \tag{5.5.5}$$

(Equation (5.5.5) is similar to a corresponding equation given by Vogl and Weise [Vo91]. Our matrix G is related to their matrix K by $G = K/4$.)

At this point, we will adopt some of the notation of [Ta95], and write $T(q^2)$ of Eq. (5.5.5) as

$$T(q^2) = \begin{bmatrix} A(q^2) & B(q^2) \\ B(q^2) & C(q^2) \end{bmatrix} , \tag{5.5.6}$$

with

$$A(q^2) = \frac{1}{\det D(q^2)} \left\{ (G_{\eta^0} G_{\eta^8} - G_{08} G_{08}) \hat{J}_{\eta^0}(q^2) - G_{\eta^8} \right\} , \tag{5.5.7}$$

$$B(q^2) = \frac{1}{\det D(q^2)} \left\{ -(G_{\eta^0} G_{\eta^8} - G_{08} G_{08}) \hat{J}_{08}(q^2) - G_{08} \right\} , \tag{5.5.8}$$

$$C(q^2) = \frac{1}{\det D(q^2)} \left\{ (G_{\eta^0} G_{\eta^8} - G_{08} G_{08}) \hat{J}_{\eta^8}(q^2) - G_{\eta^0} \right\} . \tag{5.5.9}$$

Here, the matrix $D(q^2)$ is

$$D(q^2) = \begin{bmatrix} D_{11}(q^2) & D_{12}(q^2) \\ D_{21}(q^2) & D_{22}(q^2) \end{bmatrix} , \tag{5.5.10}$$

with

$$D_{11}(q^2) = G_{\eta^8} \hat{J}_{\eta^8}(q^2) + G_{08} \hat{J}_{08}(q^2) - 1 , \tag{5.5.11}$$

$$D_{12}(q^2) = G_{\eta^8} \hat{J}_{08}(q^2) + G_{08} \hat{J}_{\eta^8}(q^2) , \tag{5.5.12}$$

$$D_{21}(q^2) = G_{\eta^0} \hat{J}_{08}(q^2) + G_{08} \hat{J}_{\eta^8}(q^2) , \tag{5.5.13}$$

$$D_{22}(q^2) = G_{\eta^0}\hat{J}_{\eta^0}(q^2) + G_{08}\hat{J}_{08}(q^2) - 1 \quad . \tag{5.5.14}$$

Note that the equations

$$\det D(m_\eta^2) = 0 \quad , \tag{5.5.15}$$

and

$$\det D(m_{\eta'}^2) = 0 \tag{5.5.16}$$

determine the masses of the η and η' mesons.

We now introduce a matrix

$$M(\theta) = \begin{pmatrix} \cos\theta & -\sin\theta \\ \sin\theta & \cos\theta \end{pmatrix} \quad , \tag{5.5.17}$$

that we use to bring $T(q^2)$ of Eq. (5.5.6) to diagonal form. (Note that θ depends upon q^2.) Thus

$$T_{diag}(q^2) = M(\theta)T(q^2)M^{-1}(\theta) \quad , \tag{5.5.18}$$

$$= \begin{bmatrix} T_1(q^2) & 0 \\ 0 & T_2(q^2) \end{bmatrix} \quad , \tag{5.5.19}$$

where

$$T_1(q^2) = A(q^2)\cos^2\theta - 2B(q^2)\cos\theta\sin\theta + C(q^2)\sin^2\theta \quad , \tag{5.5.20}$$

and

$$T_2(q^2) = A(q^2)\sin^2\theta + 2B(q^2)\sin\theta\cos\theta + C(q^2)\cos^2\theta \quad . \tag{5.5.21}$$

The off-diagonal elements are zero, if

$$\tan 2\theta(q^2) = \frac{2B(q^2)}{C(q^2) - A(q^2)} \quad . \tag{5.5.22}$$

We now introduce the functions $d_\eta(q^2)$ and $d_{\eta'}(q^2)$, defined such that

$$\frac{d_\eta(q^2)}{\det D(q^2)} = \cos^2\theta A(q^2) - 2\sin\theta\cos\theta B(q^2) + \cos^2\theta C(q^2) \quad , \tag{5.5.23}$$

and

$$\frac{d_{\eta'}(q^2)}{\det D(q^2)} = \sin^2\theta A(q^2) + 2\sin\theta\cos\theta B(q^2) + \sin^2\theta C(q^2) \quad . \tag{5.5.24}$$

If we expand $\det D(q^2)$ at its zeros,

$$\det D(q^2) = (q^2 - m_\eta^2)\frac{\partial \det D(q^2)}{\partial q^2}\Big|_{q^2 = m_\eta^2} + \ldots \quad , \tag{5.5.25}$$

and

$$\det D(q^2) = (q^2 - m_{\eta'}^2)\frac{\partial \det D(q^2)}{\partial q^2}\Big|_{q^2 = m_{\eta'}^2} + \ldots \quad , \tag{5.5.26}$$

we can identify the coupling constants of the η and η' to the quarks,

$$g_{\eta qq}^2 = \frac{d_\eta(m_\eta^2)}{\frac{\partial \det D(q^2)}{\partial q^2}\Big|_{q^2 = m_\eta^2}} \quad , \tag{5.5.27}$$

and

$$g^2_{\eta' qq} = \frac{d_{\eta'}(m^2_{\eta'})}{\frac{\partial \det D(q^2)}{\partial q^2}\Big|_{q^2 = m^2_{\eta'}}} \quad . \tag{5.5.28}$$

In Fig. 5.8 we exhibit $\det D(q^2)$. The solid line includes the effects of $\eta^0 - \eta^8$ mixing, while the dotted line is the value of $\det D(q^2)$ when $G_{08} = \hat{J}_{08}(q^2) = 0$. Note that the major effect of the mixing appears in the energy domain of the η^0, or η'. In Fig. 5.9 we show the functions of $d_\eta(q^2)$ and $d_{\eta'}(q^2)$. In Fig. 5.10 we provide values of the mixing angle $\theta(q^2)$. We obtain $\theta(m^2_\eta) = -5.60^0$ and $\theta(m^2_{\eta'}) = -29.2^0$. We will need these values when we calculate the rates for $\eta \to 2\gamma$ and $\eta' \to 2\gamma$ in the next section.

5.6. Two-Photon Decays of the η and η' Mesons

The pion, the η and the η' can decay into two photons via the triangle (anomaly) diagram shown in Fig. 5.12. The η decay rate has been calculated by Takizawa and Oka [Ta95]; however, in the absence of a model of confinement they were unable to calculate the decay rate of the η'. (Since $m_{\eta'} > 2m_u$, the calculation of the triangle diagram yields a complex result due to the quark and antiquark going on mass shell.) A comprehensive discussion of the decays of the η that makes use of the SU(3)-flavor NJL model (without confinement) is found in Ref. [Ta97]. The authors of that work report on calculated decay rates for the processes $\eta \to 2\gamma$, $\eta \to \gamma\mu^-\mu^+$ and $\eta \to \pi^0\gamma\gamma$. They also provide results for the $\eta\gamma\gamma^*$ transition form factor. In general, they find good agreement with experimental data.

In the present study, we wish to describe a method for including confinement in the calculation of the triangle diagram. For ease of reference, we will again use the notation of Ref. [Ta97]. We may define a tensor, with $q^\mu = k_1^\mu + k_2^\mu$,

$$T_{\mu\nu}(k_1, k_2) = -\int \frac{d^4p}{(2\pi)^4} \mathrm{Tr}\left\{ \frac{1}{\not p - m + i\epsilon} \gamma_5 \frac{1}{\not p - \not q - m + i\epsilon} \gamma_\nu \frac{1}{\not p - \not k_1 - m + i\epsilon} \gamma_\mu \right\} + \begin{bmatrix} k_1 \leftrightarrow k_2 \\ \mu \leftrightarrow \nu \end{bmatrix} \tag{5.6.1}$$

[See Fig. 5.11.] We have

$$T_{\mu\nu} = -4s\epsilon_{\alpha\beta\mu\nu} k_1^\alpha k_2^\beta I(k_1\ k_2) \quad , \tag{5.6.2}$$

where $s=2$ is a symmetry factor and

$$I(k_1 k_2) = i\int \frac{d^4p}{(2\pi)^4} \frac{1}{p^2 - m^2 + i\epsilon} \frac{1}{(p-q)^2 - m^2 + i\epsilon} \frac{1}{(p-k_1)^2 - m^2 + i\epsilon} \quad . \tag{5.6.3}$$

In these equations, m is the constituent mass of either the up, down, or strange quark. Note that in passing from Eq. (5.6.1) to Eq. (5.6.2), we have used the relation

$$\mathrm{Tr}\left(\gamma_5 \gamma^\alpha \gamma^\beta \gamma^\gamma \gamma^\delta\right) = -4i\epsilon^{\alpha\beta\gamma\delta} \quad . \tag{5.6.4}$$

It is useful to introduce the functions [Ta95]

$$F(u, \eta) = 32\pi^2 m_u I_u(k_1, k_2) \quad , \tag{5.6.5}$$

and

$$F(s, \eta) = 32\pi^2 m_s I_s(k_1, k_2) \quad . \tag{5.6.6}$$

(We note that $F(d, \eta) = F(u, \eta)$, if $m_u = m_d$.) In Eqs. (5.6.5) and (5.6.6), $q^2 = m_\eta^2$.

We also introduce the corresponding functions for the η': $F(u,\eta')$, $F(d,\eta')$ and $F(s,\eta')$.

The transition amplitude defined in Ref. [Ta95] takes the form, with $g_\eta \equiv g_{\eta qq}$,

$$T_{\eta\to 2\gamma} = \frac{\alpha}{\pi} g_\eta \frac{1}{3\sqrt{3}}\Big[\cos\theta_\eta \{5F(u,\eta) - 2F(s,\eta)\} - \sin\theta_\eta \sqrt{2}\{5F(u,\eta) + F(s,\eta)\}\Big] \quad . \tag{5.6.7}$$

We then find

$$T_{\eta'\to 2\gamma} = \frac{\alpha}{\pi} g_{\eta'} \frac{1}{3\sqrt{3}}\Big[\sin\theta_{\eta'} \{5F(u,\eta') - 2F(s,\eta')\} - \cos\theta_{\eta'} \sqrt{2}\{5F(u,\eta') + F(s,\eta')\}\Big] \quad . \tag{5.6.8}$$

In terms of these amplitudes, we have the widths

$$\Gamma(\eta\to 2\gamma) = \frac{m_\eta^3}{64\pi} |\, T_{\eta\to 2\gamma}\,|^2 \quad , \tag{5.6.9}$$

and

$$\Gamma(\eta'\to 2\gamma) = \frac{m_{\eta'}^3}{64\pi} |\, T_{\eta'\to 2\gamma}\,|^2 \quad . \tag{5.6.10}$$

If we use the V-A model described in Section II, we see that confinement may be included in our calculation in a particularly simple manner. Since the confining vertex has the form $\bar{\Gamma}_P(q,p) = \gamma_5 \Gamma_P(q,p)$ for the V-A model, Eq. (5.6.3) is modified to read

$$\hat{I}(k_1, k_2) = i\int \frac{d^4p}{(2\pi)^4}\Gamma_P(q,p)\ \frac{1}{p^2 - m^2 + i\epsilon}\ \frac{1}{(p-q)^2 - m^2 + i\epsilon}\ \frac{1}{(p-k_1)^2 - m^2 + i\epsilon}\ , \tag{5.6.11}$$

and may be evaluated in the frame where $\vec{q} = 0$. Note that $\Gamma_P(q^0, |\vec{p}|)$ is zero when the quark and antiquark at the η' vertex go on their positive mass shells, simultaneously. [See Fig. 5.12.]

Our evaluation proceeds by completing the integral in Eq. (5.6.11) over p^0 in the complex p^0 plane. We also use the representation of the quark propagators given in Eq. (5.3.5). With reference to Eq. (5.3.5), we may define $S(p) = S^{(+)}(p) + S^{(-)}(p)$. Since there are three propagators to consider in Eq. (5.6.1), we obtain eight terms to be evaluated. For the evaluations of $\hat{I}(k_1, k_2)$, the contour is closed either in the upper or lower p^0 plane depending upon which region has the fewer singularities. There is one term with three $S^{(+)}$ factors, and another with three $S^{(-)}$ factors, that do not contribute to the result. Thus, in a pictorial representation we would have six distinct (Goldstone) diagrams, where each quark line may be identified as either a quark or an antiquark. In Fig. 5.12b we introduce the vertex function of our V-A model of confinement. There, the shaded triangular area denotes the confinement vertex function $\Gamma_P(q^0, |\vec{p}|)$ in the frame where $\vec{q} = 0$.

In the evaluation of the diagrams of Fig. 5.12b, when first integrating over p^0, we find a factor $[q^0 - 2E(\vec{p}) + i\epsilon]^{-1}$. However, in evaluating the diagrams of Fig. 5.12a we find the factor of $\Gamma_P(q^0, |\vec{p}|)[q^0 - 2E(\vec{p})]^{-1}$, which is a real, nonsingular function. (Recall that $\Gamma_P(q^0, |\vec{p}|) = 0$ when $q^0 = 2E(\vec{p})$, so that we may drop the $i\epsilon$, as seen previously.)

The results of our calculations are given in Table 5.4. We find very good agreement between experiment and theory for $T_{\eta'} \to 2\gamma$, while the calculated value of $T_{\eta} \to 2\gamma$ is just slightly outside the range of values for that quantity as determined by experiment. [See the caption to Table 5.4.]

5.7. Meson Decay Constants

The calculation of a meson decay constant is made by evaluating the diagram shown in Fig. 5.13. We write, with the propagators being matrices in flavor space,

$$iq^{\mu}\tilde{f}_i = in_c g_{iqq} \int \frac{d^4k}{(2\pi)^4} \mathrm{Tr}\left[\gamma^{\mu}\gamma_5 \frac{\lambda^i}{2} S(q/2+k) i\gamma_5 \lambda^i S(-q/2+k)\right] \quad . \tag{5.7.1}$$

Here, the trace is over flavor and Dirac indices. Thus, upon dropping the factors that come from the flavor trace, we may consider the integral

$$f_i(q^2) = \frac{ig_{iqq}}{q^2} \int \frac{d^4k}{(2\pi)^4} \mathrm{Tr}\left[\not{q}\gamma_5 S_{m_1}(q/2+k)\gamma_5 S_{m_2}(-q/2+k)\right] \quad , \tag{5.7.2}$$

where we have written the result for two different masses, m_1 and m_2. (At a later point, we can combine the various $f_i(q^2)$, using the appropriate flavor factors, and mixing angles.) To include confinement, we replace one γ_5 by $\bar{\Gamma}(q,k)$ to obtain

$$\hat{f}_i = \frac{ig_{iqq}}{q^2} \int \frac{d^4k}{(2\pi)^4} \mathrm{Tr}\left[\not{q}\gamma_5 S_{m_1}(q/2+k)\bar{\Gamma}(q,k) S_{m_2}(-q/2+k)\right] \quad . \tag{5.7.3}$$

We then write $S_{m_1} = S^{(+)}_{m_1} + S^{(-)}_{m_1}$, as before. [See Eq. (5.3.5).] Thus,

$$\hat{f}_i = -i\frac{g_{iqq}}{q^2}\int\frac{d^4k}{(2\pi)^4}\mathrm{Tr}\left\{\not{q}\gamma_5\left[\frac{\Gamma^{+-}(q,k)\Lambda_1^{(+)}(\vec{k})\gamma_5\Lambda_2^{(-)}(-\vec{k})}{\left(q^0/2+k^0-E_1(\vec{k})\right)\left(-q^0/2+k^0+E_2(\vec{k})\right)}\right.\right. \tag{5.7.4}$$

$$\left.\left.+\frac{\Gamma^{-+}(q,k)\Lambda_1^{(-)}(-\vec{k})\gamma_5\Lambda_2^{(+)}(\vec{k})}{\left(q^0/2+k^0+E_1(\vec{k})\right)\left(-q^0/2+k^0-E_2(\vec{k})\right)}\right]\right\},$$

or

$$\hat{f}_i = \frac{g_{iqq}}{q^2}\int\frac{d^3k}{(2\pi)^3}\mathrm{Tr}\left[\frac{\Gamma^{+-}(q,k)\not{q}\gamma_5\Lambda^{(+)}(\vec{k})\gamma_5\Lambda_2^{(-)}(-\vec{k})}{q^0-E_1(\vec{k})-E_2(\vec{k})}\right. \tag{5.7.5}$$

$$\left.-\frac{\Gamma^{-+}(q,k)\not{q}\gamma_5\Lambda_1^{(-)}(-\vec{p})\gamma_5\Lambda_2^{(+)}(\vec{k})}{q^0+E_1(\vec{k})+E_2(\vec{k})}\right].$$

Finally, we have, for $\vec{q}=0$,

$$\hat{f}_i = -\frac{g_{iqq}}{q^0}\int\frac{d^3k}{(2\pi)^3}\left[\frac{m_i}{E_1(\vec{k})}+\frac{m_2}{E_2(\vec{k})}\right] \tag{5.7.6}$$

$$\times\left[\frac{\Gamma^{+-}(q^0,|\vec{k}|)}{q^0-E_1(\vec{k})-E_2(\vec{k})}+\frac{\Gamma^{-+}(q^0,|\vec{k}|))}{q^0+E_1(\vec{k})+E_2(\vec{k})}\right],$$

where q^0 is the mass of the meson considered.

Equation (5.7.6) is needed to calculate f_K. For f_π, f_η and $f_{\eta'}$, we may take $m_1=m_2$, when using Eq. (5.7.6). The various g_{iqq} may be found in Tables 2 and 3 where we also give the results obtained for the decay constants.

We note that we can obtain f_η and $f_{\eta'}$ in terms of amplitudes for the decay of the η^0 and η^8 mesons. For example, we may define q^2-dependent amplitudes for η^0 and η^8

decay, $F_{\eta^0}(q^2)$ and $F_{\eta^8}(q^2)$, which do not contain the coupling constants. Then, we use $\theta(q^2)$ to write

$$f_\eta = g_{\eta qq}\left[\cos^2\theta(m_\eta^2)F_{\eta^8}(m_\eta^2) + \sin^2\theta(m_\eta^2)F_{\eta^0}(m_\eta^2)\right] \tag{5.7.7}$$

and

$$f_\eta' = g_{\eta' qq}\left[\sin^2\theta(m_{\eta'}^2)F_{\eta^8}(m_{\eta'}^2) + \cos^2\theta(m_{\eta'}^2)F_{\eta^0}(m_{\eta'}^2)\right] \ . \tag{5.7.8}$$

We see that, in the absence of mixing, $g_{\eta qq}$ and f_η go over to $g_{\eta^0 qq}$ and f_{η^0}. We recall that mixing is quite important for the calculation of $f_{\eta'}$, since the mixing angle for the V-A model is $\theta(m_{\eta'}^2) = -28.56^0$. [See Fig. 13.]

Some experimental values for f_π, f_η and $f_{\eta'}$ are given on page 320 of Ref. [Ba96]. These are $f_{\pi^0} = 84 \pm 3$ MeV, $f_\eta = 94 \pm 7$ MeV, and $f_{\eta'} = 89 \pm 5$ MeV [Be91]. Other values obtained in a different experiment, are $f_\eta = 91 \pm 6$ and $f_{\eta'} = 78 \pm 5$ MeV [Ai90]. However, large uncertainties arise due to a need to extrapolate the current algebra results to the physical mass of the η and η'. In addition, for the η and η', there is further uncertainty due to the lack of knowledge concerning the mixing angle.

5.8. Discussion

One goal of this work was to calculate the rates for $\eta \to 2\gamma$ and $\eta' \to 2\gamma$ in a generalized NJL model that includes a model of confinement. We found a very good result for $\eta' \to 2\gamma$, while our result for $\eta \to 2\gamma$ was just slightly larger than the range of the experimental values. [See Table 5.4.] The values found for the meson masses are satisfactory. However, the decay constants obtained in the V-A model are significantly better than those of the vector confinement model. [See Tables 5.2 and 5.3.] We note, once again, that we have only changed G_S relative to the value given in Ref. [Vo91]. (Our value for κ was taken from our earlier work and was not adjusted to improve our fit to the data.)

Previously, we have seen in Section II that it is possible to do Euclidean momentum-space calculations that preserve the chiral symmetry of the Lagrangian. It remains to be seen whether our Minkowski-space calculations can be improved so as to preserve chiral symmetry. In general, that requires the use of momentum-dependent self-energies, as was seen in Section II.

Work related to ours has been presented in [Sa97]. There, a study is made of the masses and electromagnetic form factors of the pion and the kaon. The calculation is made in Euclidean space, using a phenomenological form for a non-perturbative gluon propagator. The form chosen gives rise to confinement in the sense that the quark propagator has no on-mass-shell singularities in Minkowski space. (That treatment of confinement differs from ours. Our approach is more closely related to the methods introduced by Gross and Milana [Gr91,Gr92].) The results obtained in Ref. [Sa97],

using a Euclidean momentum space, were extrapolated into the physical region. Good results were reported for various observables using a limited number of parameters.

Finally, we remark that, while the V-A model yields good results for the transition amplitudes for $\eta \to 2\gamma$ and $\eta' \to 2\gamma$, we do not claim that the V-A model will be generally useful for the study of confinement in all light meson systems. However, if we limit ourselves to the consideration of scalar or pseudoscalar mesons, the V-A model appears to be useful on a purely phenomenological level. (We recall that the meson decay constants of the V-A model were much improved when compared to those of the Lorentz-vector confinement model.) However, it appears that the model of Lorentz-vector confinement is the model of choice, if one is to make contact with recent theoretical developments [Sz97].

5.9. Appendix A Lorentz-Vector Confinement

In this appendix we discuss the vertex operator of the confining field for the case of Lorentz-vector confinement. With reference to Fig. 3.1, we may write

$$\bar{\Gamma}(q,k) = \gamma_5 - i\int \frac{d^4k'}{(2\pi)^4}\left[\gamma^\mu S(q/2+k')\bar{\Gamma}(q,k)S(-q/2+k')\gamma_\mu V^C(k-k')\right] \quad . \quad (5.9.1)$$

Here $S(p) = [\not{p} - m_u + i\epsilon]^{-1}$, if we consider an up quark and an up antiquark at the vertex. We have defined Γ^{+-} and Γ^{-+} such that

$$\Lambda^{(+)}(\vec{k})\bar{\Gamma}(q,k)\Lambda^{(-)}(-\vec{k}) = \Gamma^{+-}(q,k)\Lambda^{(+)}(\vec{k})\gamma_5\Lambda^{(-)}(-\vec{k}) \quad , \quad (5.9.2)$$

and

$$\Lambda^{(-)}(-\vec{k})\bar{\Gamma}(q,k)\Lambda^{(+)}(\vec{k}) = \Gamma^{-+}(q,k)\Lambda^{(-)}(-\vec{k})\gamma_5\Lambda^{(+)}(\vec{k}) \quad . \quad (5.9.3)$$

Recall that $\Lambda^{(+)}(\vec{k})$ and $\Lambda^{(-)}(-\vec{k})$ were defined in Eqs. (5.3.6) and (5.3.7). (See also Eq. (5.3.5).) The analysis proceeds by multiplying Eq. (5.9.1) from the left by $\gamma_5\Lambda^{(+)}(\vec{k})$ and from the right by $\Lambda^{(-)}(-\vec{k})$ and using Eq. (5.3.5) for the two quark propagators. At that point, we form the trace of the equation. If we divide the equation by $\mathrm{Tr}[\gamma_5\Lambda^{(+)}(\vec{k})\gamma_5\Lambda^{(-)}(-\vec{k})]$, we obtain an equation for $\Gamma^{+-}(q,k)$, which involves both $\Gamma^{+-}(q,k')$ and $\Gamma^{-+}(q,k')$ on the right-hand side. We neglect the coupling of $\Gamma^{+-}(q,k)$ to $\Gamma^{-+}(q,k)$. In that approximation $\Gamma^{+-}(q,k)$ satisfies an uncoupled equation, as does $\Gamma^{-+}(q,k)$. The neglect of the coupling term is equivalent to the neglect of "Z graphs", or pair-current effects. In the case of the V-A model described in Appendix B, these pair-current effects are rather small and there is not too much difference between the solution of the coupled equations and the solutions of the

uncoupled equation. On the other hand, such effects are quite large in the case of Lorentz-vector confinement and they create major problems, if one attempts to solve the coupled equations. Since the probability of the confining potential to excite pair currents is unknown, it is not unreasonable to neglect such effects in the Lorentz-vector confinement model.

Our procedure then requires that we complete the k_0' integral in the lower half of the complex k_0' plane, picking up only the pole where the quark goes on its positive mass shell. The resulting integral equation is depicted in Fig. 5.3c, where a cross on a quark line indicates that the quark is on its positive mass shell. The equation, in the frame where $\vec{q}=0$, is found to be

$$\Gamma^{+-}(q^0, |\vec{k}|) = 1 - \int \frac{d^3k'}{(2\pi)^3} \frac{V^C(\vec{k}-\vec{k}')}{q^0 - 2E(\vec{k}')} \frac{m^2 - 2E(\vec{k})E(\vec{k}')}{E(\vec{k})E(\vec{k}')} \Gamma^{+-}(q^0, |\vec{k}'|) \tag{5.9.4}$$

for the equal mass case.

To obtain the corresponding equation for $\Gamma^{-+}(q^0, |\vec{k}|)$, we multiply Eq. (5.9.1) by $\gamma_5 \Lambda^{(-)}(-\vec{k})$ from the left and $\Lambda^{(+)}(\vec{k})$ from the right and then take the trace of the equation. In this case, we divide the equation by $\mathrm{Tr}[\gamma_5 \Lambda^{(-)}(-\vec{k})\gamma_5 \Lambda^{(+)}(\vec{k})]$ to obtain an equation for $\Gamma^{-+}(q^0, |\vec{k}|)$. The integral over k_0' is completed in the lower-half k_0' plane, where we pick up only the pole that has the antiquark on its negative mass shell. The resulting (uncoupled) equation for $\Gamma^{-+}(q^0, |\vec{k}|)$ is

$$\Gamma^{-+}(q^0, |\vec{k}|) = 1 + \int \frac{d^3k'}{(2\pi)^3} \frac{V^C(\vec{k}-\vec{k}')}{q^0 + 2E(\vec{k}')} \frac{m^2 - 2E(\vec{k})E(\vec{k}')}{E(\vec{k})E(\vec{k}')} \Gamma^{-+}(q^0, |\vec{k}'|) \quad . \tag{5.9.5}$$

For completeness, we record the coupled equations obtained when we pick up both poles in the lower complex k_0' plane. These have the quark going on its positive mass shell and the antiquark on its negative mass shell. We find

$$\begin{bmatrix} \Gamma^{+-}(q^0, |\vec{k}|) \\ \Gamma^{-+}(q^0, |\vec{k}|) \end{bmatrix} = \begin{bmatrix} 1 \\ 1 \end{bmatrix} - \int \frac{d^3k'}{(2\pi)^3} \frac{V^C(\vec{k}, \vec{k}')}{E(\vec{k})E(\vec{k}')}$$

$$\times \begin{bmatrix} \dfrac{m^2 - 2E(\vec{k})E(\vec{k}')}{q^0 - 2E(\vec{k}')} & \dfrac{m^2 + 2E(\vec{k})E(\vec{k}')}{q^0 + 2E(\vec{k}')} \\ -\dfrac{m^2 + 2E(\vec{k})E(\vec{k}')}{q^0 - 2E(\vec{k}')} & -\dfrac{m^2 - 2E(\vec{k})E(\vec{k}')}{q^0 + 2E(\vec{k}')} \end{bmatrix} \begin{bmatrix} \Gamma^{+-}(q^0, |\vec{k}'|) \\ \Gamma^{-+}(q^0, |\vec{k}'|) \end{bmatrix} . \tag{5.9.6}$$

One may compare the matrix element that couples Γ^{+-} to Γ^{-+} with the element that couples Γ^{+-} to itself. [See Eq. (5.9.6).] In this manner, one can see the very large amplitude for exciting "pair currents" (or Z-graphs) in the case of Lorentz-vector confinement. That is, $m^2 + E(\vec{k})E(\vec{k}') \gg m^2 - E(\vec{k})E(\vec{k}')$, making the off-diagonal term quite important.

Solutions of Eqs. (5.9.4) and (5.9.5) are shown in Figs. 5.2 and 5.3, respectively. For our calculations, we used κ=0.05 GeV^2 and μ=0.020 GeV. The results shown are obtained for the up quark, with $m_u = 0.364$ GeV. Other sets of curves were obtained for the strange quark ($m_s = 0.522$ GeV) and for the case where we have an up quark and a strange antiquark at the vertex. In the latter case, Eq. (5.9.4) and (5.9.5) were generalized to take into account the unequal masses of the quark and antiquark.

5.10. Appendix B The V-A Model

In this appendix we review some results of [Ce97b]. A particularly simple model of confinement is obtained if we use a V-A form,

$$\bar{V}(x-y) = V^C(x-y)\left[\gamma^\mu(1)\gamma_\mu(2) - \gamma^\mu(1)\gamma_5(1)\gamma_\mu(2)\gamma_5(2)\right] , \qquad (5.10.1)$$

where symbols with a bar have a Dirac matrix structure. If we use Eq. (5.10.1), the vertex associated with the confinement potential may be written as $\bar{\Gamma}_P(q,k) = \gamma_5\Gamma_P(q,k)$, or in the frame where $\vec{q}=0$, we may put $\bar{\Gamma}_P(q^0, |\vec{k}|) = \gamma_5\Gamma_P(q^0, |\vec{k}|)$. We found the equation for $\Gamma_P(q^0, |\vec{k}|)$ to be

$$\Gamma_P(q^0, |\vec{k}|) = 1 + 4\int \frac{d^3k'}{(2\pi)^3} \frac{4E(\vec{k}')}{(q^0)^2 - [2E(\vec{k}')]^2} V^C(\vec{k}-\vec{k}')\Gamma_P(q^0, |\vec{k}'|) ,$$

(5.10.2)

when the particles entering and leaving the vertex have the same mass [Ce97b]. For the study of the kaon, we need to generalize Eq. (5.10.2). We take the quark to have mass m_1 and the antiquark to have mass m_2. Then,

$$\Gamma_P(q,k) = 1 - \int \frac{d^3k'}{(2\pi)^3} \left\{ \frac{8\left[-q^0E_1(\vec{k}') + m_1^2 - m_1m_2\right]}{2E_1(\vec{k}')\left[q^0 - E_1(\vec{k}') + E_2(\vec{k}')\right]} \frac{1}{q^0 - \left[E_1(\vec{k}') + E_2(\vec{k}')\right]} \right.$$

$$\left. + \frac{8\left[q^0E_2(\vec{k}') + m_2^2 - m_1m_2\right]}{2E_2(\vec{k}')\left[q^0 + E_2(\vec{k}') - E_1(\vec{k}')\right]} \frac{1}{q^2 + E_1(\vec{k}') + E_2(\vec{k}')} \right\} V^C(\vec{k}-\vec{k}')\Gamma_P(q,k')$$

(5.10.3)

This result reduces to that of Eq. (5.10.2), if $m_1 = m_2$. (For the kaon, $m_1 = m_u$ and $m_2 = m_s$.)

We have found that the neglect of "pair-current" effects provides a useful approximation. To study that case, we write Eq. (5.10.2) as

$$\Gamma_P(q^0, |\vec{k}|) = 1 + 4\int \frac{d^3k'}{(2\pi)^3}\left[\frac{1}{q^0 - 2E(\vec{k}')} - \frac{1}{q^0 + 2E(\vec{k}')}\right] V^C(\vec{k}-\vec{k}')\Gamma_P(q^0, |\vec{k}'|) \quad . \tag{5.10.4}$$

If we neglect the second term in the bracket, we have the following simple equation

$$\Gamma_P(q^0, |\vec{k}|) = 1 + 4\int \frac{d^3k'}{(2\pi)^3}\frac{V^C(\vec{k}-\vec{k}')}{q^0 - 2E(\vec{k}')}\Gamma_P(q^0, |\vec{k}'|) \quad . \tag{5.10.5}$$

In the present study we will make use of Eq. (5.10.5) when we consider the V-A model.

The vertex functions obtained from the solution of Eqs. (5.10.4) and (5.10.5) are shown in Figs. 5.14 and 5.15, respectively. It is seen that the inclusion of the second term of Eq. (5.10.4) mainly affects the low-energy behavior of $\Gamma_P(q^0, |\vec{k}|)$. That feature may be readily understood by comparing the structure of Eqs. (5.10.4) and (5.10.5).

Coupling Constants	Vector Confinement	V-A confinement model
G_S	21.53 GeV^{-2}	23.05 GeV^{-2}
G_D	-239.1 GeV^{-5}	-239.1 GeV^{-5}
G_π	12.82 GeV^{-2}	13.58 GeV^{-2}
G_K	12.59 GeV^{-2}	13.35 GeV^{-2}
G_{η^0}	6.964 GeV^{-2}	7.726 GeV^{-2}
G_{η^8}	12.51 GeV^{-2}	13.27 GeV^{-2}
G_{08}	0.108 GeV^{-2}	0.108 GeV^{-2}

Table 5.1. The various coupling constants used in this work are given. The condensate values are $<\bar{u}u> = <\bar{d}d> = -(0.248\ \text{GeV})^3 = -0.01525\ \text{GeV}^3$ and $<\bar{s}s> = -(0.258\ \text{GeV})^3 = -0.01717\ \text{GeV}^3$. Also, $m_u = m_d = 0.364$ GeV and $m_s = 0.522$ GeV. The values of G_D, m_u, m_d, m_s, $<\bar{u}u>$, $<\bar{d}d>$ and $<\bar{s}s>$ are the same as those used in Ref. [Vo91].

Lorentz-vector confinement model				
Meson	Mass (Expt.) [MeV]	Mass (Calculated) [MeV]	Coupling constant	Meson decay constant
π	π^+ 139.5 π^0 135.0	138	$g_{\sigma qq} = 4.74$	$f_\pi = 102$ MeV
K	K^+ 493.7 K^0 497.7	445	$g_{Kqq} = 4.72$	$f_K = 84.0$ MeV
η	547	490	$g_{\eta qq} = 4.04$	$f_\eta = 72.3$ MeV
η'	958	979	$g_{\eta' qq} = 2.87$	$f_{\eta'} = 92.7$ MeV

Table 5.2. Calculated values of the meson masses, quark-meson coupling constants and meson decay constants are given. The parameters used are μ=0.020 GeV, $G_S = 21.53$ GeV^{-2}, $G_D = -239.1$ GeV^{-5}, $m_u = m_d = 364$ MeV, $m_s = 522$ MeV, $\Lambda_3 = 0.622$ GeV, and $\kappa = 0.20/4$ GeV^2. We find that $\theta(m_\eta^2) = -5.60^0$ and $\theta(m_{\eta'}^2) = -29.2^0$. (The pion decay constant in the absence of confinement is calculated to be $f_\pi = 93.3$ MeV.)

V-A confinement model			
Meson	Mass (calculated) [MeV]	Coupling constant	Meson decay constant
π	138	$g_{\sigma qq} = 5.23$	$f_{\pi} = 102$ MeV
K	527	$g_{Kqq} = 5.19$	$f_{K} = 110$ MeV
η	571	$g_{\eta qq} = 5.33$	$f_{\eta} = 101$ MeV
η'	1071	$g_{\eta' qq} = 3.59$	$f_{\eta'} = 106$ MeV

Table 5.3. Calculated values of meson masses, coupling constants and meson decay constants for the V-A model. Here $G_S = 23.05$ GeV^{-2} and $G_D = -239.1$ GeV^{-5}. (See caption to Table 5.2.) The mixing angles are $\theta(m_{\eta}^2) = -6.02^0$ and $\theta(m_{\eta'}^2) = -28.6^0$ for the V-A model. Here κ=0.20/8 GeV^2.

	Experiment	Calculated
$T_{\eta\to 2\gamma}$	$2.38 \pm 0.25 \times 10^{-2}$ GeV^{-1}	2.73×10^{-2} GeV
$\Gamma_{\eta\to 2\gamma}$	0.46 ± 0.04 keV	0.609 keV
$T_{\eta'\to 2\gamma}$	$3.13 \pm 0.25 \times 10^{-2}$ GeV^{-1}	3.06×10^{-2} GeV^{-1}
$\Gamma_{\eta'\to 2\gamma}$	4.26 ± 0.25 keV	4.09 keV

Table 5.4. Calculated and experimental values of the amplitudes and widths for the processes $\eta\to 2\gamma$ and $\eta'\to 2\gamma$. The V-A confinement model is used. (Here κ=0.20/8 GeV^2.) Note that for the quantities defined in Eqs. (5.6.7) and (5.6.8) we have $F(u,\eta) = 2.62$ GeV^{-1}, $F(s,\eta) = 1.90$ GeV^{-1}, $F(u,\eta') = 3.73$ GeV^{-1} and $F(s,\eta') = 2.22$ GeV^{-1}. The experimental values for $\Gamma_{\eta\to 2\gamma}$ and $\Gamma_{\eta'\to 2\gamma}$ are taken from [Ba96].

VIII. Figure Captions

Fig. 2.1 (a) The figure shows the contributions to the quark self-energy, $\Sigma(k)$. Here the double line represents the quark propagator, $iS(k') = i\left[\not{k} - \Sigma(k') + i\epsilon\right]^{-1}$ and the wavy line is the confining interaction. (As a diagrammatic element, the wavy line introduces $-iV^C(k-k')$ when evaluating the diagram. The filled circle denotes a factor of iG_S.)

(b) The equation for the quark propagator is given in terms of the self-energy, $\Sigma(k)$, seen in Fig. 2.1a. The single line is the propagator of a massless quark in this figure.

Fig. 2.2 Values of $A(k^2)$ are shown for $k^2 \leq 0$. The calculations are made in Euclidean momentum space using a regulator function, $C(k^2) = 2\Lambda^4[k^2 + A^2(k^2) + \Lambda^2]^{-1}[k^2 + A^2(k^2) + 2\Lambda^2]^{-1}$, with $\Lambda = 0.78$ GeV. Here $\kappa = -0.14/8$ GeV^2 and $G_s = 8.30$ GeV^{-2}.

Fig. 2.3 The integral equation for a vertex function of the confining interaction. The filled triangular area denotes the vertex functions. [We may write integral equations for either $F_S(q,k)$ or $F_P(q,k)$.] Here the wavy line is the confining interaction $V^C(k-k')$. The resulting equation is solved with either the quark on its positive mass shell or the antiquark on its negative mass shell. [See the text.] The double line denotes the propagator $iS(k+q/2) = i\left[\not{k} + \not{q}/2 - A_+(q,k)\right]^{-1}$ or $iS(k-q/2) = i\left[\not{k} - \not{q}/2 - A_-(q,k)\right]^{-1}$.

Fig. 2.4 The function $\Gamma_S(q^0, |\vec{k}|)$ is shown for $\kappa = 0.0175$ GeV^2 and various values of q^0. Note that $\Gamma_S(q^0, |\vec{k}_{on}|) = 0$, when $\vec{k}_{on}^2 = (q^0/2)^2 - m_q^2$. Starting at the lowest curve and moving higher, we have $q^0 = 0.7$ GeV, $q^0 = 0.6$ GeV, $q^0 = 0.5$ GeV, $q^0 = 0.4$ GeV, $q^0 = 0.3$ GeV, $q^0 = 0.2$ GeV, and $q^0 = 0.0$ GeV. (The values for $q^0 = 0.1$ GeV are quite close to those for $q^0 = 0.0$ GeV.) The results are for a constant mass, $m_q = 260$ MeV. If m_q is replaced by $A(k^2)$ only some small changes are observed near $|\vec{k}| = 0$. A cutoff on the three-momenta has been used ($|\vec{k}'| < \Lambda_3$), with $\Lambda_3 = 0.702$ GeV. [See the text.]

Fig. 2.5 The equation satisfied by the pseudoscalar-isovector vertex of the total interaction, $F_T(q, k)$, is shown as a crosshatched triangular area. The wavy line is the confining interaction, $V^C(k - k')$, and the filled circle represents a factor of iG_S. The driving term for this equation $\gamma_5 \tau^i$. [See Eqs. (2.5.1) and (2.5.2).]

Fig. 2.6 Solutions of the coupled equations for $A(k^2)$ and $B(k^2)$, generalized to include a current mass, $m_q^0 = 5.5$ MeV, are shown. [See Eqs.(2.8.1) and (2.8.2).] Here we use vector confinement with $k = -0.14/4$ GeV^2 and $G_s = 8.65$ GeV^{-2}. (For this calculation we have used a Pauli-Villars regularization procedure. See caption of Fig. 2.2)

Fig. 3.1 (a) The diagram represents the equation for the vertex, $\bar{\Gamma}_S(q, k)$, that sums a series of confining interactions. These interactions are shown here as dashed lines.

(b) A perturbative expansion for $\bar{\Gamma}_S(q,k)$ is shown.

(c) The vertex $\Gamma_S^{*-}(q,k)$ is obtained in our analysis when the quark is on its mass shell. (Here the cross denotes a quark on its positive mass shell.)

(d) A perturbative expansion for $\Gamma_S^{*-}(q,k)$ is shown. The dashed line introduces a factor $-iV^C(k-k')\gamma^\mu(1)\gamma_\mu(2)/4$ when applying the Feynman rules in the evaluation of the diagrams.

Fig. 3.2 Values of $\Gamma_S^{*-}(q^0, |\vec{k}|)$ are shown. Starting from the uppermost curve and moving downward, the values of q^0 are 0, 0.10, 0.20, 0.30, 0.40, 0.50, 0.55, and 0.60 MeV. For the last two of these curves, $\Gamma_S^{*-}(q^0, |\vec{k}_{on}|) = 0$. Here $\vec{k}_{on}^2 = (q_0/2)^2 - m_q^2$, $m_q = 0.260$ GeV, $\mu = 0.030$ GeV and $\kappa = 0.20$ GeV^2.

Fig. 3.3 Values of $\Gamma_S^{*-}(q^0, |\vec{k}|)$ are shown. Starting with the uppermost curve and moving downward, the values of q^0 are 0, 0.4, and 0.6 GeV. (Here $m_q = 0.260$ GeV, $\mu = 0.030$ GeV, and $\kappa = 0.20$ GeV^2.)

Fig. 3.4 (a) The zero-range quark interaction of the NJL model is shown.

(b) The quark-loop integral in the scalar-isoscalar channel is shown.

(c) The quark-loop integral including a series of confining interactions (dashed line) is shown. The filled triangular region denotes the vertex function that serves to sum the ladder of confining interactions.

(d) The function $K_S(q^2)$ describes effects of coupling to the two-pion continuum.

(e) The function $\hat{K}_S(q^2)$ includes two confinement vertex functions and has a cut for $q^2 > 4m_\pi^2$.

Fig. 3.5 The quark-quark T matrix, $t_{qq}(q^2)$, is obtained by summing the diagrams shown. The t-channel exchanges are summed by the expression given as Eq. (3.3.9). In a limited region of $q^2(-0.25\ \text{GeV}^2 < q^2 < 0)$, these effects are well represented by the exchange of an effective sigma meson with $m_\sigma = 540$ MeV.

Fig. 3.6 The figure shows $J_S(q^2)$ and $\hat{J}_S(q^2)$ calculated for $q^2 \geq 0$. (We use a cutoff on the three-momenta in the loop integral of $|\vec{k}| \leq \Lambda_3$, with $\Lambda_3 = 0.689$ GeV.) The dotted curve is the result in the absence of confinement and the solid line shows $\hat{J}_S(q^2)$ for Lorentz-vector confinement with $\kappa = 0.20\ \text{GeV}^2$. For the dotted curve ($\kappa$=0) we have $G_S = 7.91\ \text{GeV}^{-2}$ and for the solid curve ($\kappa = 0.20\ \text{GeV}^2$) we have $G_S = 8.516\ \text{GeV}^{-2}$. Without confinement we find $m_\sigma = 540$ MeV, while, with confinement included, we find $m_\sigma = 800$ MeV. The horizontal dashed lines represent G_S^{-1} for the two cases. The intersection of the appropriate dashed line with the dotted or solid lines determines the mass of the sigma. Here $J_S(0) = 0.088\ \text{GeV}^2$ and $\hat{J}_S(0) = 0.0708\ \text{GeV}^2$.

Fig. 3.7 The diagram corresponding to $\mathcal{F}_S(q^2, q\cdot\kappa, \kappa^2)$ is shown. Here, the wavy lines are pions. (The only factors of i introduced in the definition are those from the propagators. [See Eq. (3.4.1).] The diagram is evaluated

for $q^2 > 0$ by first completing the integral over k^0 in the complex k^0 plane.

(a) These diagrams introduce the factor $\Gamma_S^{++}(q, k)$.

(b) These diagrams introduce the factor $\Gamma_S^{--}(q, k)$.

(c) The first diagram introduces a factor of $\Gamma_S^{++}(q, k)$, while the second diagram introduces a factor of $\Gamma_S^{--}(q, k)$.

Fig. 3.8 (a) The diagram that corresponds to $F_1(q^2)$ is shown. Here, the pions are on mass shell, so that $F_1(q^2) = \mathcal{F}_S(q^2, q\cdot\kappa = 0, \kappa^2 = m_\pi^2 - q^2/4)$, where $\mathcal{F}_S(q^2, q\cdot\kappa, \kappa^2)$ is depicted in Fig. 3.7. $F_1(q^2)$ is needed in the evaluation of $\mathrm{Im}\,\hat{K}_S(q^2)$.

(b) The diagram that corresponds to $F_2(\kappa^2)$ is shown, with $F_2(\kappa^2) = \mathcal{F}_S(0, 0, \kappa^2)$.

Fig. 3.9 Values of $F_2(\kappa^2)$ are shown. For $\kappa^2 < 0$ the calculation is made in a Euclidean momentum space with a cutoff $\Lambda_E = 1.0$ GeV. For $\kappa^2 > 0$, the calculation is made in Minkowski space with a cutoff $|\vec{k}| \le \Lambda_3 = 0.816$ GeV placed upon the integration variable. That cutoff is used for loop integrals having three quark propagators.

Fig. 3.10 Values of $\mathrm{Im}\,\hat{K}_S(q^2)$ are shown. Here we use $\kappa = 0.20$ GeV^2, $g_{\pi qq} = 2.58$ and Lorentz-vector confinement. We also have $m_q = 260$ MeV and a cutoff on the three-momenta, $|\vec{k}| \le \Lambda_3$, with $\Lambda_3 = 0.816$ GeV. (Note that the result is quite insensitive to the model

of confinement used.) To obtain the values for $g_{\pi qq} = 2.68$, we need to multiply the values in the figure by $(2.68/2.58)^4 = 1.16$.

Fig. 3.11 Values of $\mathrm{Re}\,\hat{K}_S(q^2)$ obtained from the once-subtracted dispersion relation of Eq. (3.5.6) are shown. Here, $g_{\pi qq} = 2.68$ was used in the calculation of $\mathrm{Im}\,\hat{K}_S(q^2)$. [See Fig. 3.10, which shows $\mathrm{Im}\,\hat{K}_S(q^2)$ calculated for $g_{\pi qq} = 2.58$.]

Fig. 3.12 The dashed line shows $\mathrm{Re}\,\hat{K}_S(q^2)$. [See Fig. 3.11] The dotted line shows the values of $\hat{J}_S(q^2)$ calculated in Minkowski space, with $m_q = 260$ MeV and a cutoff $\Lambda_3 = 0.689$ GeV. The solid line shows $\hat{J}_S(q^2) + \mathrm{Re}\,\hat{K}_S(q^2)$. The dot-dash line shows the value of $G_S^{-1} = (1/8.516)$ GeV^2. The intersection of the solid line with the dot-dash line depicts the solution of the equation $G_S^{-1} - [\hat{J}_S(m_\sigma^2) + \mathrm{Re}\,\hat{K}_S(m_\sigma^2)] = 0$. We find $m_\sigma = 823$ MeV. (For these calculations $\kappa = 0.20$ GeV^2 and $\mu = 0.030$ GeV.)

Fig. 3.13 Values of $\hat{J}_S(q^2) + \mathrm{Re}\,\hat{K}_S(q^2)$ [see Fig. 3.12] and $\mathrm{Im}\,\hat{K}_S(q^2)$ [see Fig. 3.10] are used to form $\mathrm{Re}\,t_{qq}(q^2)$, shown as a solid line, and $\mathrm{Im}\,t_{qq}(q^2)$, shown as a dotted line. (The large dip in the value of $\mathrm{Re}\,t_{qq}(q^2)$ corresponds to the opening of the two-pion continuum at $q^2 = 4m_\pi^2$.)

Fig. 3.14 Values of $|t_{qq}(q^2)|^2$ are shown. [See Fig. 3.13 for $\mathrm{Re}\,t_{qq}(q^2)$ and $\mathrm{Im}\,t_{qq}(q^2)$.]

Fig. 3.15 Values of $|t_{qq}(q^2)|^2$ are shown in an expanded scale relative to that used in Fig. 3.14. The enhanced values for $q^2 \sim 0.7$ GeV^2 correspond to the zero of $\mathrm{Re}\,t_{qq}(q^2)$ at $q^2 = 0.677$ GeV^2. [See Fig. 13.]

Fig. 4.1 (a) The equation for the quark-antiquark T matrix is shown for the case $\hat{K}_S(q^2) = 0$. The circle is the effective interaction. [See Eqs. (4.1)-(4.3) and (c) below.] The filled triangular region denotes the vertex for the confining interaction.

(b) An expansion of the T matrix is given in terms of the effective interaction (circle) and the vacuum-polarization integrals $\hat{J}(q^2)$.

(c) The effective interaction (open circle) is composed of the original (two-quark) NJL interaction and the three-quark 't Hooft interaction.

Fig. 4.2 (a) The diagram represents the function $K_S(q^2)$, which has cuts starting at $q^2 = 4m_u^2$ and at $q^2 = 4m_\pi^2$. The wavy lines denote pions.

(b) The inclusion of the confining vertex defines the function $\hat{K}_S(q^2)$, which has only one cut starting at $q^2 = 4m_\pi^2$.

(c) The calculation of $\mathrm{Im}\hat{K}_S(q^2)$ may be made by placing the pions on mass shell, as denoted by a cross on the wavy line.

(d) A form factor needed in the calculation of the diagram in (c) is shown. (See Ref. [1].)

(e) A form factor needed in the calculation of $\hat{K}_S(0)$ is shown. (See Ref. [1].)

Fig. 4.3 The figure shows $\mathrm{Re}[\det D(q^2)]$ for the case where both $\mathrm{Re}\hat{K}_S(q^2)$ and $\mathrm{Im}\hat{K}_S(q^2)$ are included, as is singlet-octet coupling. The zeros of this function correspond to the states σ_1 and σ_2. The first of these states is predominantly $\sigma^0(1P)$. (The vertical line shows the position of the

singularity at $q^2 = 1.48$ GeV^2 that is due to the presence of a bound state in the confining potential.)

Fig. 4.4 The figure shows $\mathrm{Im}[\det D(q^2)]$.

Fig. 4.5 The figure shows $\mathrm{Re}\,T_{\sigma}(q^2)$ [dashed line] and $\mathrm{Re}\,T_{\sigma'}(q^2)$ [solid line]. The cusp behavior for $q^2 \simeq 4m_{\pi}^2$ is only prominent in $\mathrm{Re}\,T_{\sigma}(q^2)$. Resonances appear at 1.00 GeV and 1.28 GeV, where $\mathrm{Re}\,T_{\sigma}(q^2)$ rises through zero from negative values. (No resonance appears for $\mathrm{Re}\,T_{\sigma'}(q^2)$ in this energy range.) Note that there is no singularity at $q^2 = 1.48$ GeV^2 in the T matrix.

Fig. 4.6 The figure shows $\mathrm{Im}\,T_{\sigma}(q^2)$ [dashed line] and $\mathrm{Im}\,T_{\sigma'}(q^2)$ [solid line].

Fig. 4.7 The figure shows $\mathrm{Re}[\det D(q^2)]$. The solid line is the result obtained when including $\mathrm{Re}\,\hat{K}_S(q^2)$ and $\mathrm{Im}\,\hat{K}_S(q^2)$, as well as singlet-octet coupling. The dashed line is the result with $\hat{K}_S(q^2) = 0$ and in the absence of singlet-octet coupling. The dotted line represents a linear approximation to $\mathrm{Re}[\det D(q^2)]$ (solid line) in the region $q^2 \simeq 0$. For the dotted line, $\mathrm{Re}[\det D(q^2)] \simeq 0.97\left[\left(m_{\sigma}^{eff}\right)^2 - q^2\right]$, with $m_{\sigma}^{eff} = 0.520$ GeV.

Fig. 4.8 (a) The one-boson-exchange (OBE) amplitude due to sigma exchange between nucleons is shown. The large open circles denote the vertex cutoffs of the OBE model.

(b) A representation of sigma exchange in the NJL model based upon the use of a valence-quark nucleon form factor is shown.

(c) The nucleon-nucleon interaction is related to a quark-quark T matrix. A sigma-dominance model of the T matrix is shown in b)

Fig. 5.1 (a) The equation for the quark self-energy, $\Sigma(p^2) = A(p^2) + \not{p}B(p^2)$, is shown. Here V^c denotes the confining field. The double line represents the dressed quark propagator for the theory with SU(2)-flavor symmetry [4].

(b) An equation for the dressed quark propagator is given in terms of the quark self-energy.

(c) The equation for a vertex of a pseudoscalar bound state. The filled circle denotes the interaction of the NJL model that has SU(2)-flavor symmetry.

Fig. 5.2 Values obtained for $\Gamma^{+-}(q^0, |\vec{k}|)$ are shown for Lorentz-vector confinement. We note that $\Gamma^{+-}(q^0, |\vec{k}_{on}|) = 0$, where $k_{on}^2 = (q^0)^2/4 - m_q^2$. (A more general definition is needed for k_{on} when the quark and antiquark have different masses.) Starting with the uppermost curve and moving downward, we have

(a) $q^0 = 0.0$ GeV,

(b) $q^0 = 0.2$ GeV,

(c) $q^0 = 0.4$ GeV,

(d) $q^0 = 0.6$ GeV,

(e) $q^0 = 0.7$ GeV,

(f) $q^0 = 0.8$ GeV.

The calculation is made for the up quark. Here, $m_u = 364$ MeV, $\mu = 0.020$ GeV and $\kappa = 0.20/4$ GeV^2. The values shown are obtained from the solution of Eq. (A4).

Fig. 5.3 Values of $\Gamma^{-+}(q^0, |\vec{k}|)$ ares shown for Lorentz-vector confinement. Here the antiquark is on its negative mass shell. Starting with the uppermost curve and moving downward, we have

(a) $q^0 = 0.0$ GeV,

(b) $q^0 = 0.2$ GeV,

(c) $q^0 = 0.4$ GeV,

(d) $q^0 = 0.6$ GeV,

(e) $q^0 = 0.7$ GeV,

(f) $q^0 = 0.8$ GeV.

The calculation is made for the up quark. Here, we have solved Eq. (A5). (See the caption to Fig. 4.)

Fig. 5.4 Values of $\hat{J}_u(q^2)$, $\hat{J}_s(q^2)$ and $\hat{J}_{us}(q^2)$ are shown. The quark masses are $m_u = 364$ MeV and $m_s = 522$ MeV. Here, the cutoff is $\Lambda_3 = 0.622$ GeV and $\kappa = 0.20/4$ GeV^2. The dotted, dashed, and dot-dash lines represent $J_u(q^2)$, $J_s(q^2)$ and $J_{us}(q^2)$, respectively, and are given in the region where these functions are real.

Fig. 5.5 The figure shows values of $\hat{J}_\pi(q^2)$, $\hat{J}_K(q^2)$, $\hat{J}_{\eta'}(q^2)$ and $\hat{J}_\eta(q^2)$ for Lorentz-vector confinement. The calculation is made for

$m_u = m_d = 364$ MeV and $m_s = 522$ MeV. A cutoff of $\Lambda_3 = 0.622$ GeV is used, $\mu = 0.020$ GeV and $\kappa = 0.20/4$ GeV^2.

Fig. 5.6 The solid lines show the values of $\hat{J}_\pi(q^2)$ and $\hat{J}_K(q^2)$. The dashed line represents $J_K(q^2)$ and the dotted line represents $J_\pi(q^2)$. The latter two curves rise rapidly as the thresholds of the $q\bar{q}$ continuum at $q^2 = (m_u + m_d)^2 = 0.530$ GeV^2 or $q^2 = (m_u + m_s)^2 = 0.785$ GeV^2, are approached. Beyond these thresholds $J_\pi(q^2)$ and $J_K(q^2)$ are complex functions.

Fig. 5.7 Values of $\hat{J}_{\eta^8}(q^2)$ and $\hat{J}_{\eta^0}(q^2)$ are shown. The dashed line represents $J_{\eta^8}(q^2)$ and the dotted line represents $J_{\eta^0}(q^2)$. Beyond $q^2 = (2m_u)^2 = 0.530$ GeV^2, $J_{\eta^8}(q^2)$ and $J_{\eta^0}(q^2)$ are complex functions, while $\hat{J}_\pi(q^2)$ and $\hat{J}_K(q^2)$ remain real.

Fig. 5.8 The functions $d_{\eta'}(q^2)$ and $d_\eta(q^2)$ are shown for the case of vector confinement. [See Eqs. (5.5.24) and (5.5.25).]

Fig. 5.9 The values of the determinant of the matrix $D(q^2)$ are shown as a solid line. The dotted line is the result when the $\eta^0 - \eta^8$ mixing is neglected ($G_{08} = \hat{J}_{08}(q^2) = 0$). Note that the relations $\det D(m_\eta^2) = 0$ and $\det D(m_{\eta'}^2) = 0$ provide the values of the masses of the η and η' mesons.

Fig. 5.10 The mixing angle, $\theta(q^2)$, is shown for the case of vector confinement. We find $\theta(m_\eta^2) = -5.60^0$ and $\theta(m_{\eta'}^2) = -29.2^0$. [See Table 5.2.]

Fig. 5.11 The experimental values and the calculated values of the meson masses are shown. (See Tables 5.2 and 5.3.) Here the pion mass is used to fix the

value of the parameter G_S. The other mass values are predictions of the model.

Fig. 5.12 The triangle (anomaly) diagram that describes the decays $\pi \to 2\gamma$, $\eta \to 2\gamma$, $\eta' \to 2\gamma$. Here k_1 and k_2 are the momenta of the on-mass-shell photons.

(a) These diagrams appear in the absence of a model of confinement. For the η', the diagrams would yield complex amplitudes due to the quark and antiquark going on their positive mass shells, simultaneously.

(b) The triangle diagrams are shown including the confining vertex $\bar{\Gamma}_P(q,p)$ of the V-A confinement model.

Fig. 5.13 The diagram shown forms the basis of the calculation of the meson decay constant. Here g_{iqq} is either $g_{\pi qq}$, g_{Kqq}, $g_{\eta qq}$ or $g_{\eta' qq}$. The shaded area is the confinement vertex $\bar{\Gamma}(q,k)$. [See Tables 5.2 and 5.3.]

Fig. 5.14 The function $\Gamma_P(q^0, |\vec{k}|)$ is shown for the V-A model. Here we have solved Eq. (B4) of Appendix B. The calculation is made for $m_q = 0.364$ GeV and $\kappa = 0.20/8$ GeV^2. (No cutoff is needed for the three-dimensional integral, which is convergent.) Here we solve the coupled equations that include "Z graphs" (or pair currents). The values of q^0, starting at the uppermost curve and moving down, are $q^0 = 0.0$ GeV, $q^0 = 0.2$ GeV, $q^0 = 0.4$ GeV, $q^0 = 0.6$ GeV, $q^0 = 0.7$ GeV, and $q^0 = 0.8$ GeV.

Fig. 5.15 Similar caption to that of Fig. 14, except that we have solved Eq. (B5). Here, we neglect pair-current (or "Z graph") effects. These effects are only significant for small values of q^0. [Compare Figs. 14 and 15.]

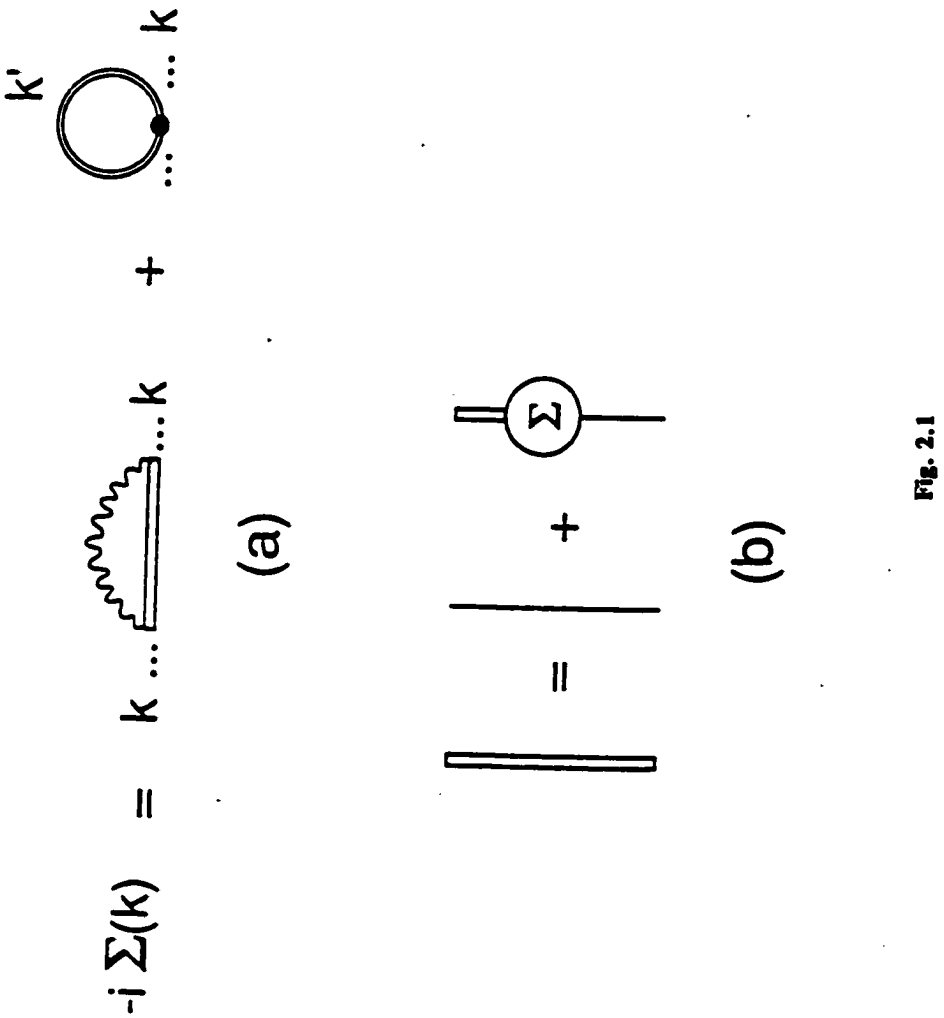

Fig. 2.1

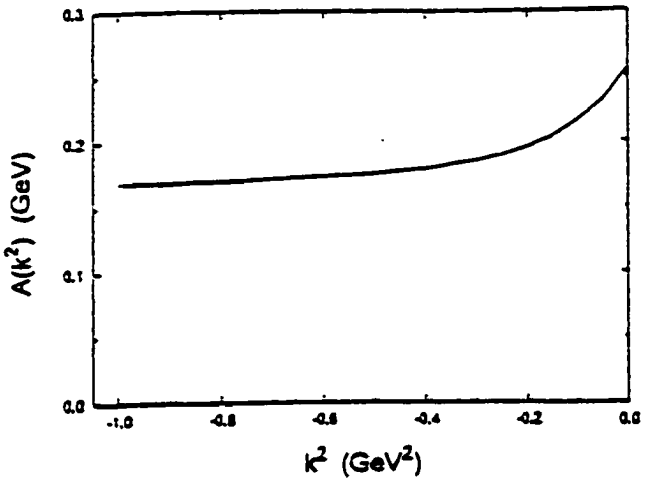

Fig. 2.2

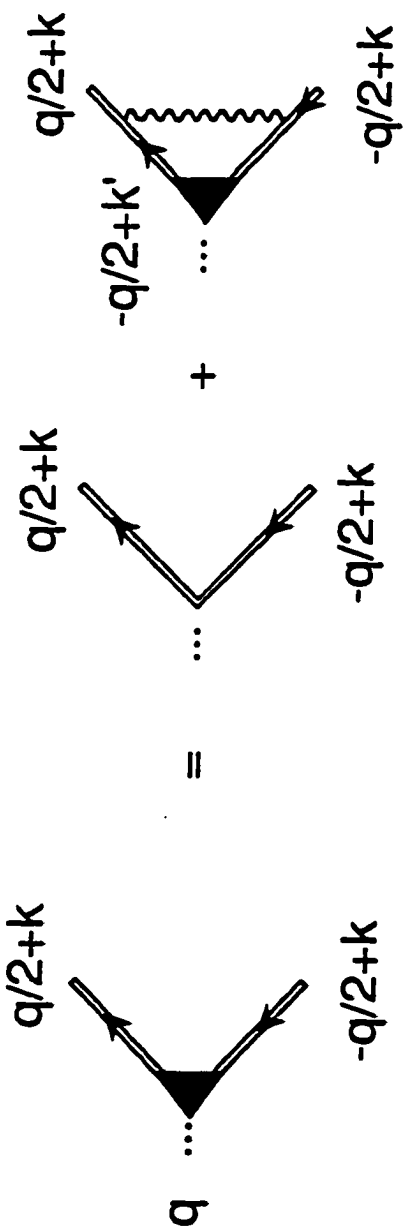

Fig. 2.3

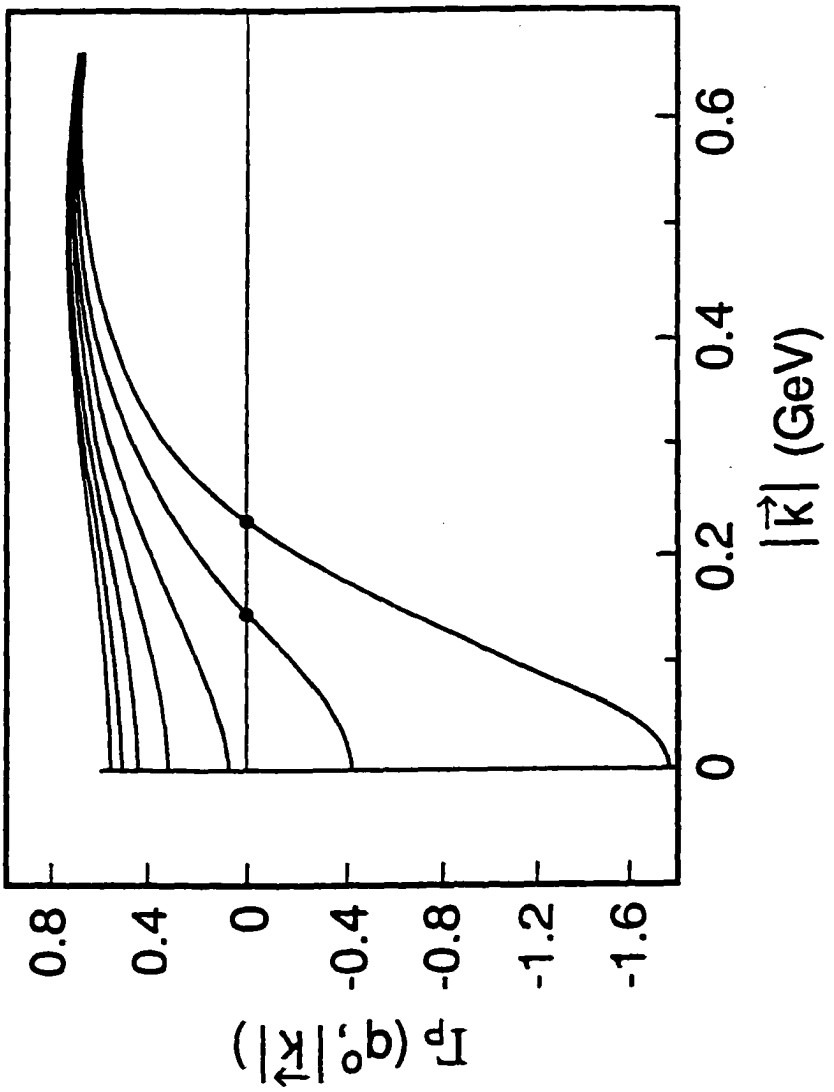

Fig. 2.4

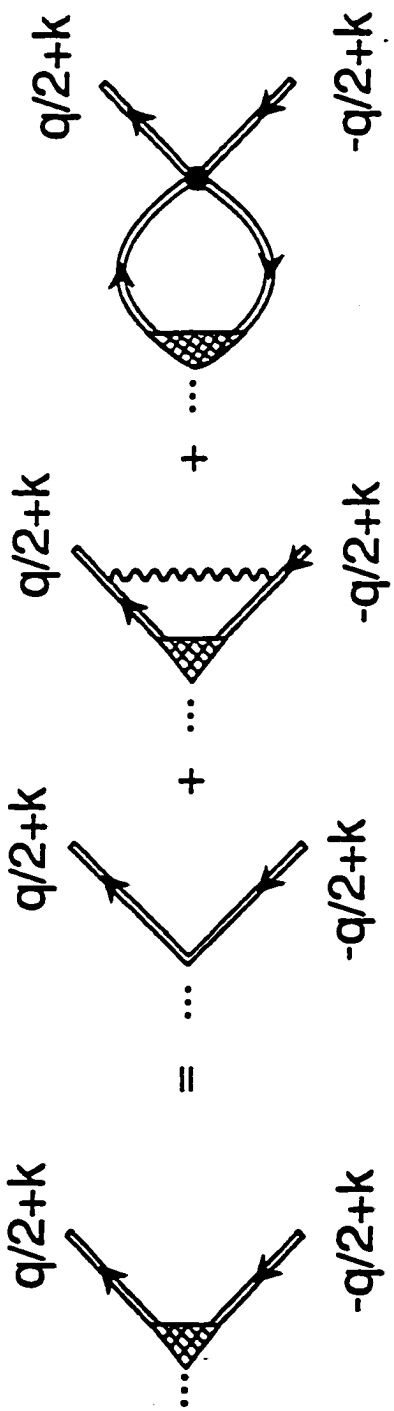

Fig. 2.5

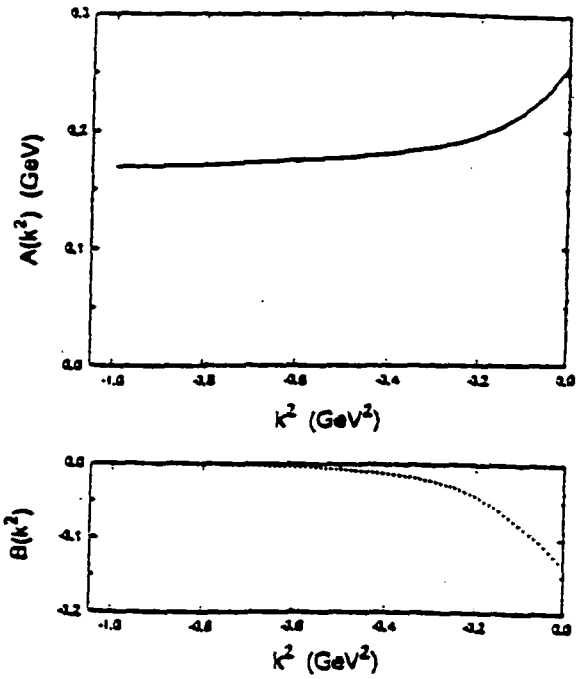

Fig. 2.6

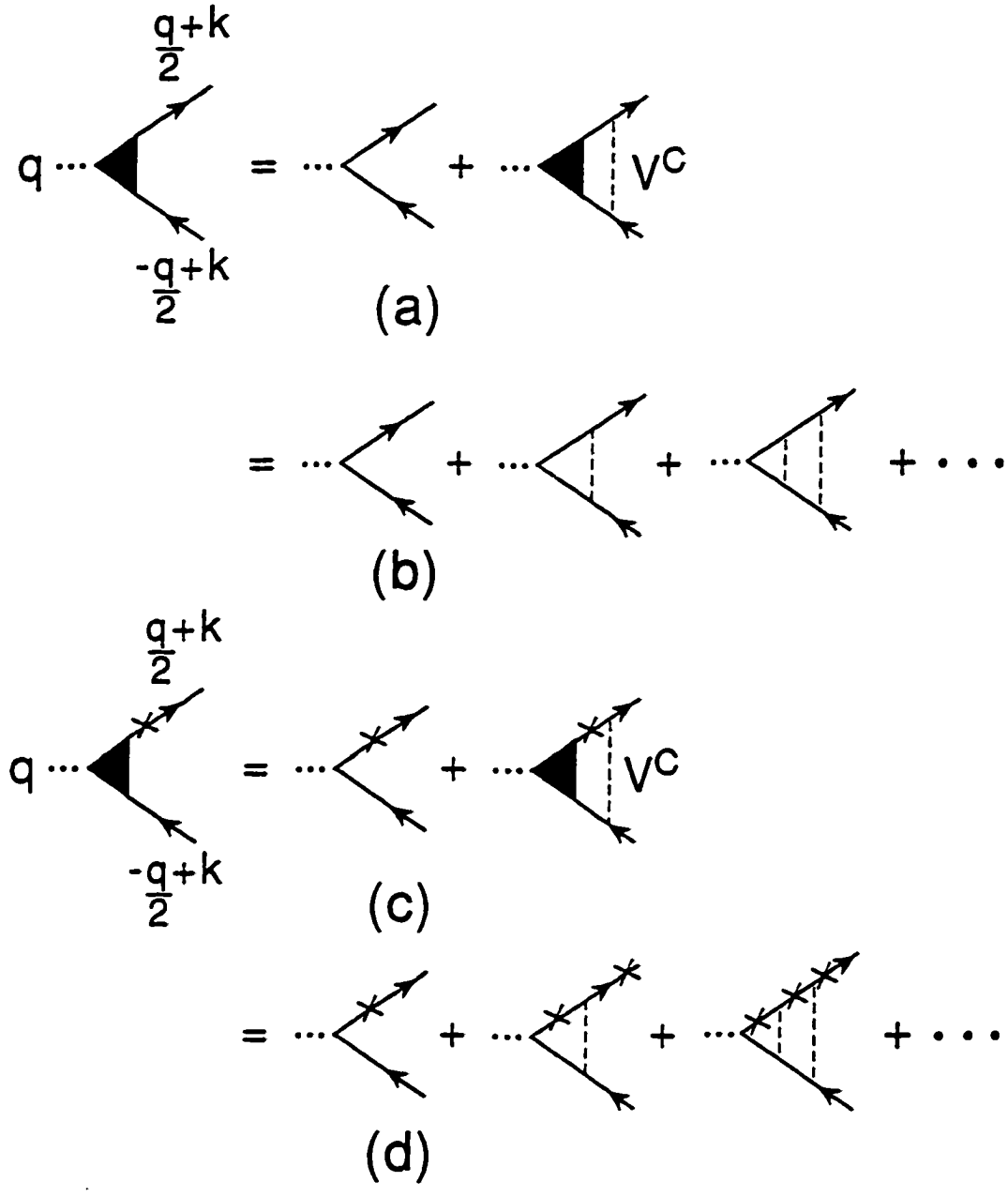

Fig. 3.1

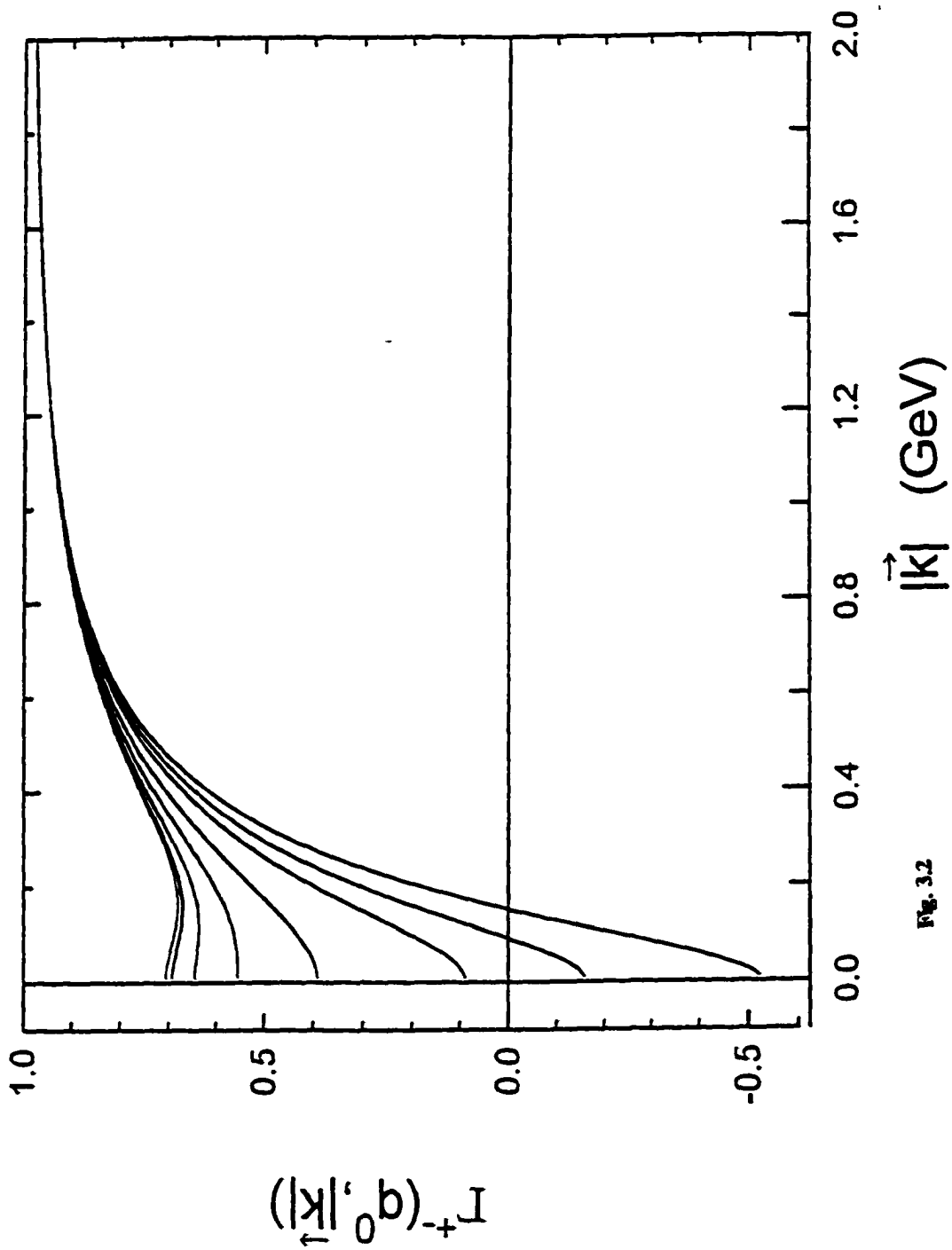

Fig. 3.2

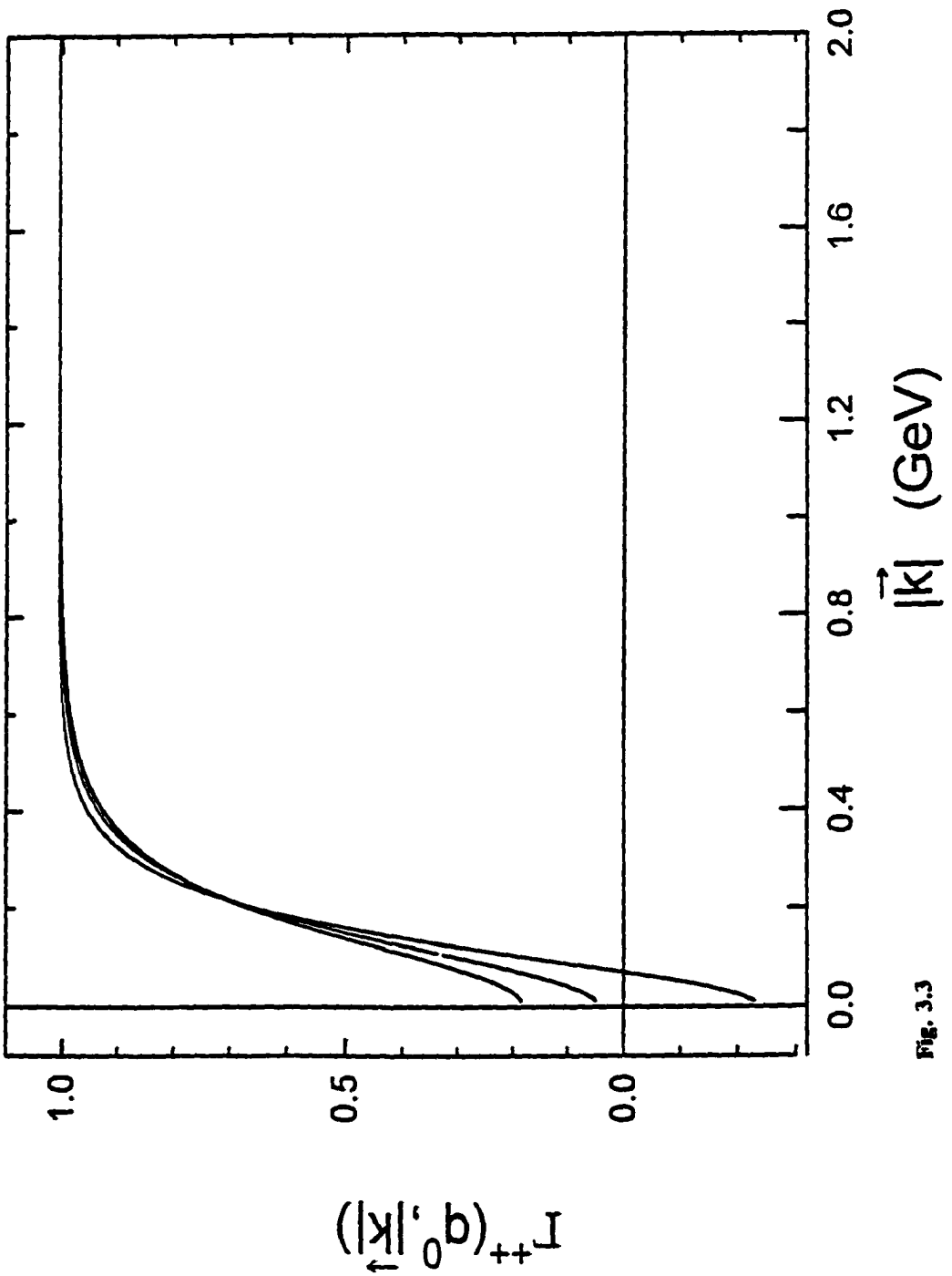

Fig. 3.3

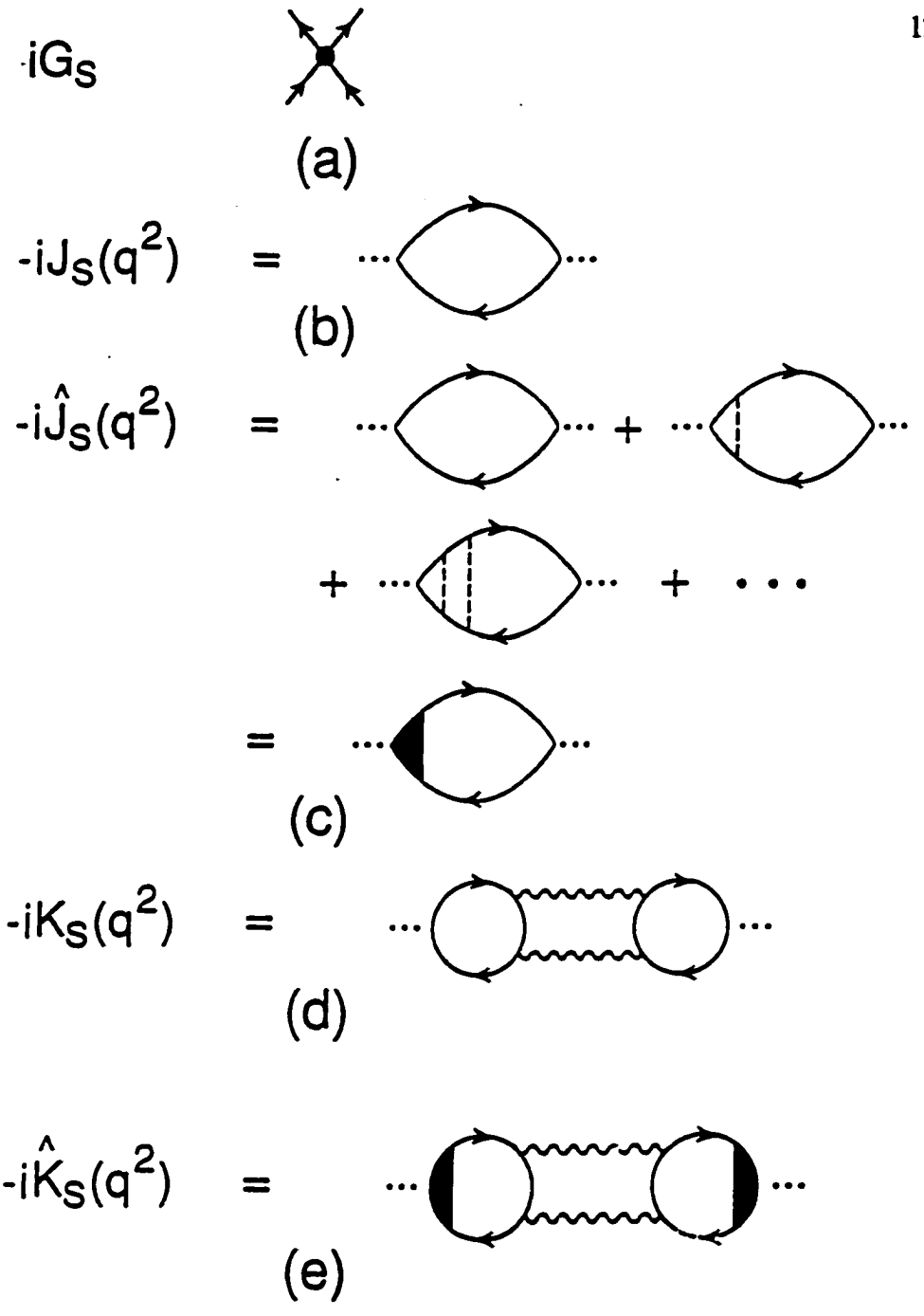

Fig. 3.4

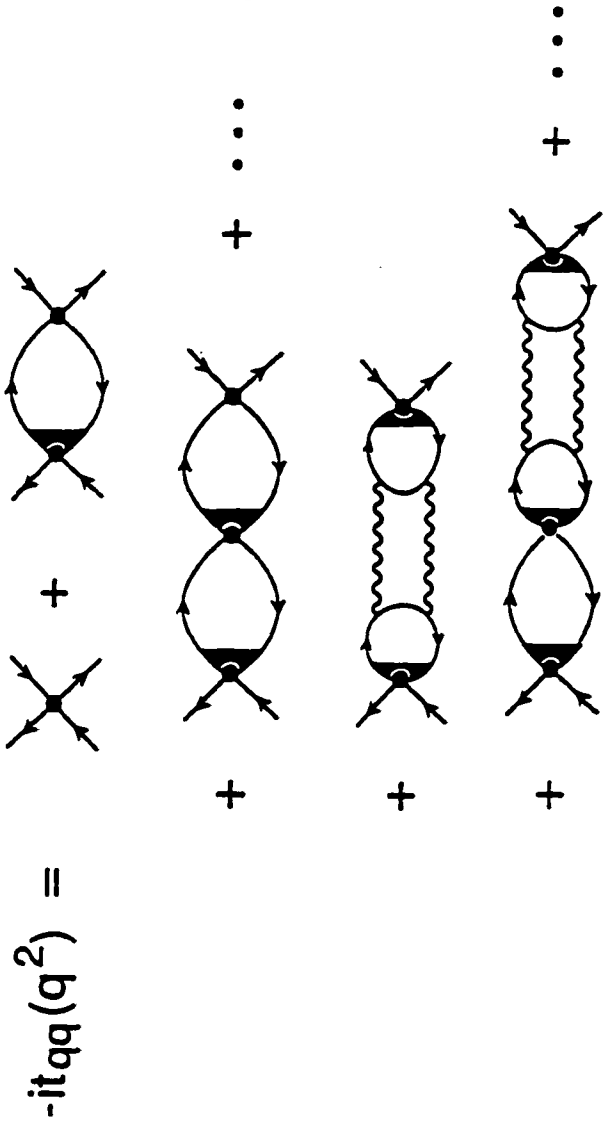

Fig. 3.5

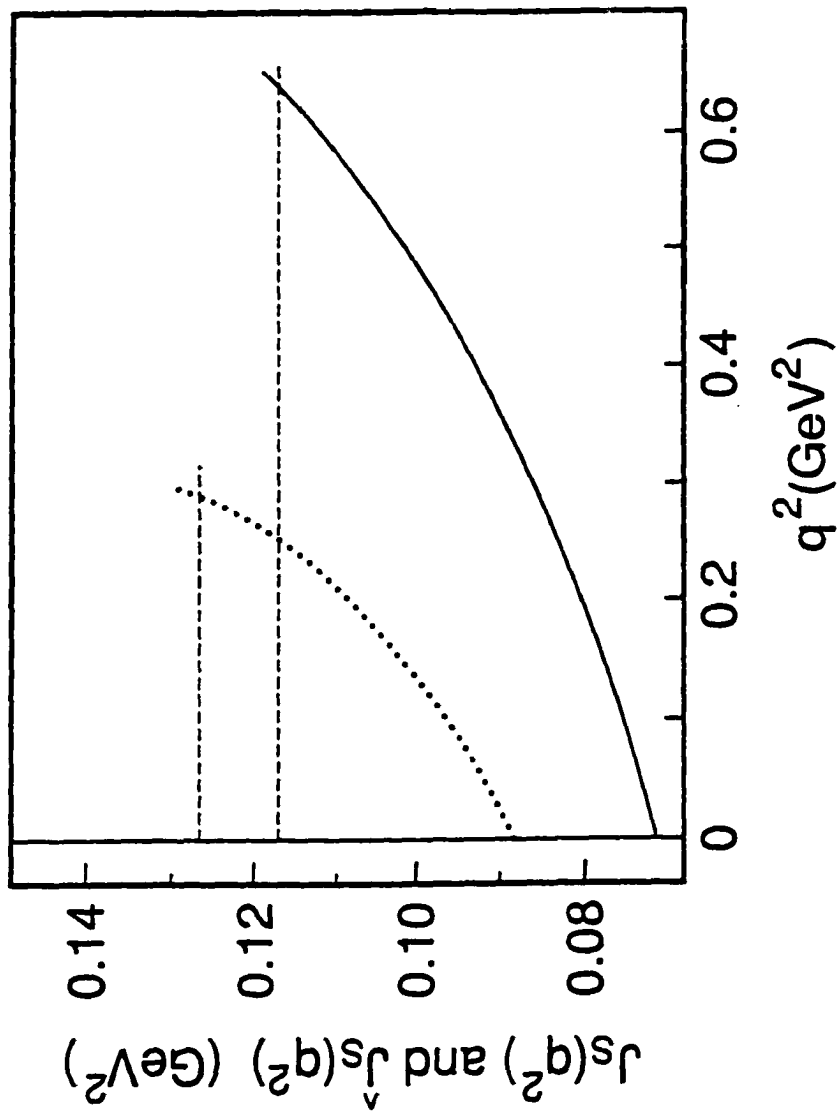

Fig. 3.6

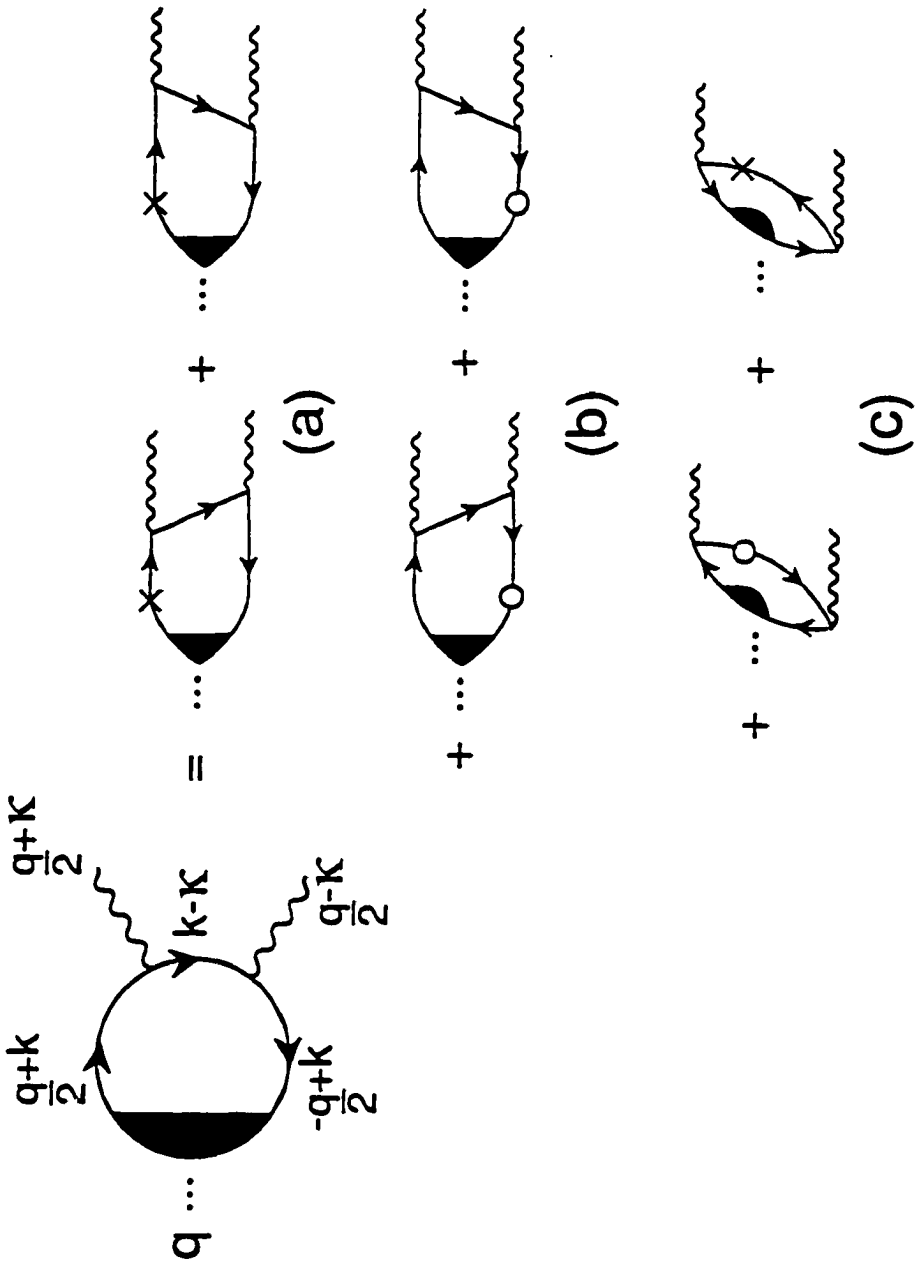

Fig. 3.7

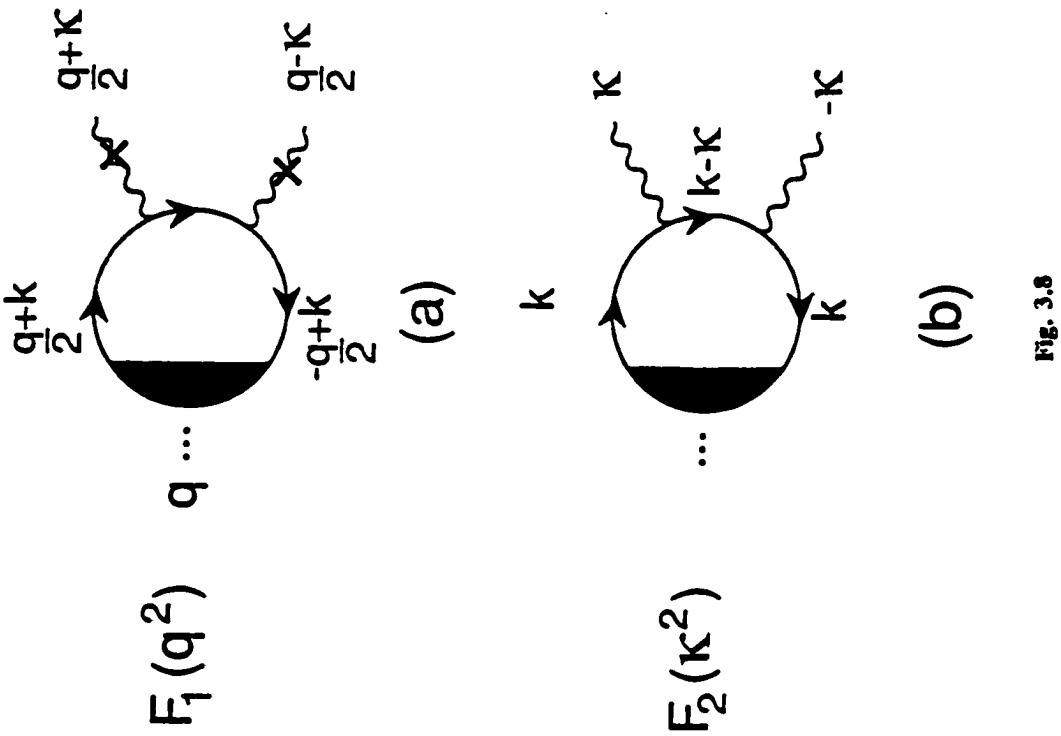

Fig. 3.8

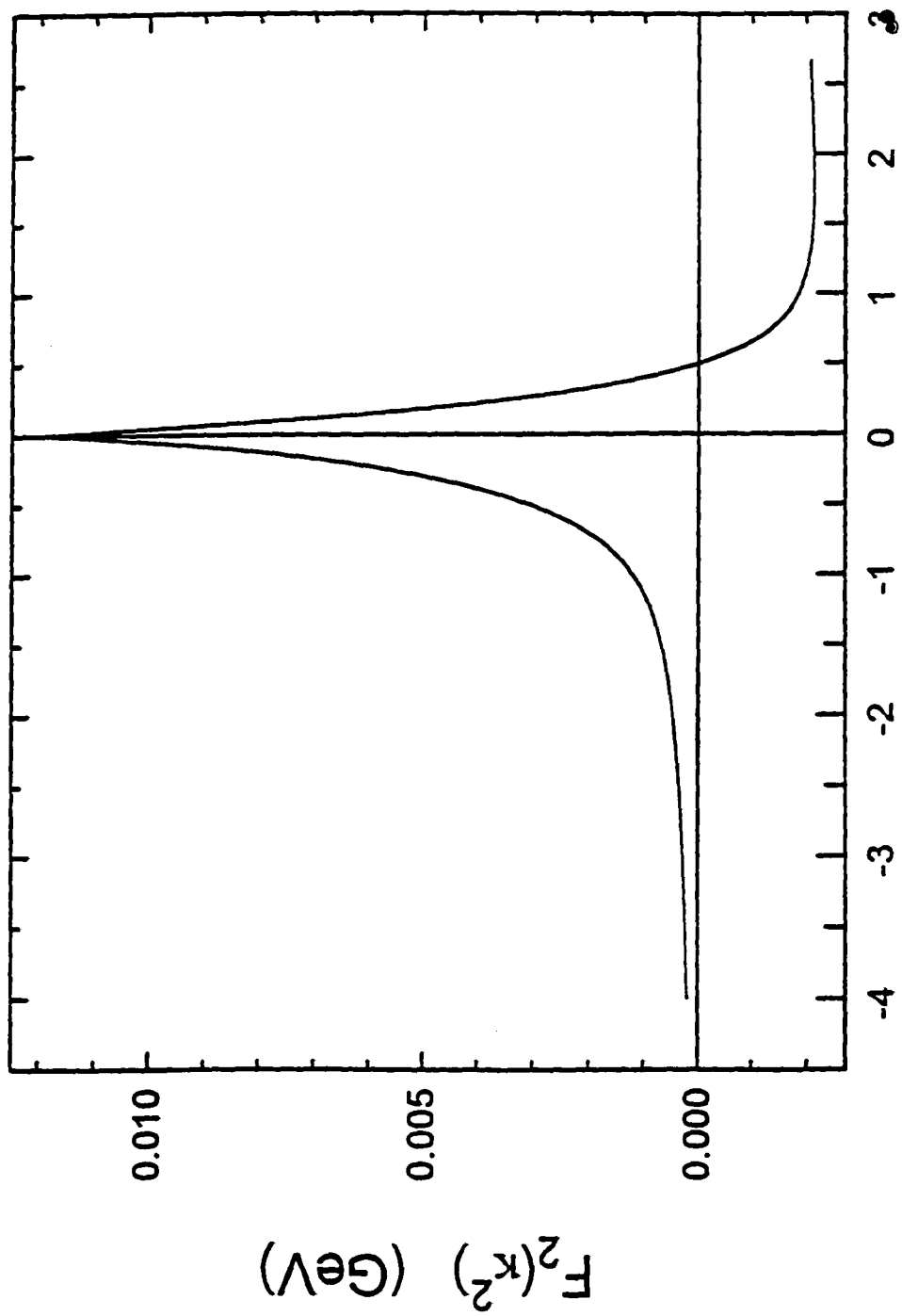

Fig. 3.9

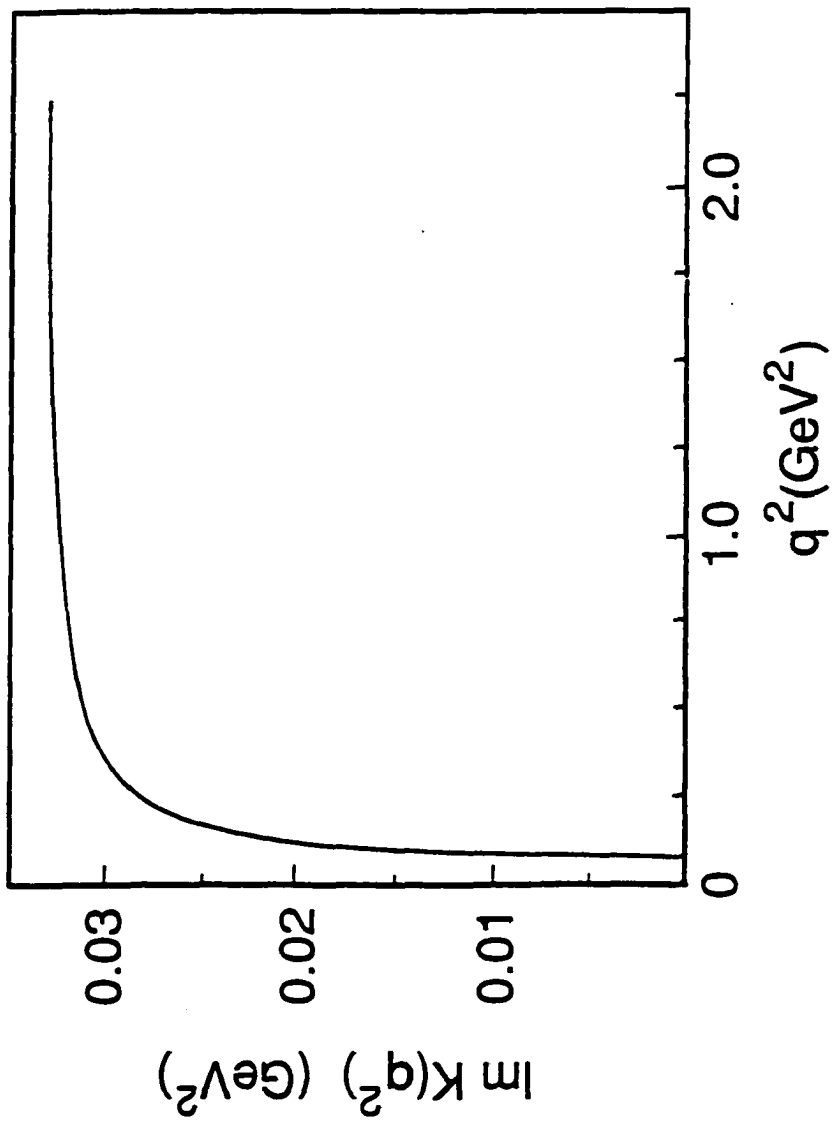

Fig. 3.10

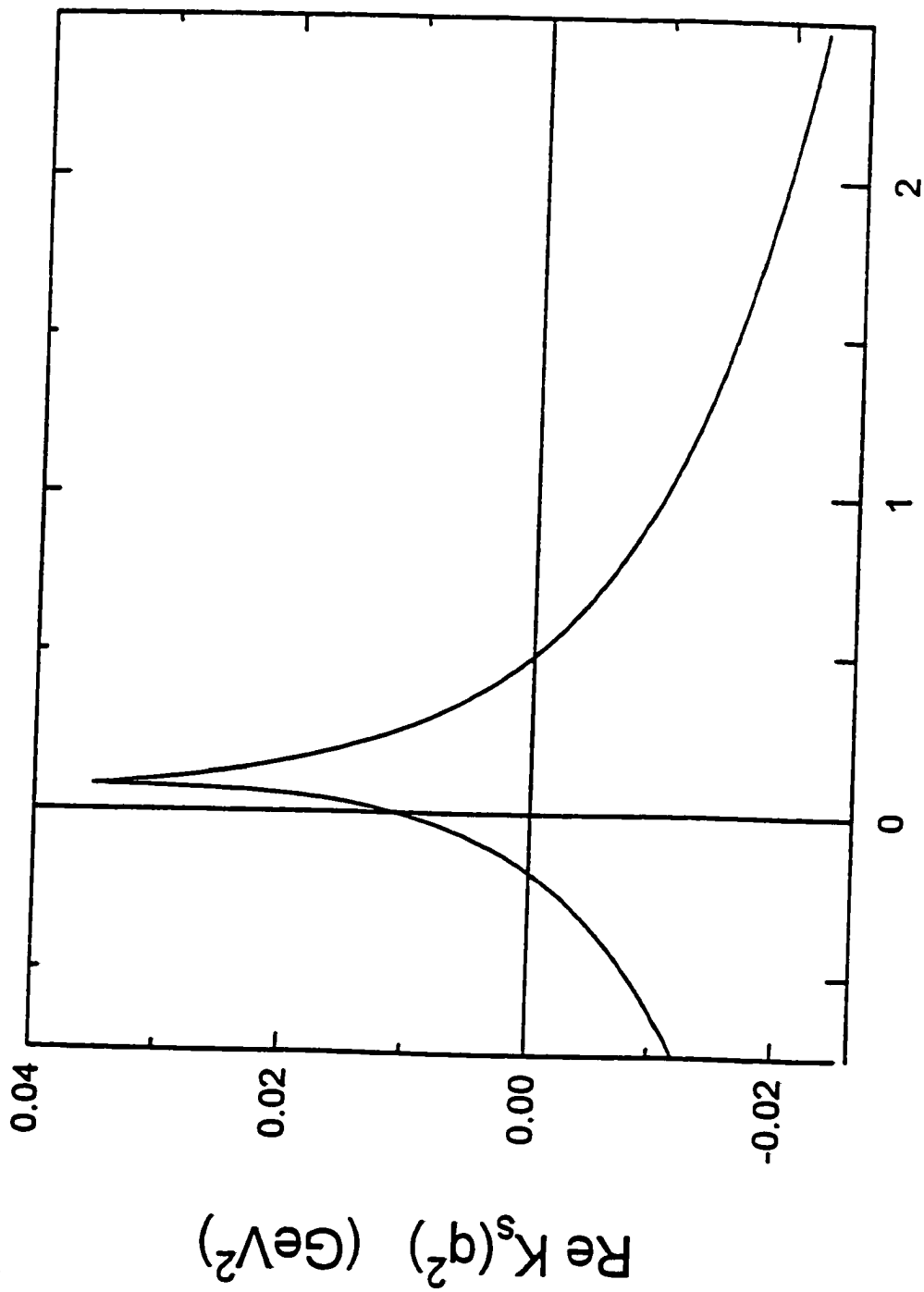

Fig. 3.11

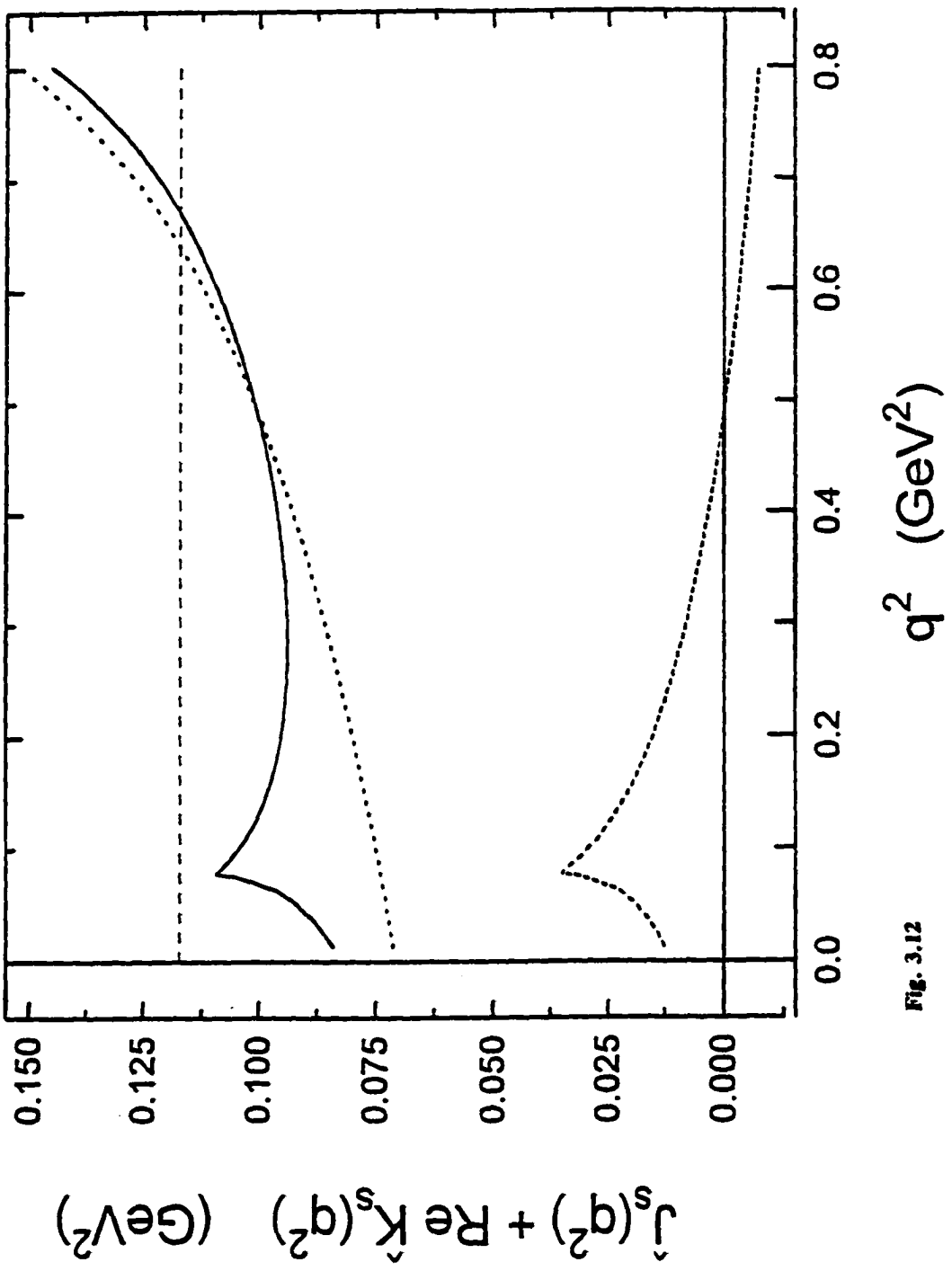

Fig. 3.12

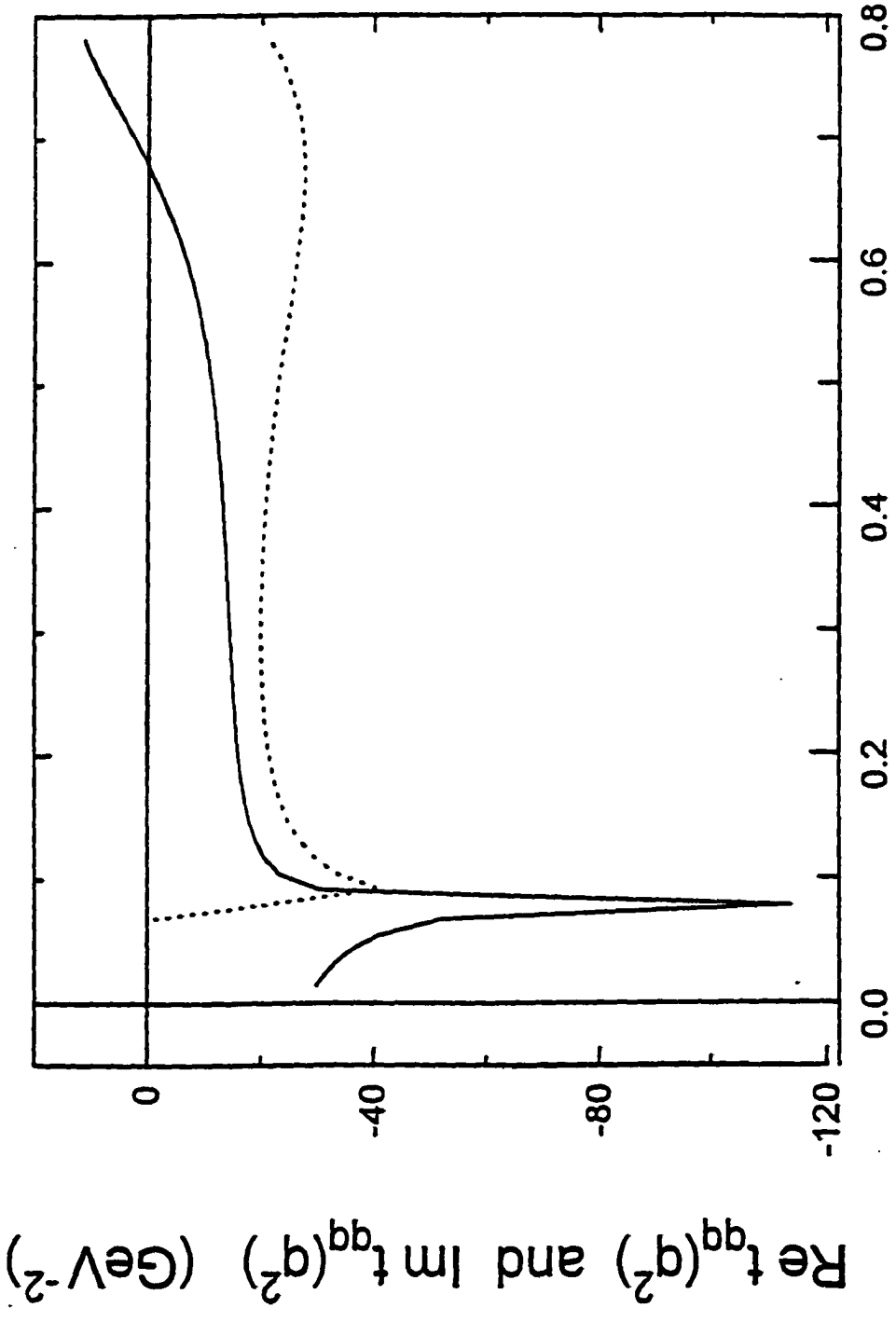

Fig. 3.13

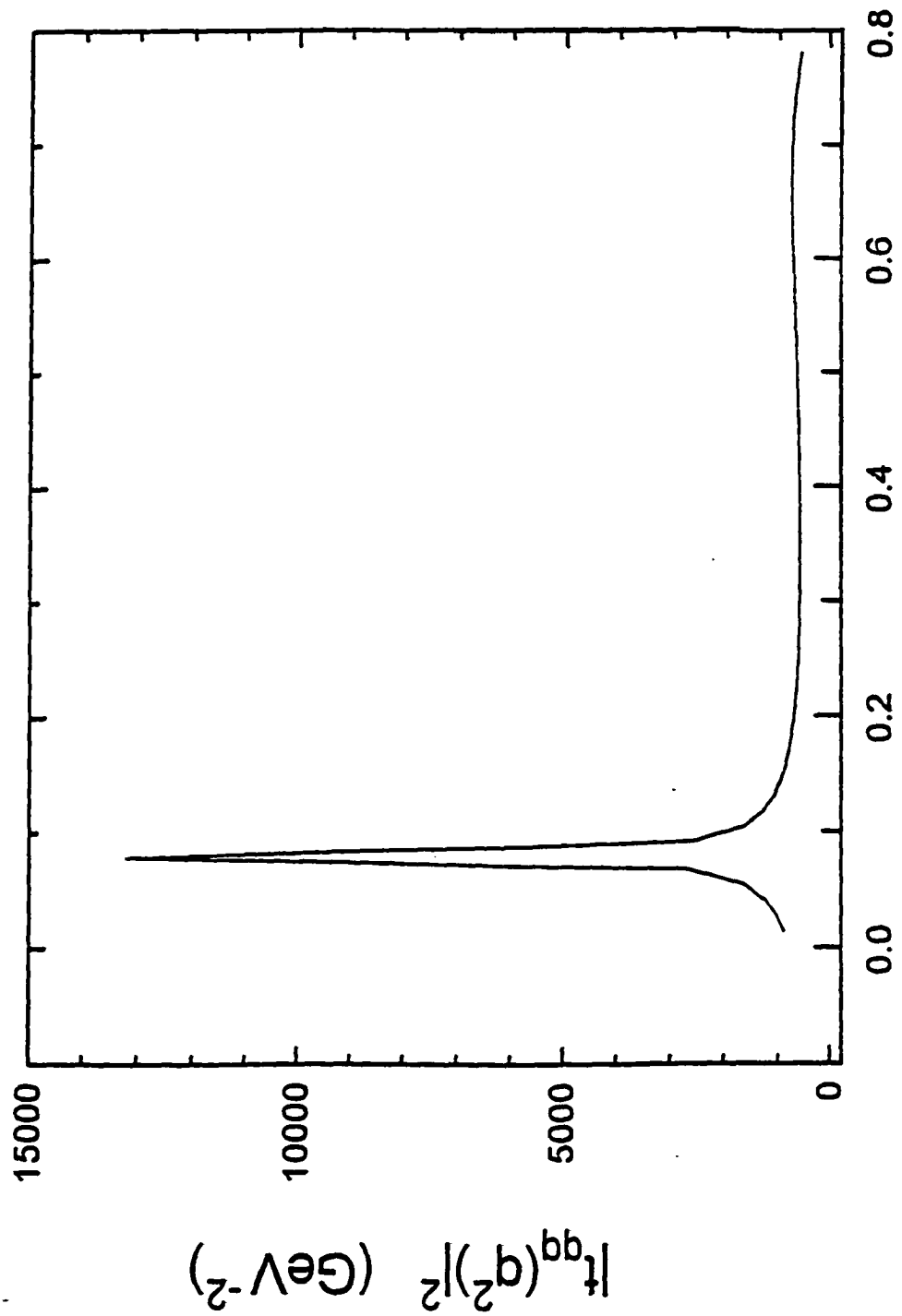

Fig. 3.14

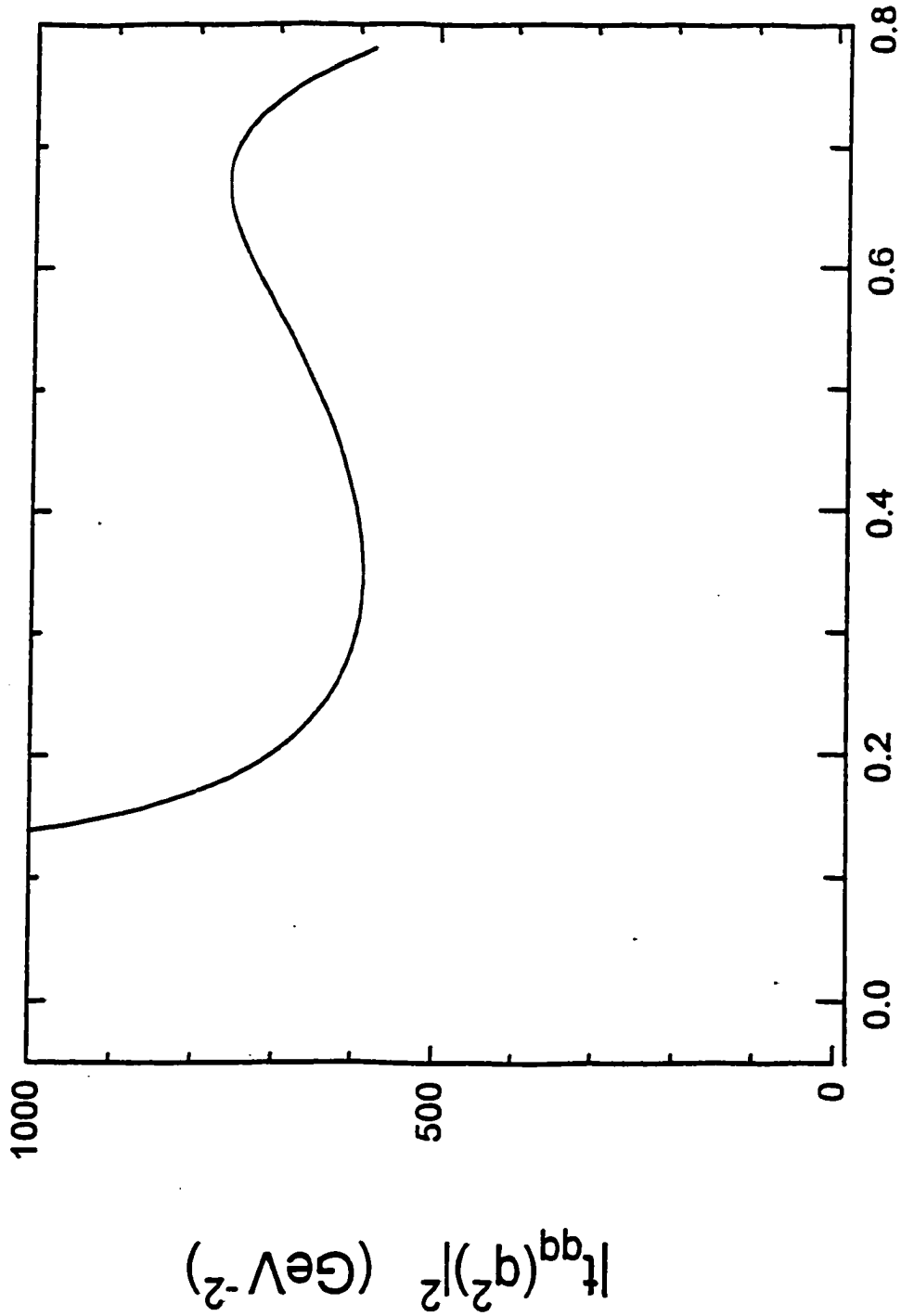

Fig. 3.15

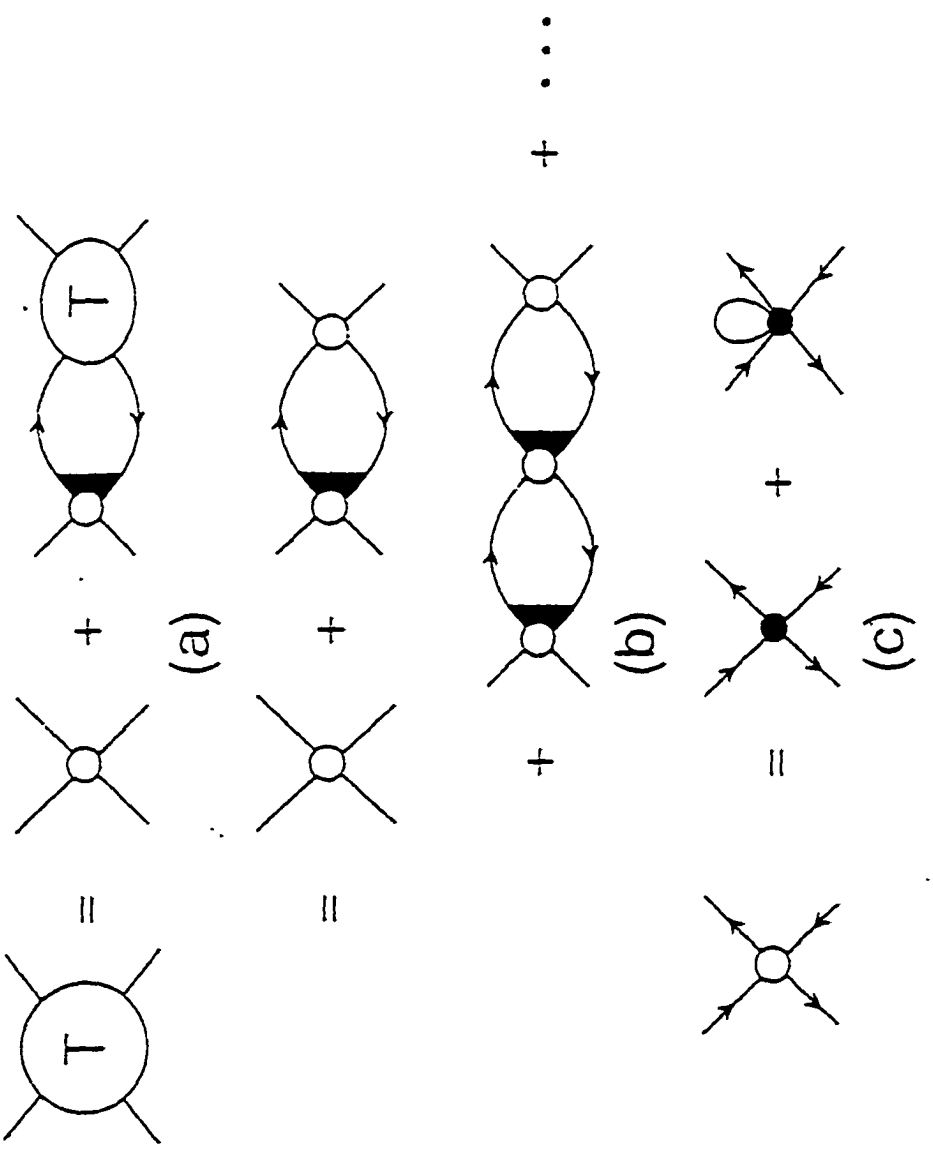

Fig. 4.1

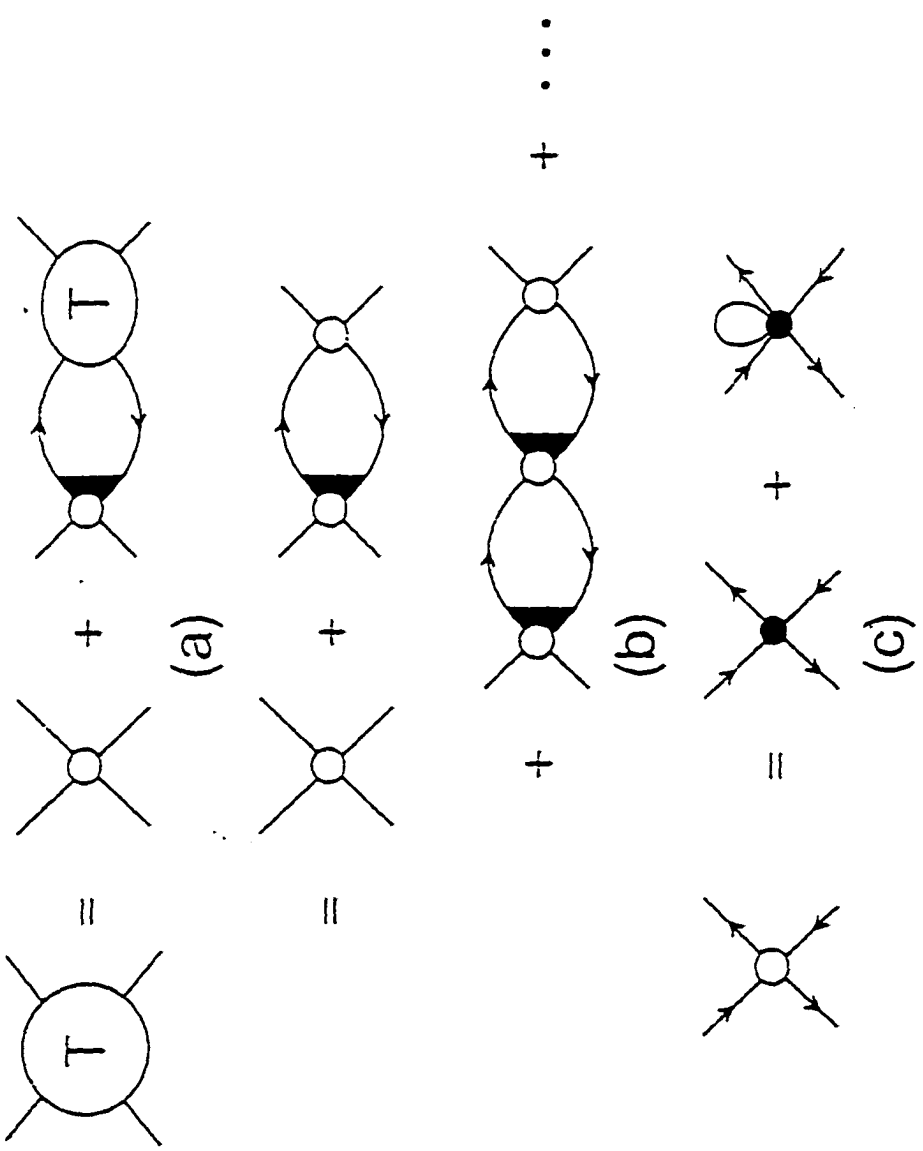

Fig. 4.1

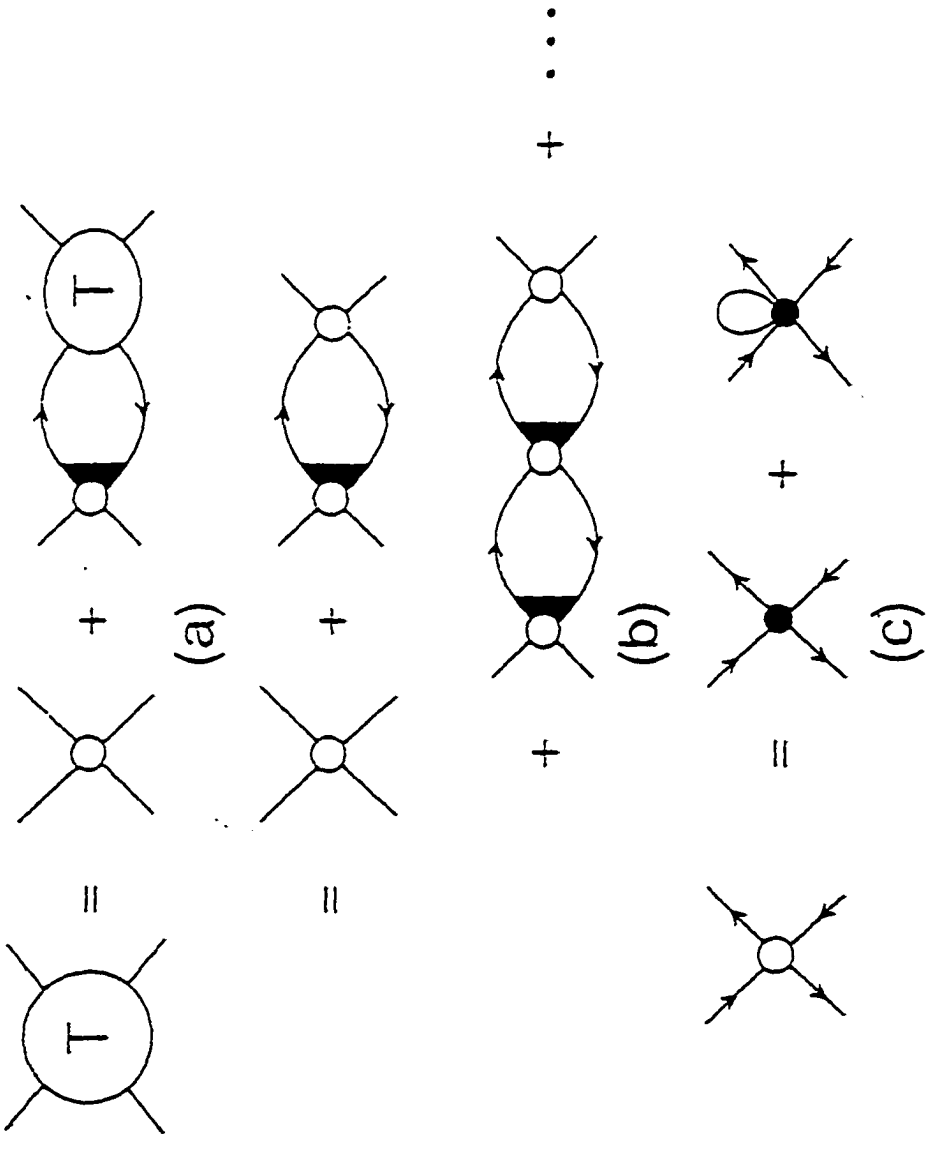

Fig. 4.1

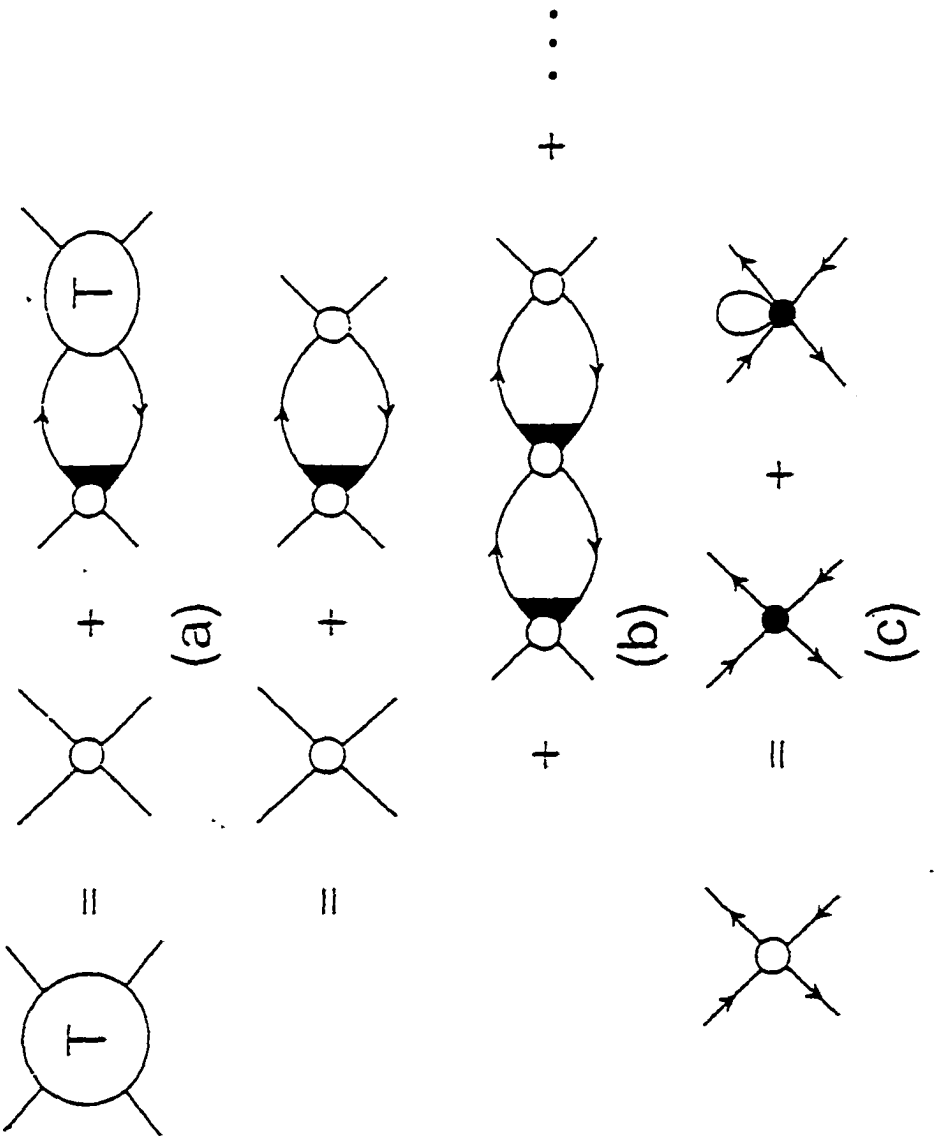

Fig. 4.1

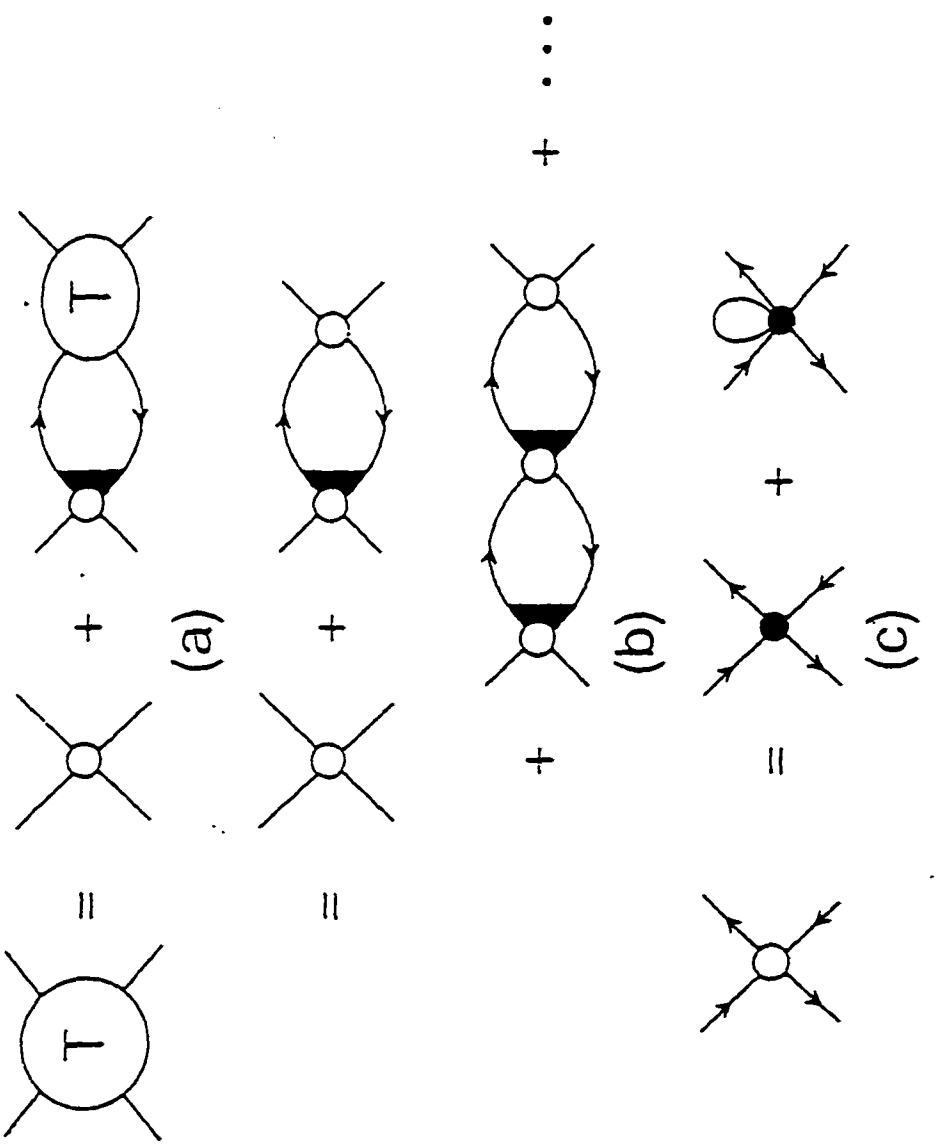

Fig. 4.1

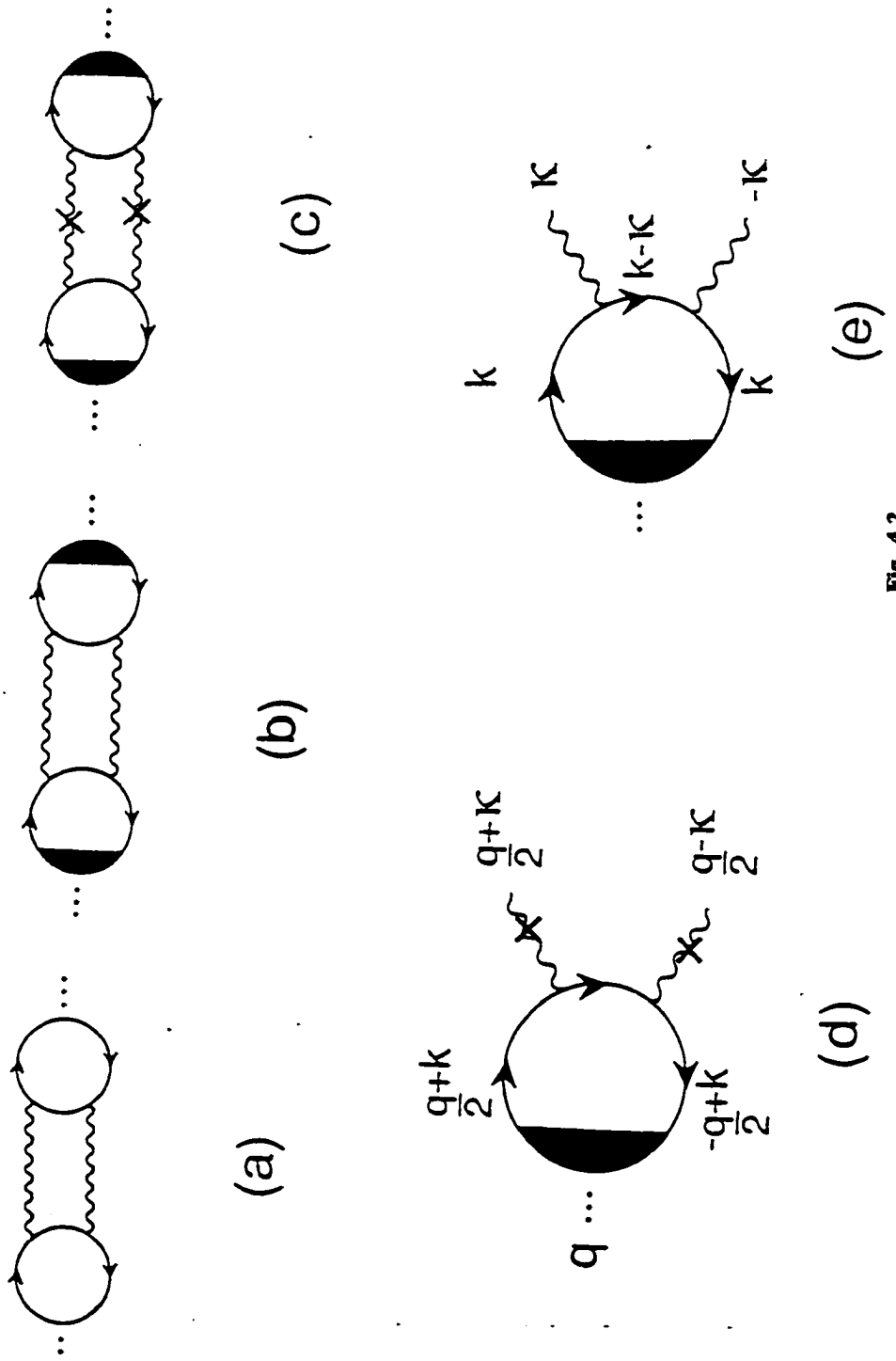

Fig. 4.2

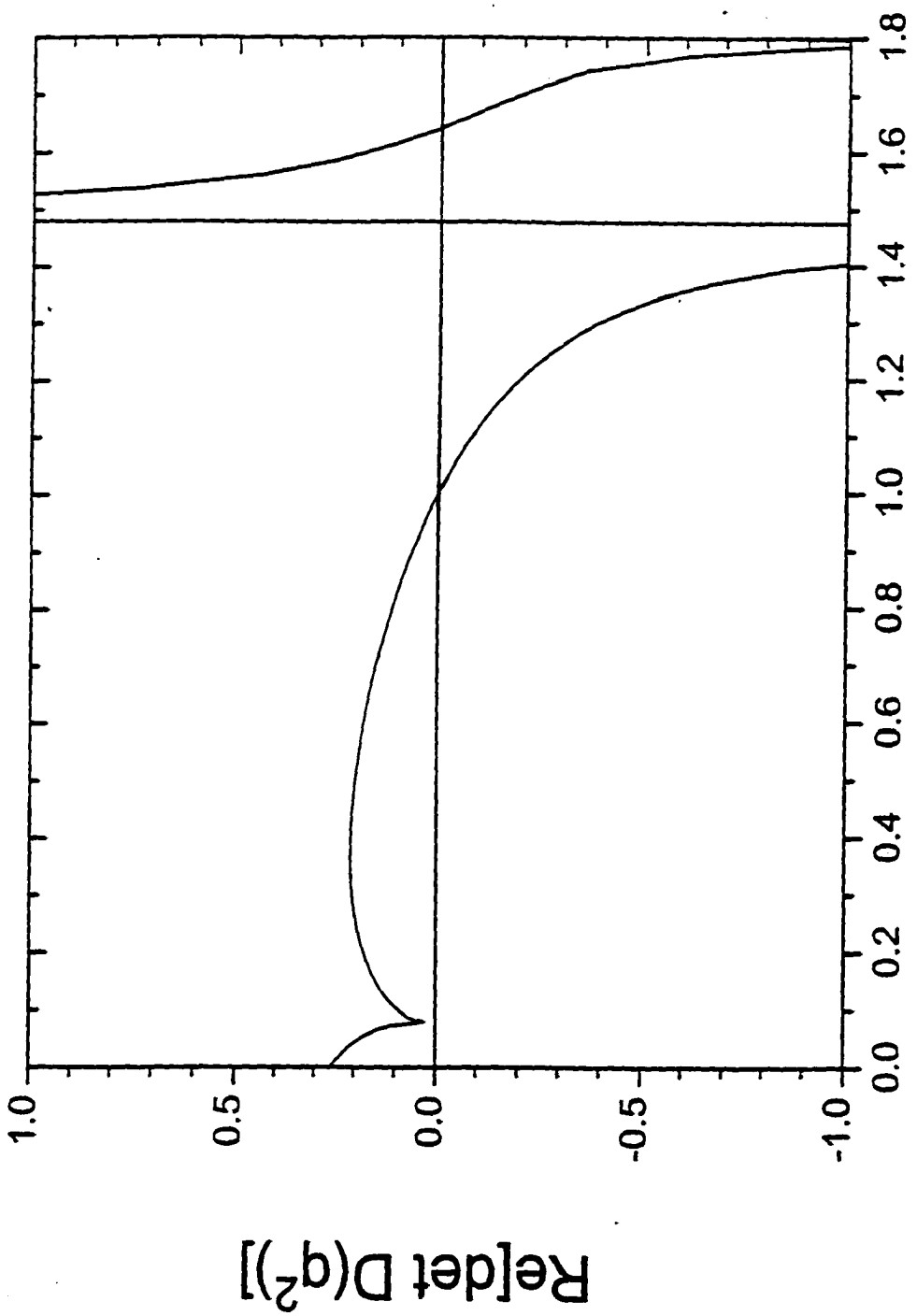

Fig. 4.3

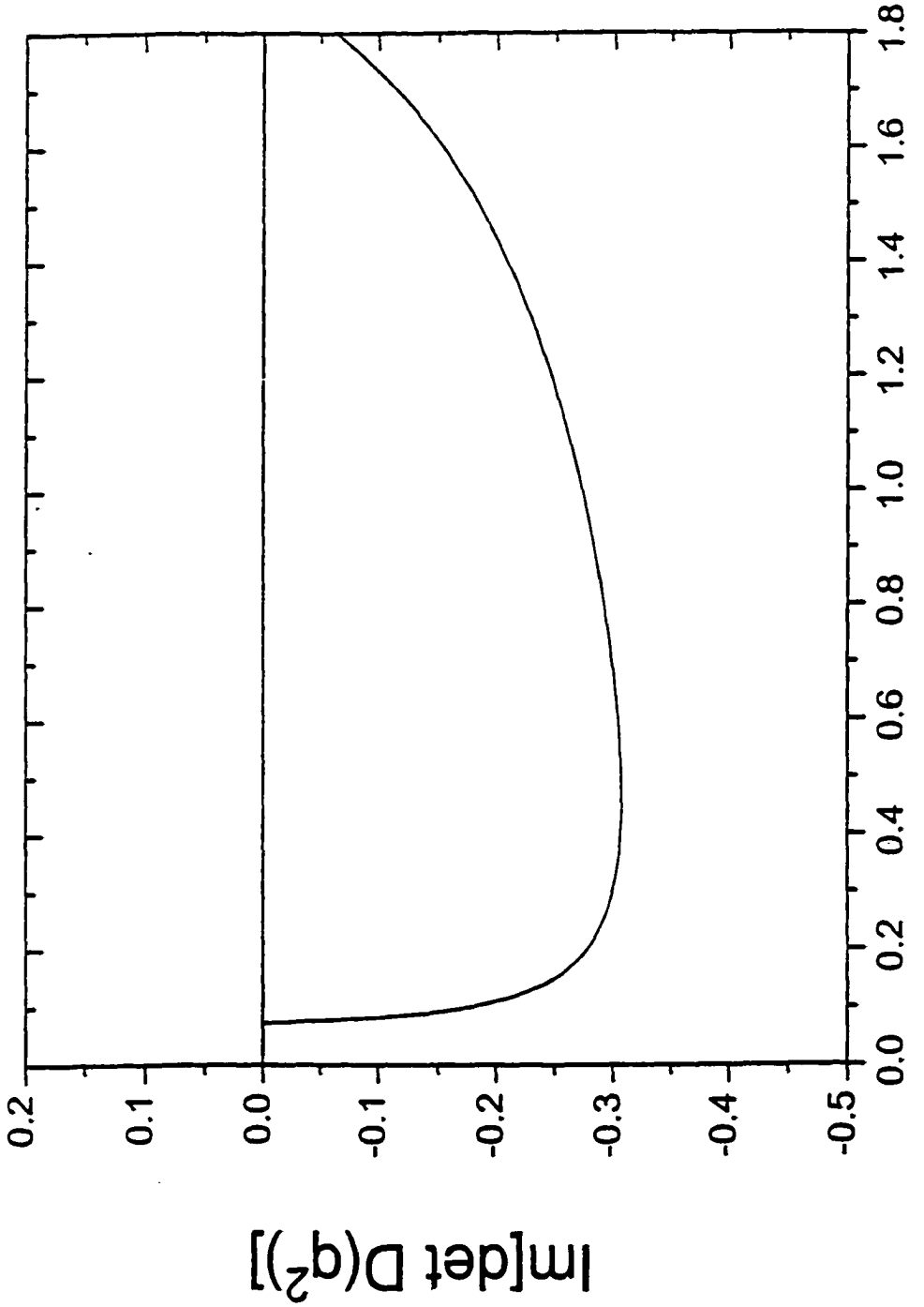

Fig. 4.4

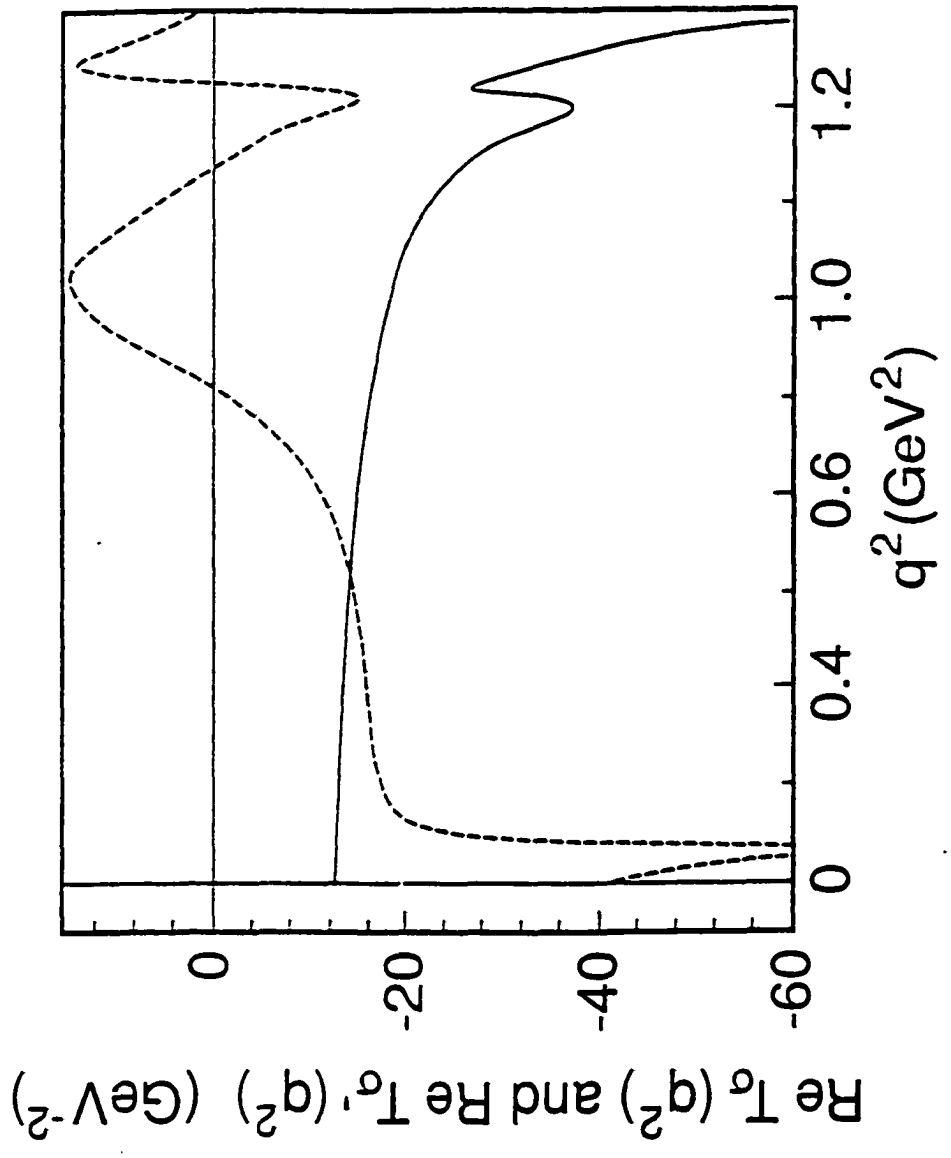

Fig. 4.5

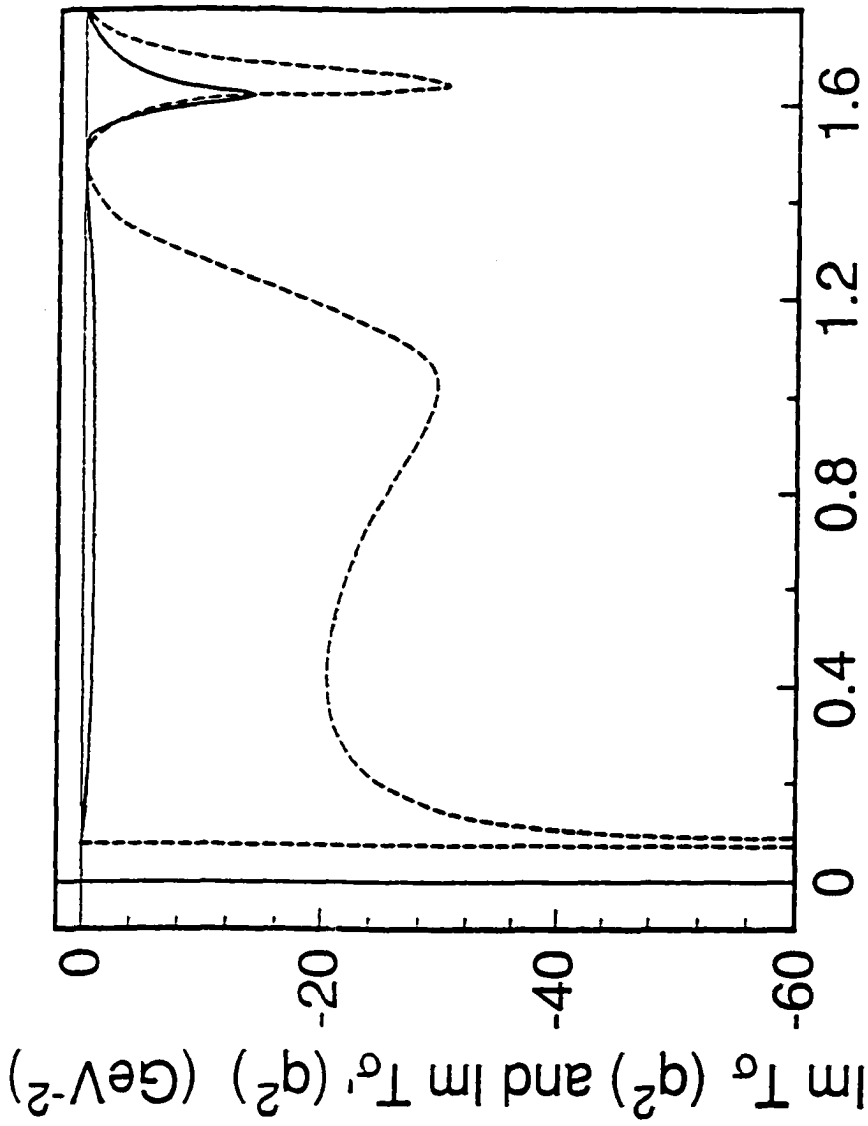

Fig. 4.6

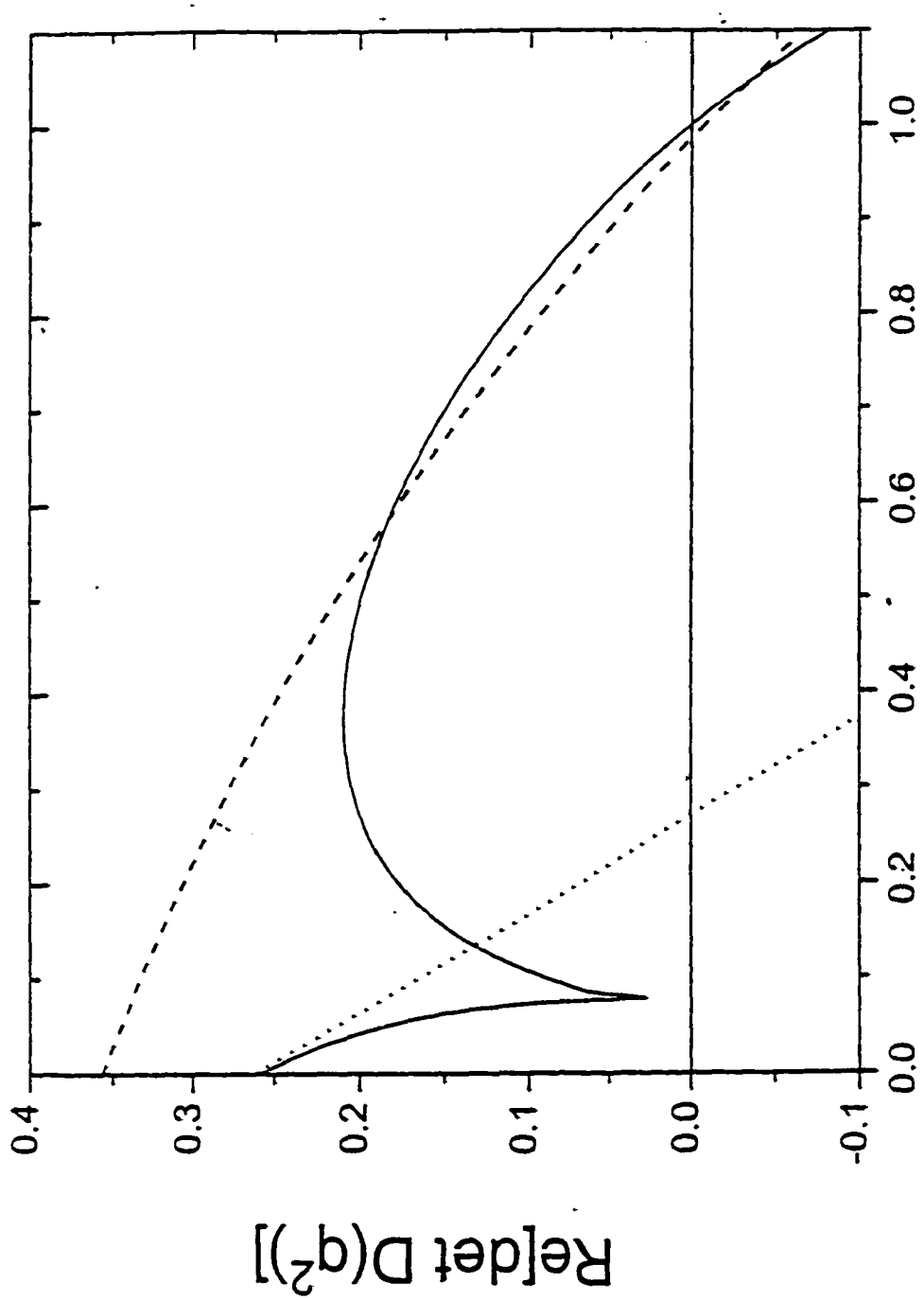

Fig. 4.7

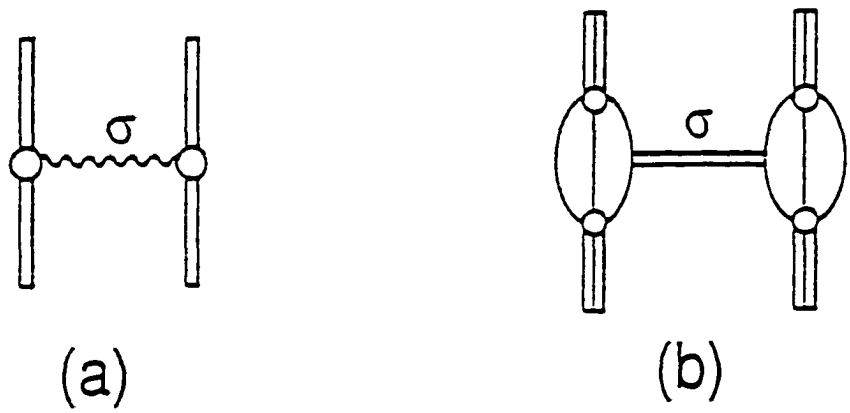

(a) (b)

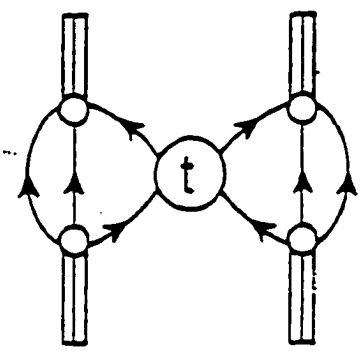

(c)

Fig. 4.8

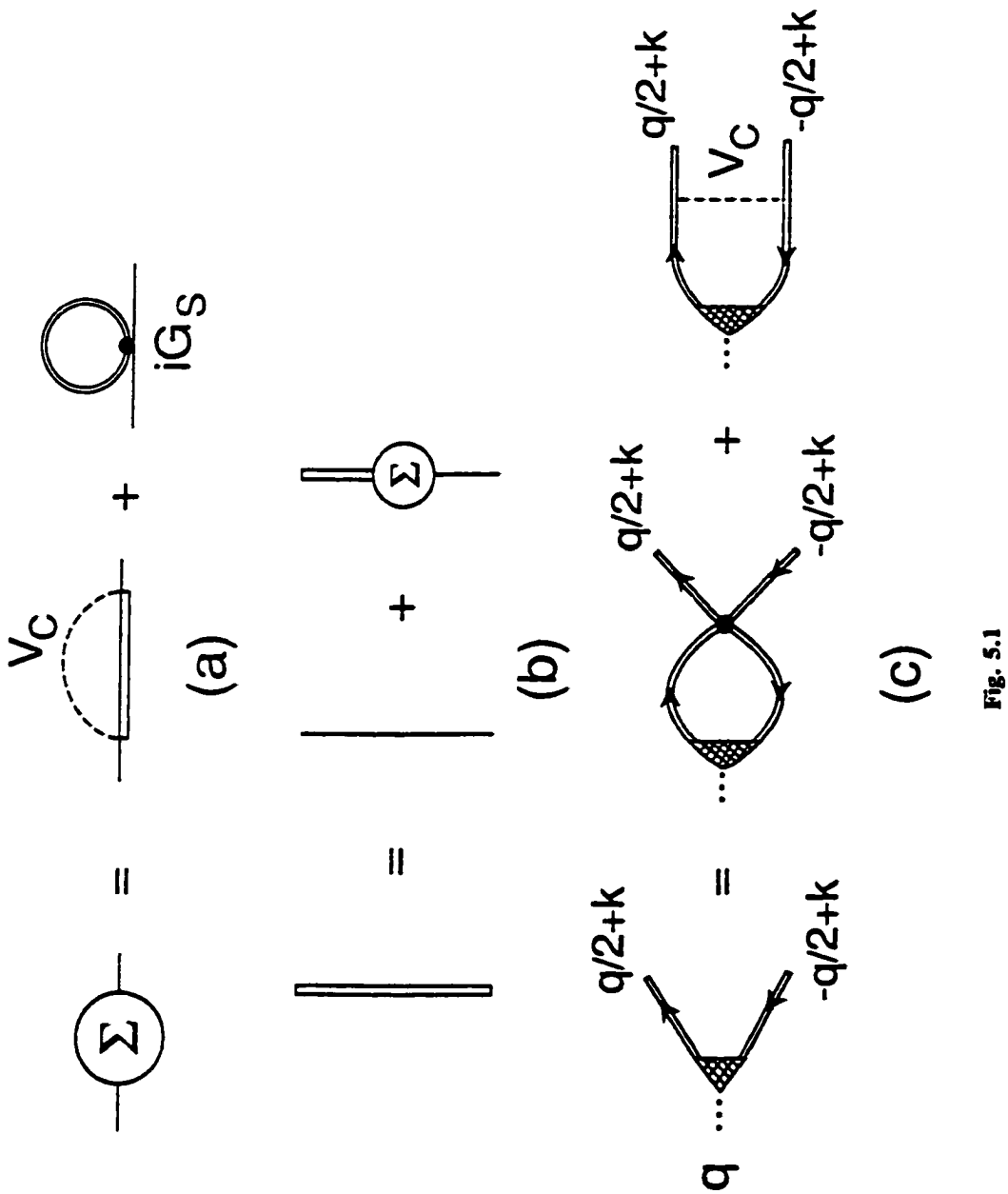

Fig. 5.1

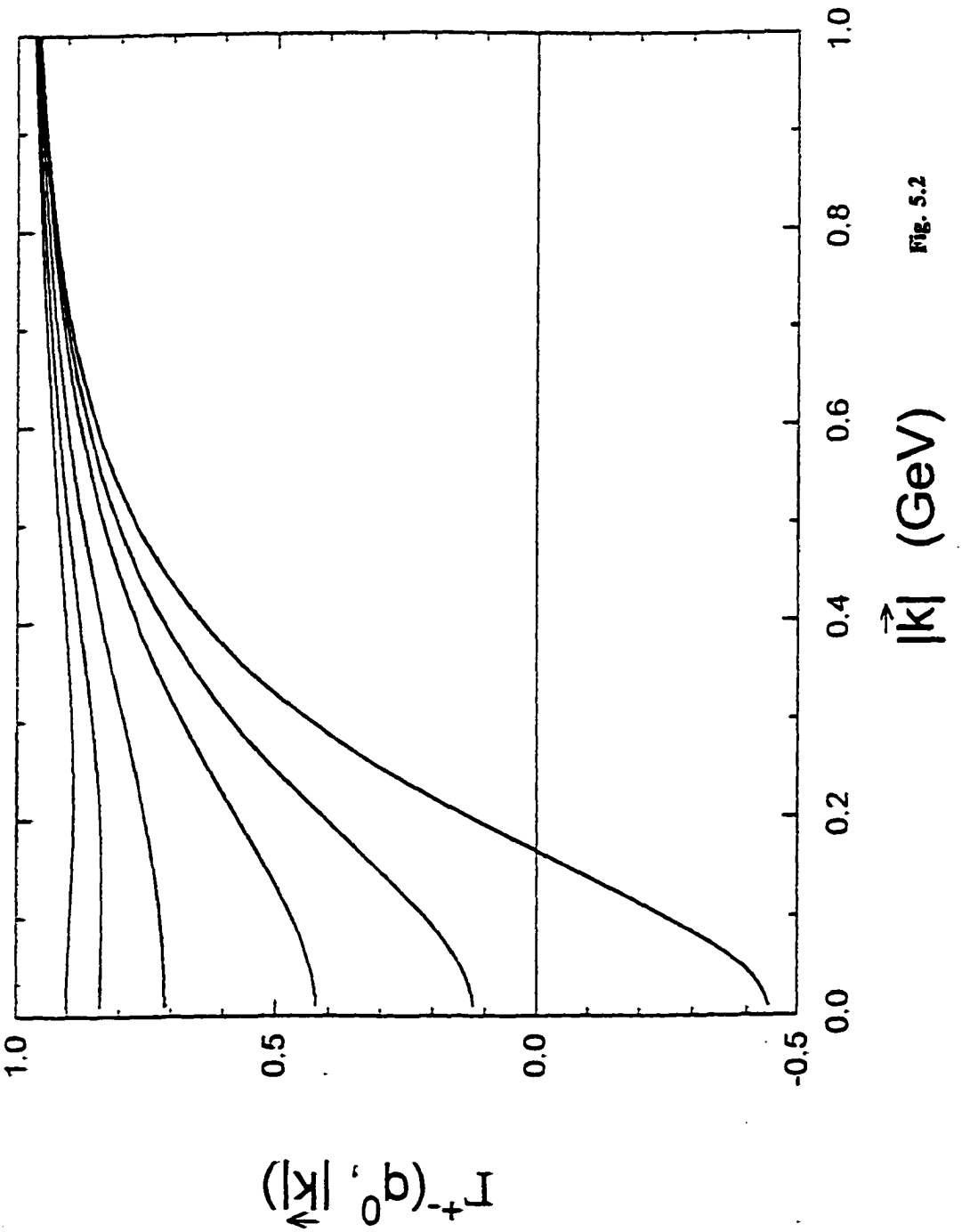

Fig. 5.2

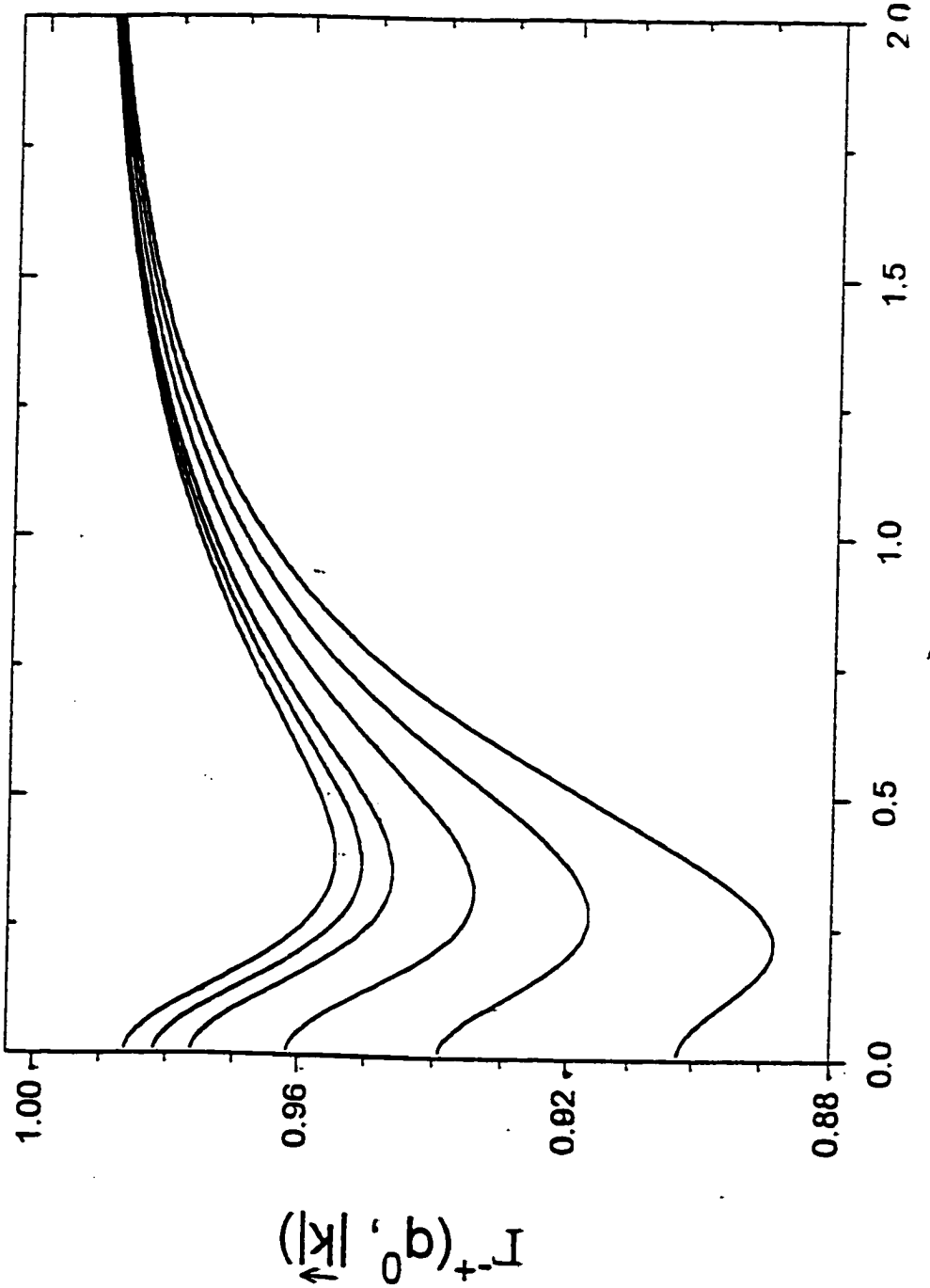

Fig. 5.3

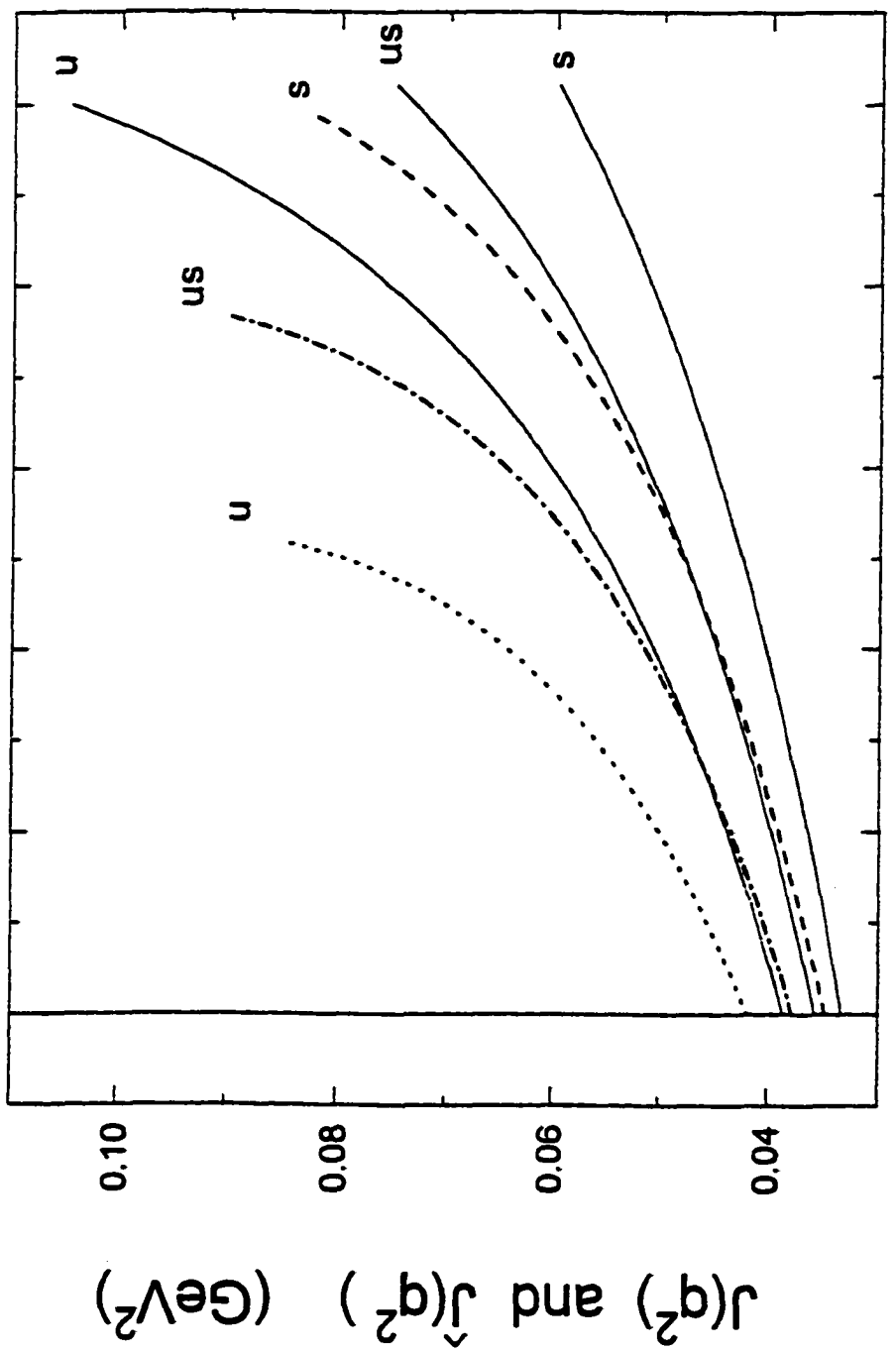

Fig. 5.4

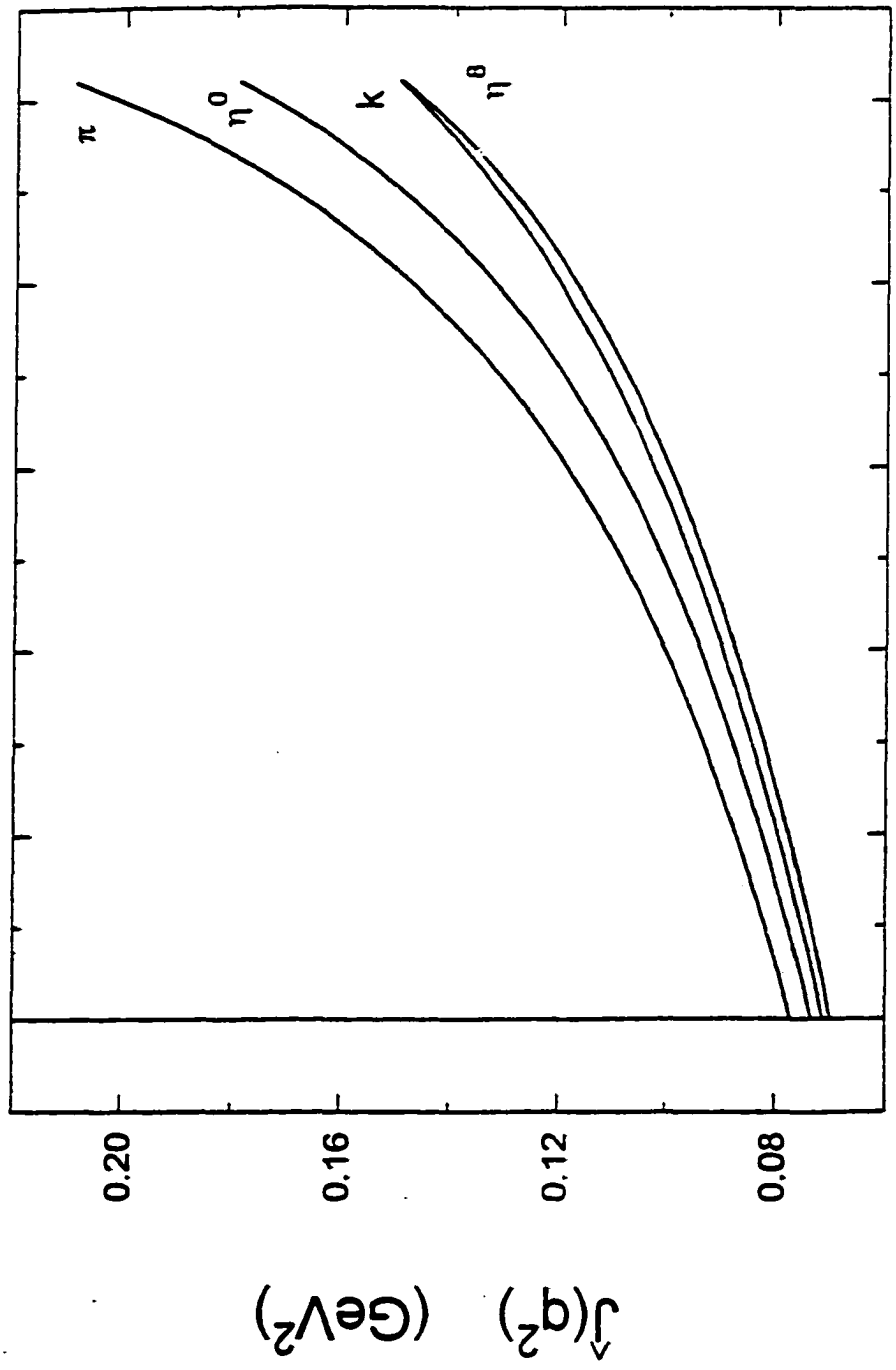

Fig. 5.5

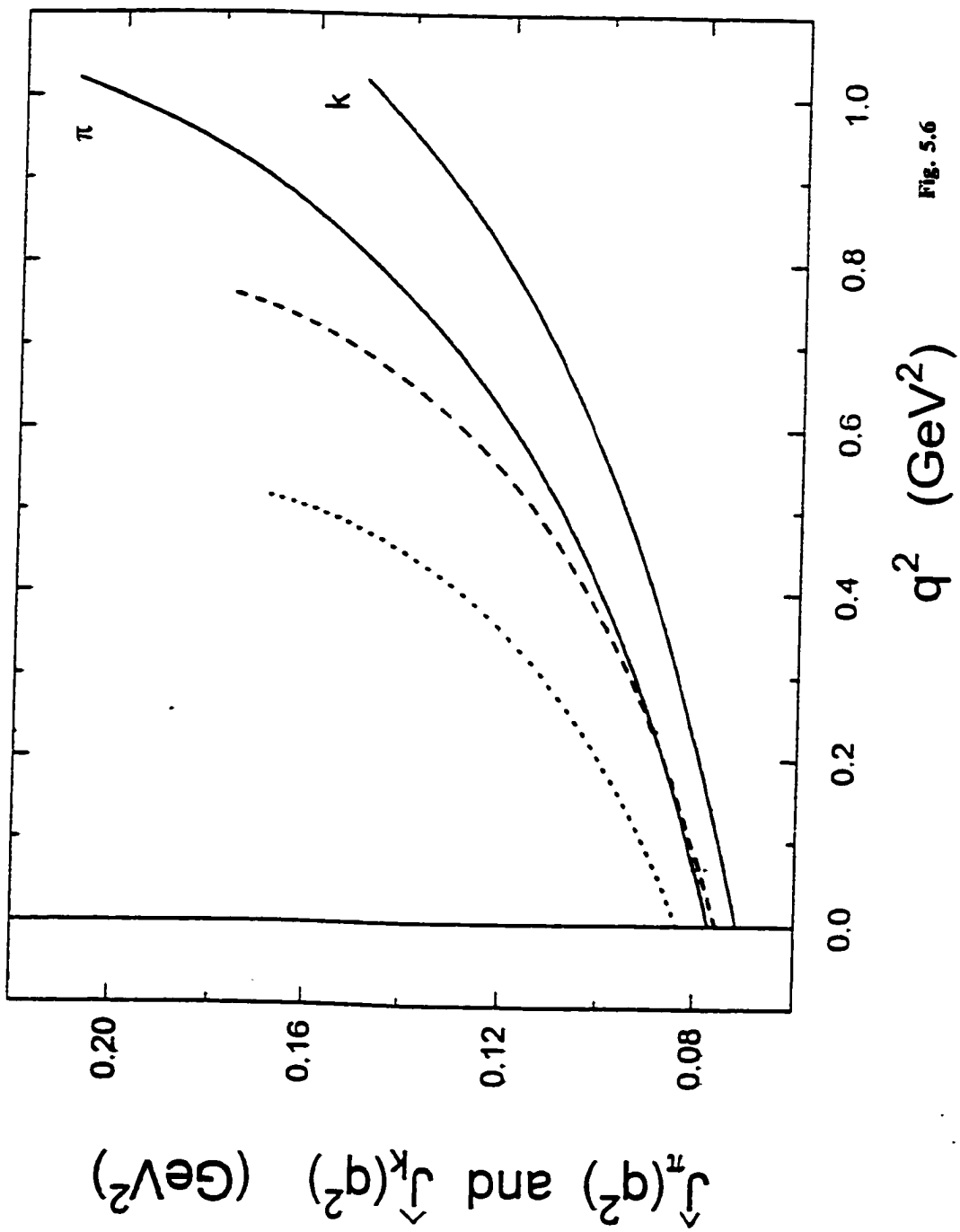

Fig. 5.6

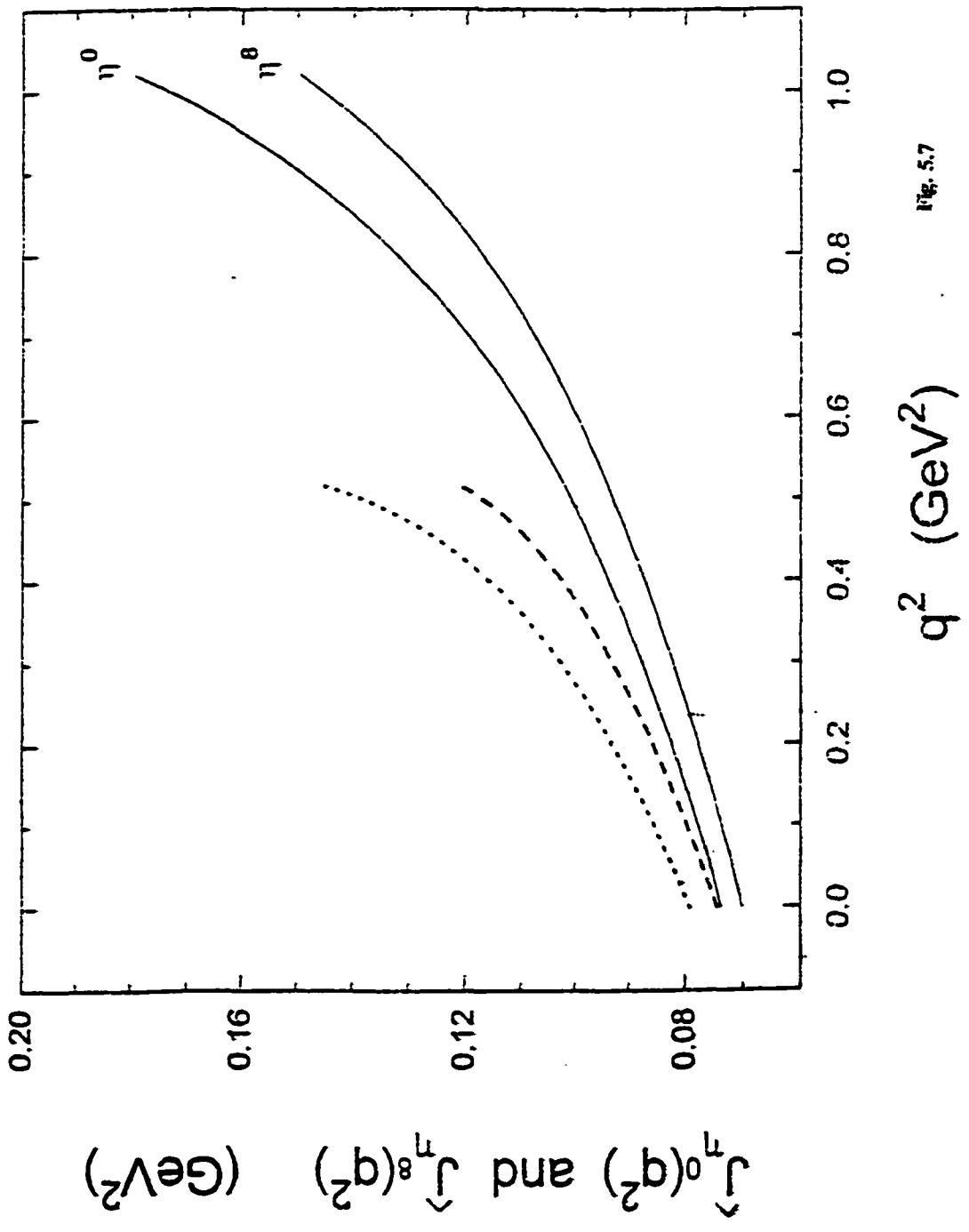

Fig. 5.7

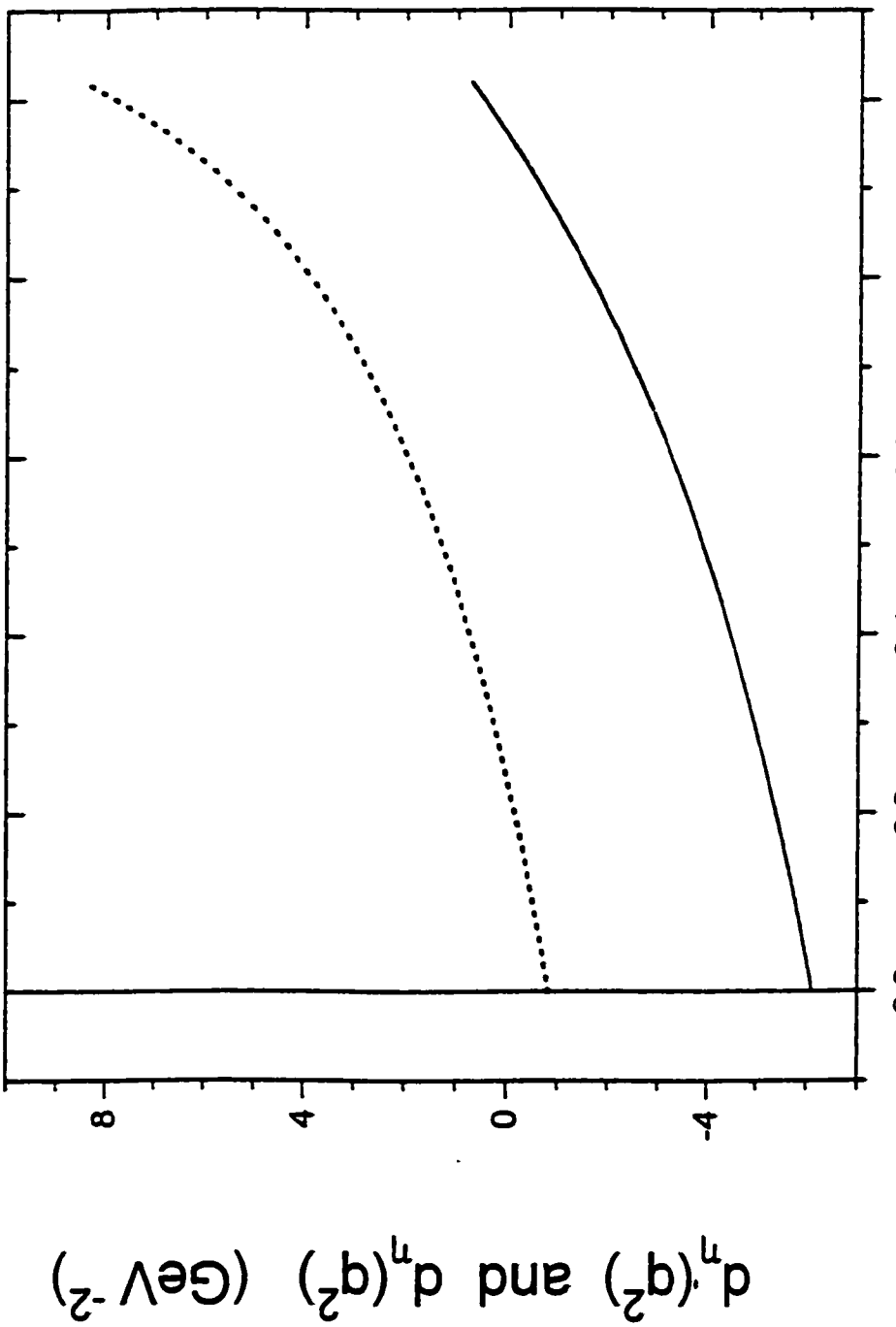

Fig. 5.8

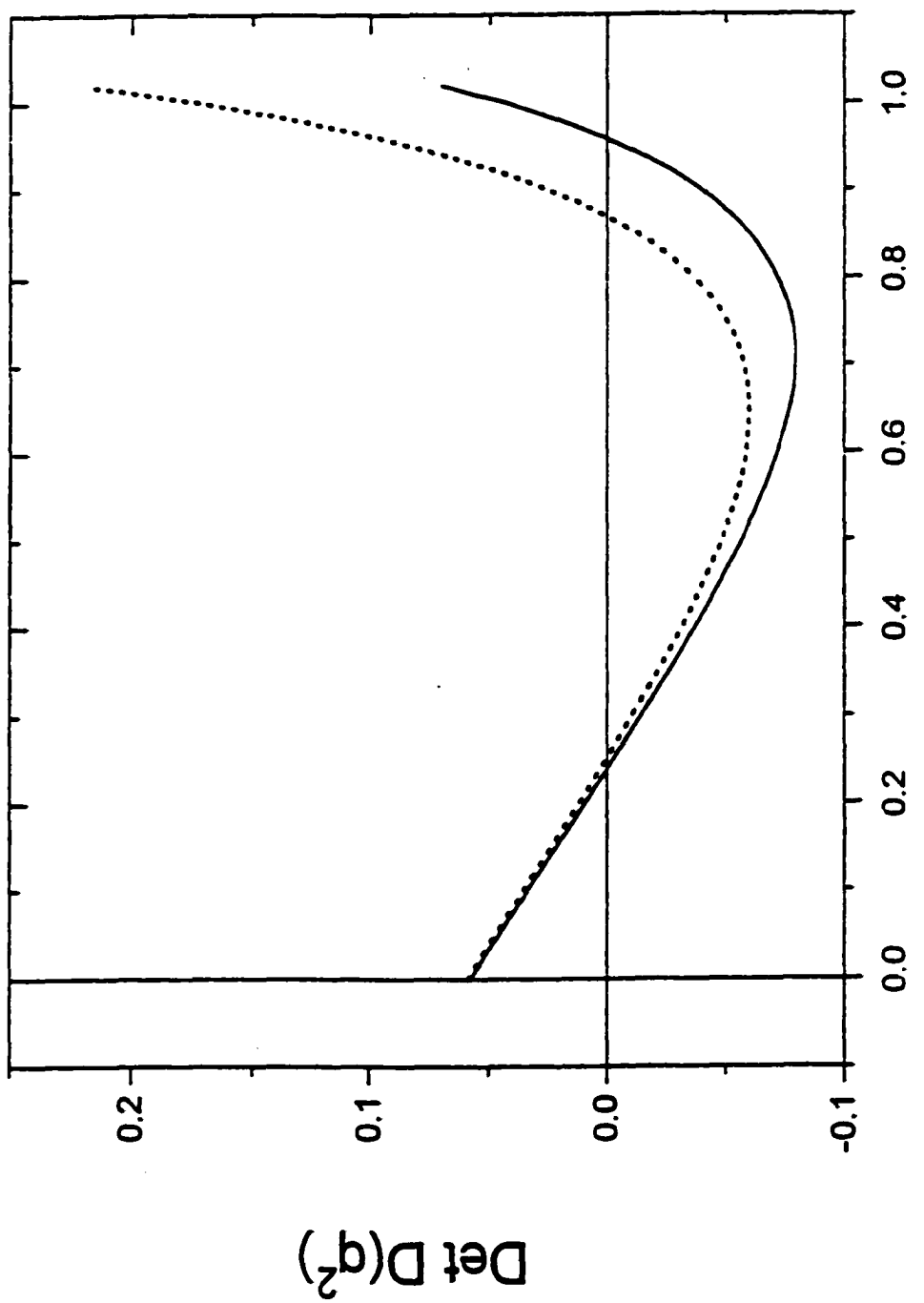

Fig. 5.9

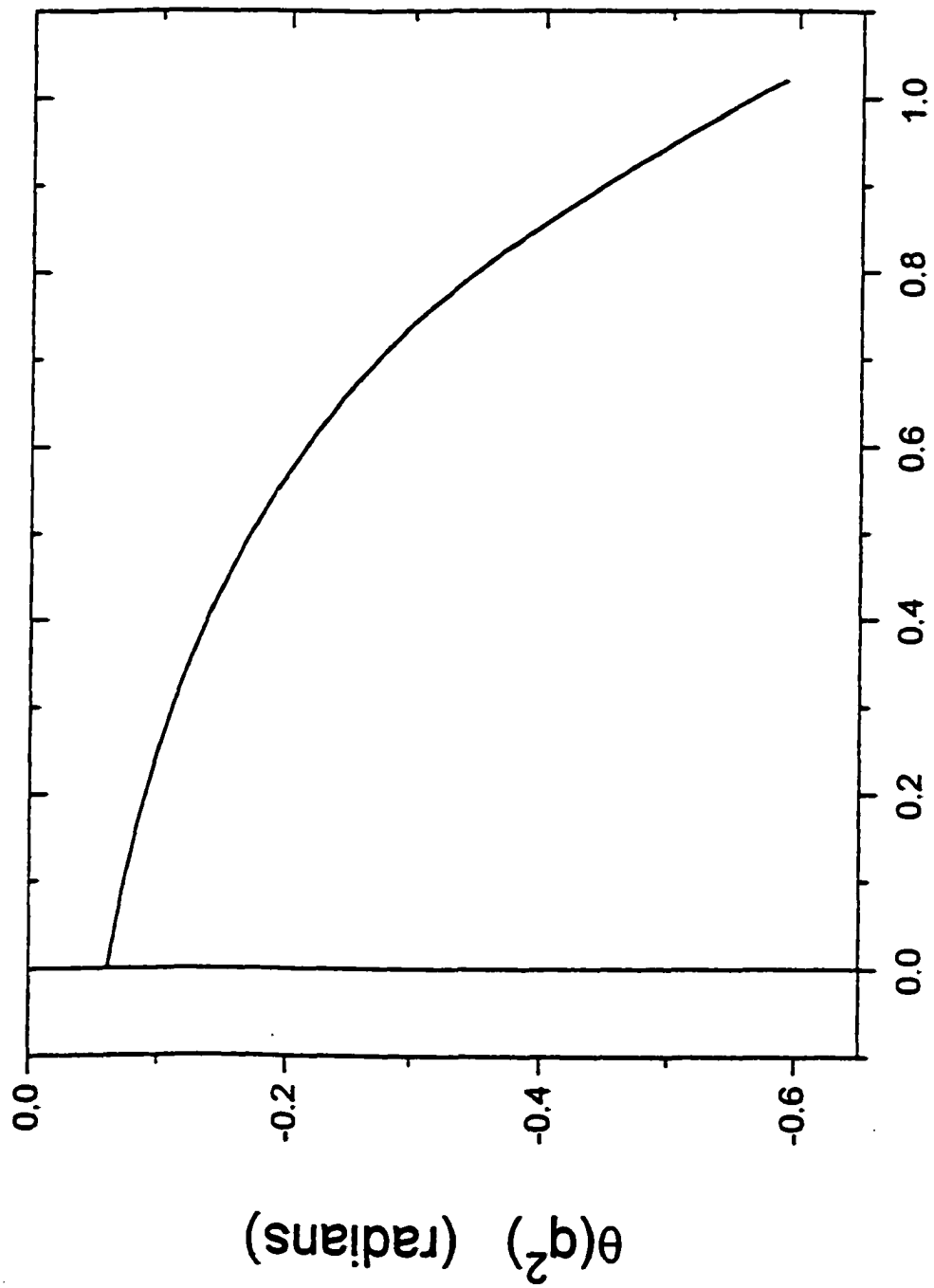

Fig. 5.10

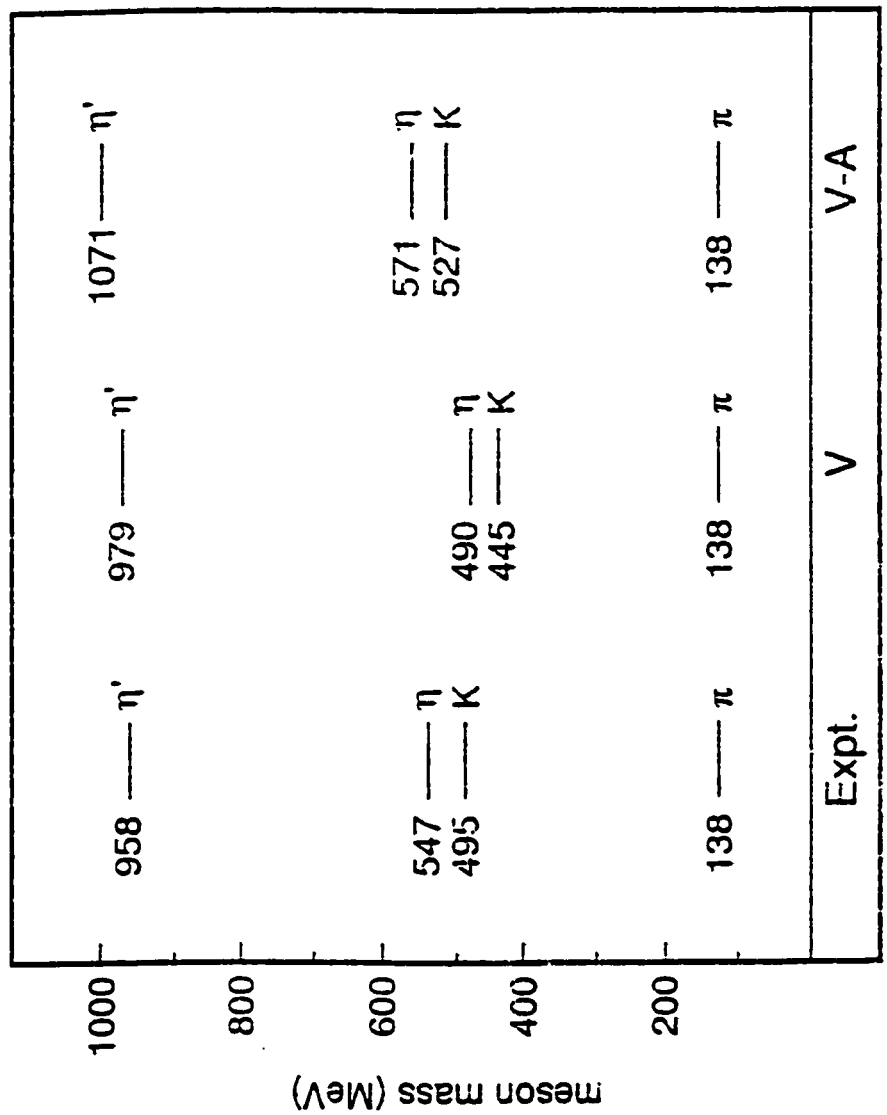

Fig. 5.11

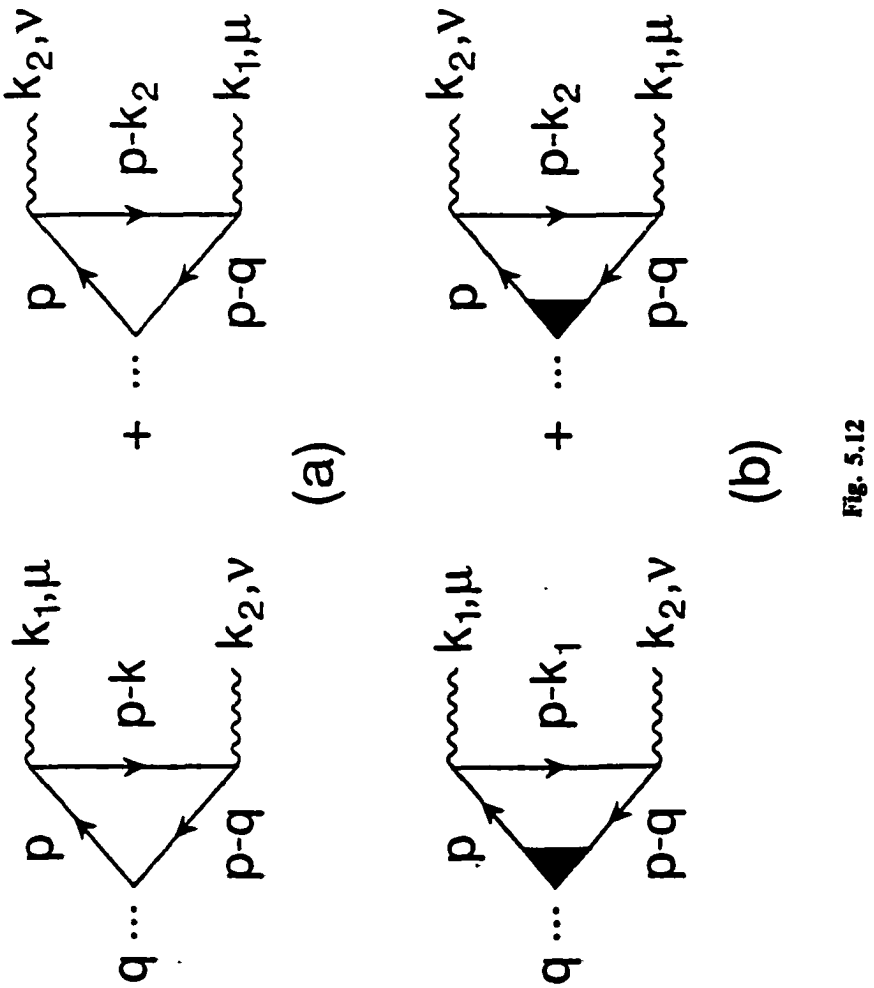

Fig. 5.12

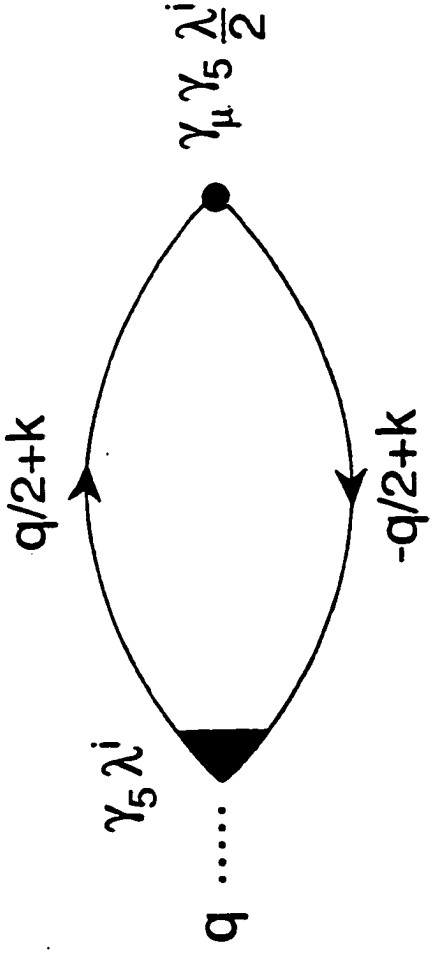

Fig. 5.13

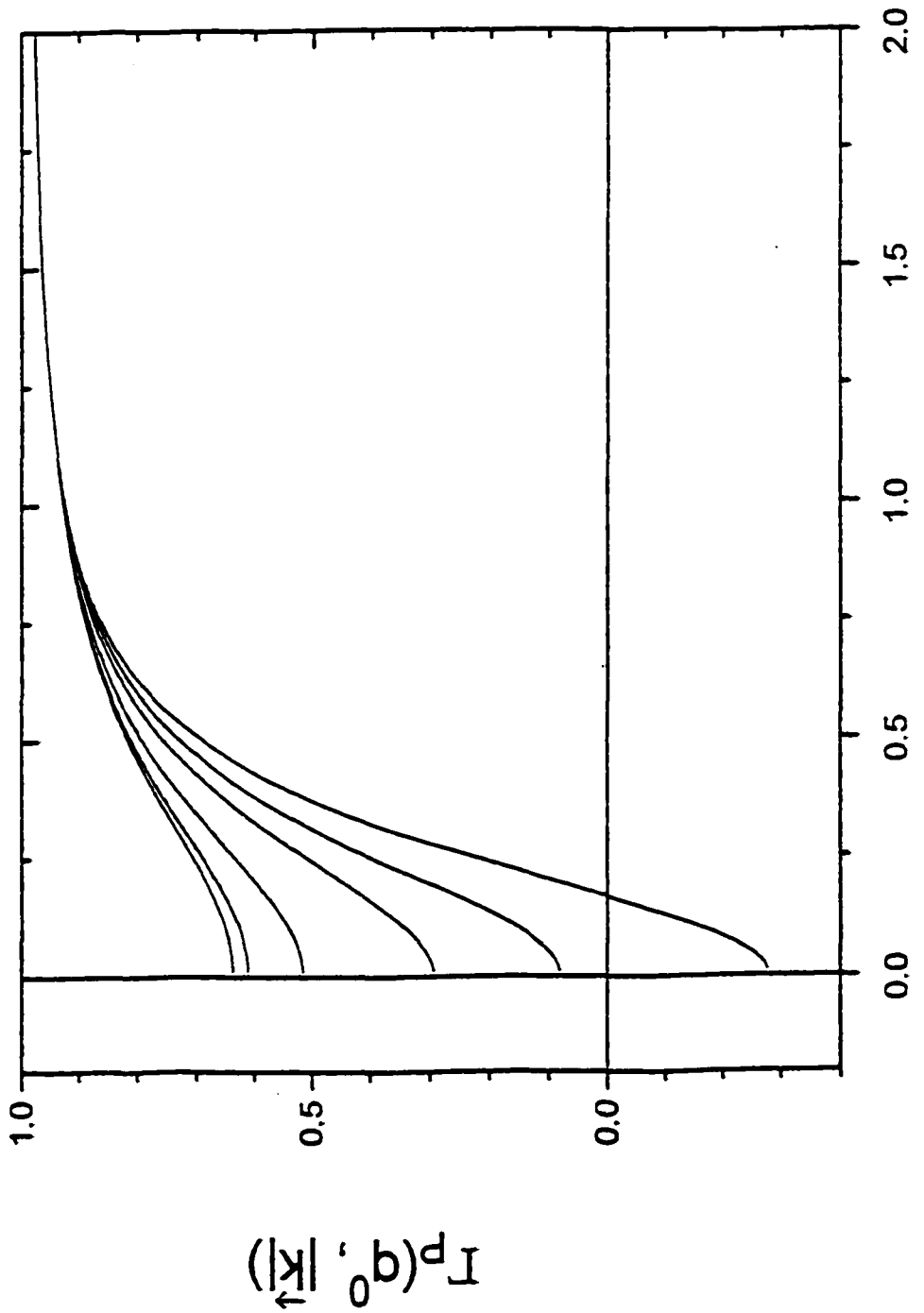

Fig. 5.14

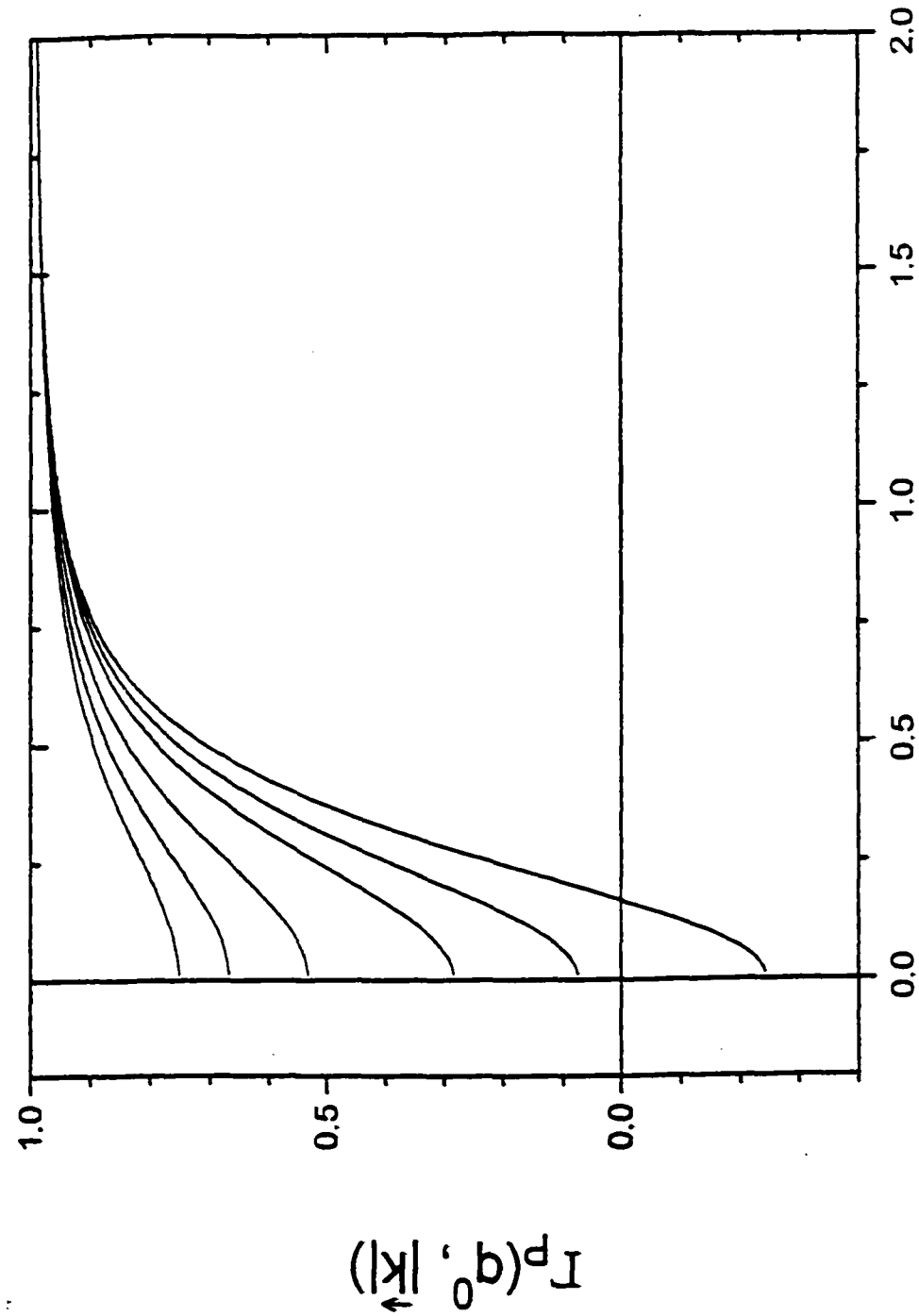

Fig. 5.15

References

[Ai90] H. Aihara *et al.*, Phys. Rev. Lett. 64, 172 (1990). (See Ref. [20] of this letter.)

[Ba96] R.M. Barnett *et al.*, Phys. Rev. D54, 1 (1996). This reference contains a comprehensive survey of elementary particle properties.

[Be88] V. Bernard, R.L. Jaffe and U.-G. Meissner, Nucl. Phys. B308, 753 (1988).

[Be91] H.-J. Behrend *et al.*, Zeit. für Phys. C49, 401 (1991).

[Ce81] L.S. Celenza, B. Goulard and C.M. Shakin, Phys. Rev. D24, 912 (1981).

[Ce86] L.S. Celenza and C.M. Shakin, Relativistic Nuclear Physics: Theories of Structure and Scattering (World Scientific, Singapore, 1986).

[Ce92a] L.S. Celenza, A. Pantziris, C.M. Shakin, and Wei-Dong Sun, Phys. Rev. C45, 2015 (1992).

[Ce92b] L.S. Celenza, A. Pantziris, C.M. Shakin, and Wei-Dong Sun, Phys. Rev. C46, 571 (1992).

[Ce93] L.S. Celenza, C.M. Shakin, Wei-Dong Sun, and Xiquan Zhu, Phys. Rev. C48, 159 (1993).

[Ce93a] L.S. Celenza, C.M. Shakin, Wei-Dong Sun, J Szweda, and Xiquan Zhu, Intl. J. Mod. Phys. E2, 603 (1993).

[Ce93b] L.S. Celenza, C.M. Shakin, Wei-Dong Sun, J Szweda, and J. Szweda, Intl. J. Mod. Phys. E2, 437 (1993).

[Ce93c] L.S. Celenza, C.M. Shakin, Wei-Dong Sun, J. Szweda, and Xiquan Zhu, Intl. J. Mod. Phys. E2, 603 (1993).

[Ce95a] L.S. Celenza, C.M. Shakin, Wei-Dong Sun, J Szweda, and Xiquan Zhu, Phys. Rev. D51, 3638 (1995).

[Ce95b] L.S. Celenza, C.M. Shakin, Wei-Dong Sun, J Szweda, and Xiquan Zhu, Ann. Phys. (N.Y.) 241, 1 (1995).

[Ce96a] L.S. Celenza, Shun-fu Gao, C.M. Shakin, Wei-Dong Sun, and J. Szweda, Phys. Rev. C53, 1936 (1996).

[Ce96b] L.S. Celenza, C.M. Shakin, and Wei-Dong Sun, Phys. Rev. C54, 487 (1996).

[Ce97a] L.S. Celenza, Xiang-Dong Li, and C.M. Shakin, Phys. Rev. C55, 3083 (1997).

[Ce97b] L.S. Celenza, Xiang-Dong Li, and C.M. Shakin, Phys. Rev. C55, 1492 (1997).

[Dm96] V. Dmitrašinović, Phys. Rev. C53, 1383 (1996).

[Gr91] F. Gross and J. Milana, Phys. Rev. D43, 2401 (1991).

[Gr92] F. Gross and J. Milana, Phys. Rev. D45, 969 (1992).

[Ha87] T. Hatsuda and T. Kunihoro, Phys. Lett. B185, 304 (1987); B198, 126 (1987).

[Ha94] T. Hatsuda and T. Kunihiro, Phys. Rep. 247, 223 (1994).

[Kl90] S. Klimt, M. Lutz, U. Vogl and W. Weise, Nucl. Phys. A516, 429 (1990);

[Kl92] S.P. Klevansky, Rev. Mod. Phys. 64, 649 (1992);

[Ma89] R. Machleidt, in Advances in Nuclear Physics, edited by J.W. Negele and E. Vogt (Plenum, New York, 1989) Vol. 19.

[Mu96] C.R. Münz, Two-photon decays of mesons in a relativistic quark model, hep-ph/9601206 (1996).

[Na92] Nan-Wei Cao, C.M. Shakin, and Wei-Dong Sun, Phys. Rev. C46, 2535 (1992).

[Pa95] J. Parramore and J. Piekarewicz, Nucl. Phys. A585, 705 (1995).

[Re95] J. Resag and C.R. Münz, Nucl. Phys. A590, 735 (1995).

[Re96] P. Rehberg, S.P. Klevansky and J. Hüfner, Phys. Rev. C53, 410 (1996).

[Sa97] C. Savkli and F. Tabakin, preprint, College of William and Mary WM-97-103 (1997); LANL e-print archive hep-ph/9702251.

[Se86] B.D. Serot and J.D. Walecka, in Advances in Nuclear Physics, edited by J.W. Negele and E. Vogt (Plenum, New York, 1986) Vol. 16.

[Sh94] C.M. Shakin, Phys. Rev. C50, 1129 (1994).

[Sh95a] C.M. Shakin, Wei-Dong Sun, and J. Szweda, Phys. Rev. C52, 3353 (1995).

[Sh95b] C.M. Shakin, Wei-Dong Sun, and J. Szweda, Phys. Rev. C52, 3502 (1995).

[Sh97] C.M. Shakin and Wei-Dong Sun, Phys. Rev. C55, 614 (1997).

[Sz97] A. Szczepaniak and E.S. Swanson, Phys. Rev. D55, 3987 (1997).

[Sz97] A. Szczepaniak, private communication.

[Sw97] Eric Swanson, private communication.

[Ta95] T. Takizawa and M. Oka, Phys. Lett. B359, 210 (1995); erratum: Phys. Lett. B 364, 249 (1995).

[Ta97] M. Takizawa, Y. Nemoto and M. Oka, Phys. Rev. D55, 4083 (1997).

[To96] N.A. Törnqvist and M. Roos, Phys. Rev. Lett. 76, 1575 (1996).

[Vo90] U. Vogl, M. Lutz, S. Klimt and W. Weise, Nucl. Phys. A516, 469 (1990).

[Vo91] U. Vogl and W. Weise, Prog. Part. Nucl. Phys. 27, 195 (1991).